STUDIES OF CRUSTAL SHEAR WAVES AND POISSON'S RATIO.

by

Marcelo Sousa de Assumpção
(B.Sc., Univ. of S. Paulo)

Thesis submitted for the degree of Ph.D.

University of Edinburgh
Department of Geophysics

December 1978.

TO

CECÍLIA

ABSTRACT

A large deep crustal and upper mantle seismic refraction experiment was carried out in 1974 with the cooperation of many British and German institutions --- the Lithospheric Seismic Profile in Britan (LISPB). Sixty portable 3-component stations and 10 shot-points produced a series of reversed and overlapping profiles along a distance of 1000 Km from north of Scotland to south of England. The experiment has produced valuable detailed information about the deep crust and upper mantle structure in Britain. The present work is an interpretation of the shear waves recorded in the northern part of the LISPB profile (mainly Scotland), complementing the information derived from the compressional waves.

The ratio of compressional to shear wave velocities in various parts of the crust of Northern Britain was determined by a method using the observed travel time ratio of shear to compressional waves (ts/tp). Basically the method involves fitting the observed ts/tp data with a theoretical curve of ts/tp versus station distance that is a function of the various Poisson's ratios along the ray paths. A knowledge of the P velocity model is necessary, but uncertanties in this model have very little effect on the calculated Poisson's ratios which means that only an approximate P velocity model is sufficient for the method to be applicable.

The resulting Poisson's ratios in northern Britain are close to the conventional value of 0.25 (equivalent to a velocity ratio of $Vp/Vs = \sqrt{3}$) except in the Southern Uplands upper crustal and Midland Valley mid crustal layers (about 0.23). The pre-Caledonian basement of Lewisian granulites thought to continue beneath the Highlands down to the Southern Upland Fault shows different Poisson's ratios under the Midland Valley and under the Northern Highlands which might be interpreted as significant differences in mineral composition.

The Poisson's ratio structure was used to help analyse a PS reflection from the Moho (P converted to S). The high apparent velocity of this phase was interpreted as due to a localized dip in the Moho discontinuity which is in agreement with Pn time-term data for the area. The Poisson's ratio structure was also used for accurate determination of epicentres of an earthquake swarm in the Kintail area of NE Scotland. The S wave arrival times of these earthquakes are in general agreement with the LISPB results showing that the Poisson's ratio determined in the LISPB profile north of the Highland Boundary Fault are representative of the rest of the Highlands.

ACKOWLEDGEMENTS

I wish to express my very sincere thanks to all those who helped me complete this thesis. Working in the Global Seismology Unit of the Institute of Geological Sciences and in the Geophysics Department of Edinburgh University was a very stimulating experience which I enjoyed very much. The high level of scientific research and enthusiasm that I saw in Edinburgh much contributed to enhance my interest in geophysics. Many times during the last four years I experienced a great joy after a good result in my work as well as big disappointments when realizing that many "brilliant" results were not so brilliant after all. I had many long depressing spells of hard work with no useful outcome as well as great contentment after unexpectedly producing good results. Many times I felt the distress of not understanding a particular topic in my studies as well as relief of suddenly grasping its meaning (or regarding it as unimportant !). Many times my opinions (and those of other people) ranged between unfounded optimism and ruthless scepticism. All that helped me to see how scientific progress is made and how interesting and motivating science can be.

I wish to thank Dr. P.L.Willmore, head of the Global Seismology Unit, and Prof. K.M.Creer, head of the Geophysics Department, for accepting me to Edinburgh and allowing me full use of their facilities for my project. I am specially indebted to the Global Seismology Unit for having provided me with all possible assistance and support throughout my work. I am grateful to Graham Neilson for my first lessons on seismological practice and also for patiently answering all my questions ever since. I am much obliged to all GSU technical staff who first showed me how to operate seismic equipments and who since then have continuously helped me either in the field or in the laboratory. The assistance of Douglas Houliston, Keith Chappel, Bob McGonigle, Pete Marrow, Alistair Miller, Stan Morgan, John

Laughlin and Gordon Waugh was much appreciated.

I was very lucky to have David Booth as a colleague during an early field exercise in Brazil. His work was extremely helpful for which I am very grateful. I also thank Remy Antezana and Jesus Berrocal for the help I had then as well as Dr. Willmore whose enthusiasm greatly impressed me.

The work of this thesis was carried out under the supervision of Dave Bamford. I enjoyed his supervision very much. Quite often instead of answering my questions he would ask me other questions as if I knew what I was doing --- this much contributed to building up my self-confidence. He carefully read and corrected earlier drafts of this thesis and his criticisms were always very constructive and extremely helpful. I had the great pleasure of working together with Brian Jacob for over a year. He supported and encouraged me throughout my work and the many discussions I had with him were very fruitful. I am also indebted to Stuart Crampin for being so interested in my project and for his constant assistance. I profited a great deal from several discussions I had with him over these years and I would like to thank him for the computer programs he made available to me. I also benefited from the many discussions I had with Dr. Willmore and I am thankful for his advices and suggestions. David Booth and Charlie Fyfe have also helped me a lot with various computer programs, digitization of seismic records and instructions on the operation of the PDP-11/50 computer of IGS, and Bob McGonigle helped me with various discussions on the problems of local epicentre determination.

I would like to express my gratitude to all other members of the Global Seismology Unit and of the Geophysics Department (too numerous to mention here) who helped me in one way or another to complete this work. All my student colleagues deserve special thanks for the enjoyable time I have had in the past four years.

Finally I am deeply indebted to Cecília Torres de Assumpção for the

strong support and encouragement she gave me during my work. Her constant help with data preparation, typing, corrections and comments were immensely appreciated and her willingness to understand the seismology I was doing made my work even more rewarding.

This project was partly financed by the Fundação de Amparo à Pesquisa do Estado de S. Paulo, Brazil, under grant no. 74/627. The Instituto Astronômico e Geofísico of the University of S. Paulo also financially supported this work.

CONTENTS

CHAPTER 5. PS MOHO REFLECTION AND LOWER CRUST STRUCTURE

CHAPTER 6. KINTAIL EARTHQUAKE SERIES

LIST OF ABBREVIATIONS

GGF = Great Glen Fault

HBF = Highland Boundary Fault

LTF = Loch Tay Fault

MT = Moine Thrust

MV = Midland Valley

SU = Southern Uplands

SUF = Southern Upland Fault

Z = Vertical component

R = X = Radial horizontal component

T = Y = Transverse horizontal component

'a' = Upper crustal refraction

'c' = Moho wide-angle reflection

'd' = Uppermantle refraction

'e' = Lower crust wide-angle reflection

ts (tp) = S (P) travel time

Vs (Vp) = S (P) velocity

K = Vp/Vs

SNR = Signal to noise ratio

PR = σ = Poisson's ratio

N2-->ALPHA = profile from shot-point N2 recorded on segment ALPHA

unf. = unfiltered seismograms

smoo. = smoothed seismog.(low pass filtered)

$$\sigma = \frac{1}{2}\cdot\frac{(K^2-2)}{(K^2-1)}$$

σ	K
0.22	1.669
0.25	1.732 (=$\sqrt{3}$)
0.28	1.809
0.30	1.871
0.333	2.000

CHAPTER 1

INTRODUCTION

1.1 STUDIES OF CONTINENTAL CRUSTAL STRUCTURE.

1.1.1 Seismic velocity structure

Structural models for the continental crust have developed quite rapidly in the last decade or so. For a long time the continental crust was modelled with two constant velocity layers, an upper granitic and a lower crustal basaltic layer, with occasionally a superficial sedimentary layer. However modern interpretation techniques using as much information as possible from the seismograms such as secondary arrivals, amplitude and frequency, have revealed that the crust is more complex with many features not previously detected. Such new features are : more than two crustal layers, vertical velocity gradients, velocity inversions and transition zones of a few kilometers instead of sharp discontinuities. Large lateral variations in the lower crust and upper mantle have also been found. Fig 1.1 shows an example of a possible P velocity crustal section.

Upper crustal low velocity layers were reported for example by Mueller & Landisman (1966) and seem to be quite a general feature, although not always of sufficient horizontal occurrence to be easily detected by refraction studies. Quite often a velocity gradient either in the upper or lower crust seems to better fit the seismic data, specially when amplitudes, in addition to travel times, are modelled (e.g., Fuchs & Müller 1971, Mueller & Landisman 1971 and Berry & Fuchs 1973).

The Moho transition is very seldom a sharp discontinuity (Fuchs 1975) but more often a gradational transition between lower crust and upper mantle. In tectonically active regions (such as the Rhinegraben rift system in Europe, Edel et al. 1975) the "thickness" of the Moho can be as much as 4 - 5 Km. Below the Moho the upper mantle has been found to have a fine

structure consisting of several discontinuities and velocity inversions (e.g., Kind 1974, Hirn et al. 1975 and Faber 1978).

All the details discussed above have been found by interpretation of P waves only. S wave arrivals are not usually clear enough for a detailed determination of the various crustal interfaces. Nevertheless determination of S velocities are essential for a better understanding of other aspects of the crustal structure such as explained below.

1.1.2 Constitution of the continental crust.

The idea of the upper crust consisting of a granitic layer is still valid as an average composition and this is supported by surface geology. Although in tectonically active regions extreme exceptions may occur (such as in the Ivrea zone in the southern Alps where a slab of basic rocks from the lower crust or mantle was injected in the upper crust, Berckhemer 1969), the upper crust on a world wide average basis was estimated by Ronov & Yaroshevsky (1969) to be composed mainly of acidic granitoids and metamorphic rocks in roughly the same proportion with basic and ultra basic rocks being less than 15%.

The lower crust on the other hand is not a simple basaltic or gabbroic layer as previously thought. Ringwood & Green (1966) showed that under the pressure and temperature conditions of the lower continental crust and Moho the mineral assemblies of gabbro or basalt are likely to be unstable and would change to eclogite. To compensate for the high density and high seismic velocities of the eclogite assemblies those authors suggested that the lower crust would necessitate minerals like quartz and alkali-feldspars indicating that the lower crust could have a composition of acidic to intermediate rocks in the eclogite facies. Christensen & Fountain (1975) also showed that metamorphic rocks of the granulite facies could be major constituents of the lower crust and used one of the Canadian Shield

velocity structures to derive possible mineralogical models under that interpretation. Ronov & Yaroshevky (1969) proposed that the lower crust, on the average, is formed of deeply metamorphosed rocks of basic and acidic composition, basic rocks being about half the volume of the lower crust.

Studies of the lower crust and upper mantle composition are based mainly on the comparison of seismic velocities obtained in refraction profiles with those measured in the laboratory. To this end measurement of S as well as P velocity is essential because a wide range of different rock types can give the same P velocity (e.g. Mackenzie 1969). Measurements of Poisson's ratio can then significantly constrain the range of possible mineralogical models of the crust and upper mantle (e.g. Crosson & Christensen 1967, Christensen 1969, Christensen & Fountain 1975). Fig. 1.2 is a plot of Poisson's ratio and P velocity for a range of different rock types. The data is from laboratory measurements at 4 Kb (equivalent to about 15 Km depth) and room temperature compiled from various sources. The classification of rock types shown in Fig. 1.2 is rather arbitrary but helps to show how mineral constitution can affect Poisson's ratio. Granitic rocks usually have PR around 0.25 whereas basic and ultrabasic rocks tend to have higher Poisson's ratio. In granitic and metamorphic rocks an increase of quartz content can significantly decrease Poisson's ratio. In basic rocks pyroxene content decreases PR. Serpentinization of basic and metamorphic rocks decreases P velocity and increases Poisson's ratio.

It is important to point out that large variations in crustal seismic structure are found from one region to another. For example Poisson's ratios as reported in crustal refraction studies can easily range from 0.22 to 0.29 . This is equivalent to a deviation of +/- 5 % , in terms of velocity, from the normal value of 0.25 . This indicates that the crustal and upper mantle composition can vary enormously between different regions (e.g., Fagernes & Kanestrom 1973).

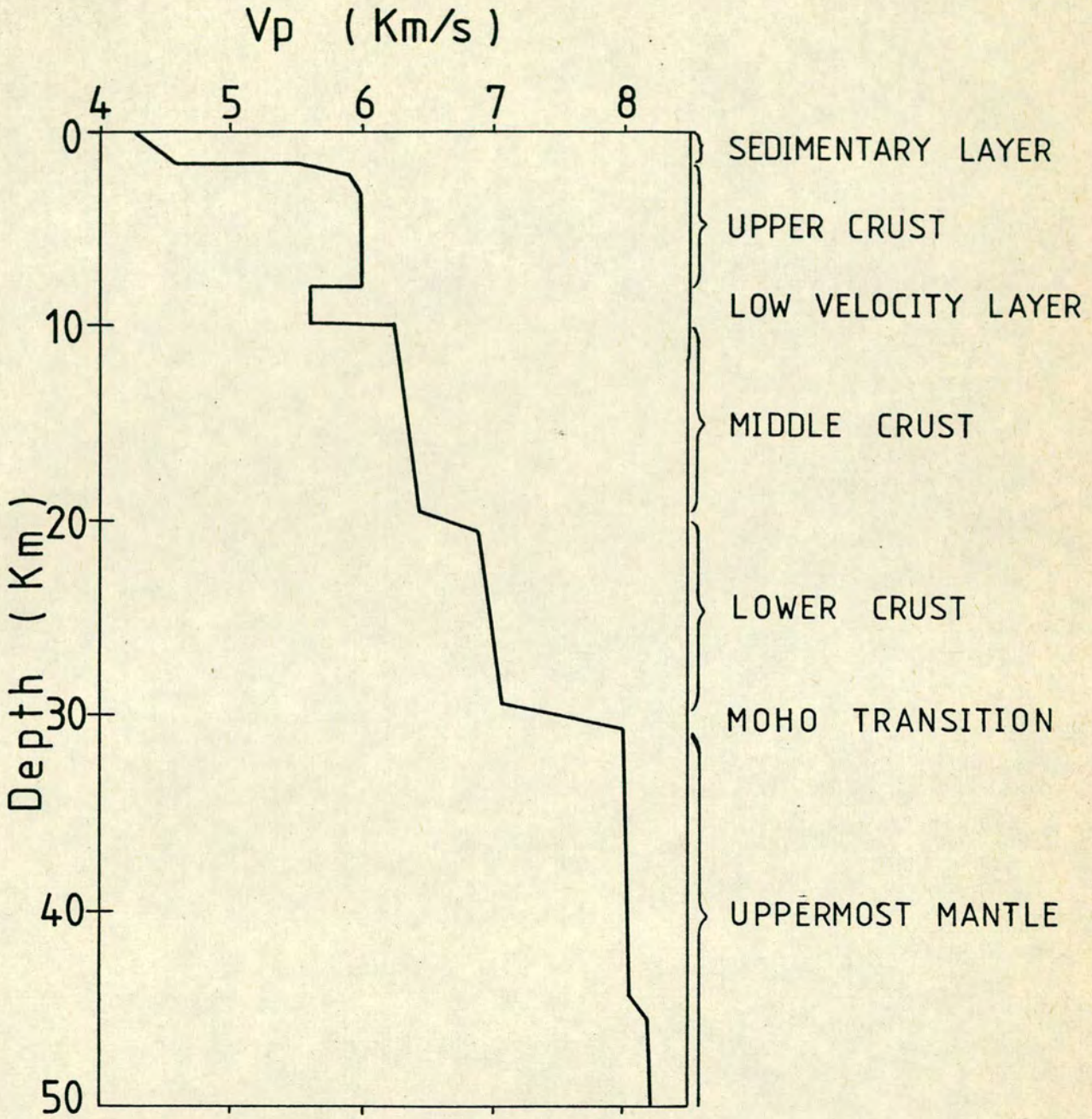

Fig. 1.1 An example of crustal P velocity structure.

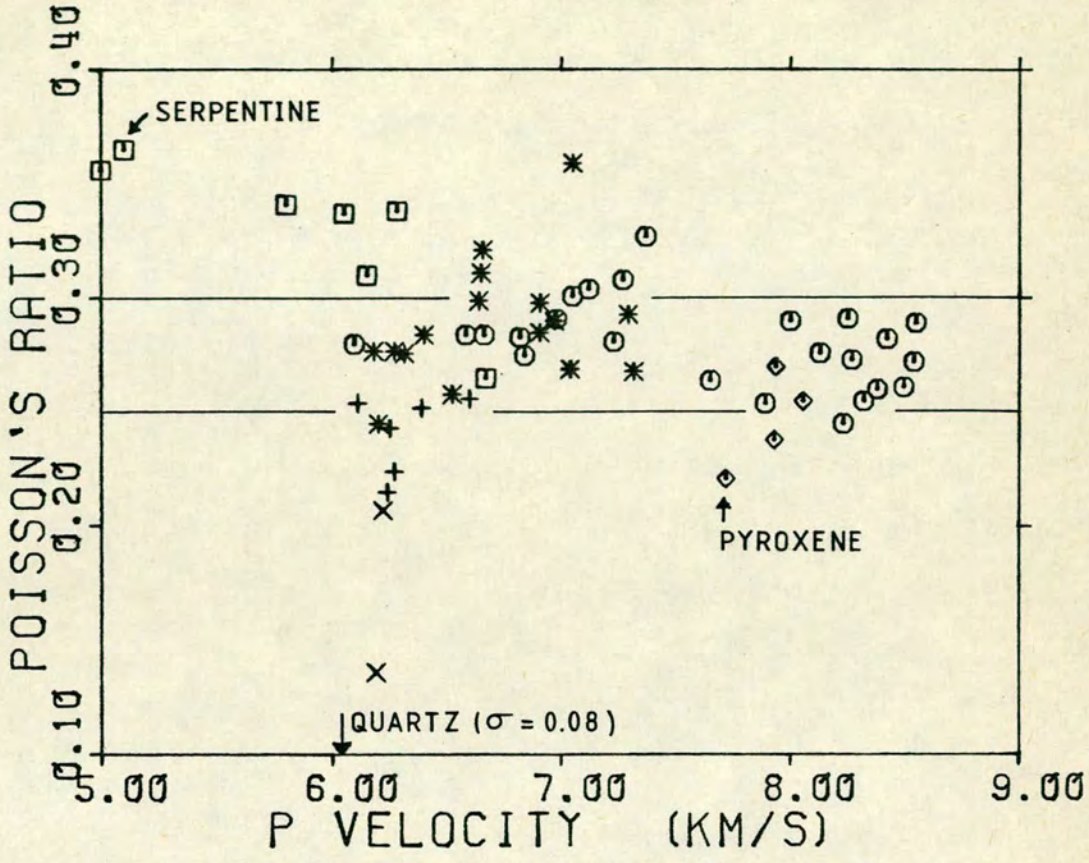

× QUARTZITE

\+ GRANITE

✱ METAMORPHIC (Gneiss, Schist, Granulite)

◈ PYROXENITE

⊡ SERPENTINITE

⊙ OTHER BASIC AND ULTRABASIC

Fig. 1.2 P velocity and Poisson's ratio for various rock types at 4 Kb and room temperature. Data compiled from : Birch 1960, 61; Simmons 1964; Christensen 1965, 66a, 1966b, 71, 72, 74, and Christensen & Fountain 1975.

1.1.3 Poisson's ratio and rock crack/porosity.

Apart from the bearing on the chemical composition of the crust and upper mantle, Poisson's ratio can also provide a good indication on the state of crack/porosity of the rock as well as partial melting.

A large amount of field and laboratory research has been done lately about the effect on seismic velocities (and velocity ratio Vp/Vs) of cracks and porosity in order to study the dilatancy phenomena in earthquake mechanisms with application to earthquake prediction. Increase of crack/porosity usually leads to a decrease in the Vp/Vs ratio if the cracks are dry but to an increase in Vp/Vs if the cracks are saturated with water (e.g., Nur 1972). Examples of observations of earthquake precursors being interpreted as dilatancy and its effect on Vp/Vs can be found for example in Scholtz et al. 1973, Whitcomb et al. 1973 and Aggarwal et al. 1975. Observed variations in seismic velocities with crack formation (dilatancy) can be up to 20% and decreases in travel time ratios (ts/tp) about 10% (equivalent to a decrease in Poisson's ratio from 0.26 to less than 0.20). Theoretical studies of the effect on Poisson's ratio of cracks and pore fluid saturation can be found for example in O'Connell & Budiansky 1977 and Crampin 1978. An interesting example of the variation of Poisson's ratio with fluid saturation was found at a dam in the southern Alps (Wittlinger & Haessler 1976) where the Poisson's ratio of the underlying rocks increased from about 0.27 to 0.33 after filling of the lake (equivalent to a velocity change of 10%), accompanied by increased seismicity, indicating the possibility that variations in Poisson's ratio could be used to help study the depth of penetration of water in the upper crust in relation to earthquake triggering.

At lower crustal depths Poisson's ratio is not much affected by changes in temperature (Fagerness & Kanestrom 1973, Birch 1969 and Fielitz

1976) provided there is no partial melting. A small degree of partial melting can significantly decrease Vs much more than Vp thus increasing Poisson's ratio dramatically (e.g. from $\sigma = 0.24$ to $\sigma = 0.27$ for 10% partial melting in Olivine, Birch 1969). In tectonically active regions Poisson's ratio can be very useful for detecting areas of the lower crust and upper mantle where partial melting exists (Ruegg 1975).

1.1.4 Location of local earthquakes.

Shear wave velocity structures are also very important for the determination of earthquake epicentres in local networks. As noted before a deviation of Poisson's ratio of 0.03 from the "normal" value of 0.25 is not uncommon in the crust and is equivalent to a difference in S travel times of about 0.3 s at an epicentral distance of only 20Km. This difference can be greater than the uncertainties usually associated with S arrivals, specially if 3-component stations are employed, so that an improvement in the location of local earthquakes should be expected when a good knowledge of S velocity structure is available.

1.2 THE CALEDONIAN TECTONICS.

A simplified tectonic map of the British Isles is shown in Fig. 1.3 where the main units are :

a) Precambrian basement at NW Scotland characterized by the Lewisian granulites.

b) A metamorphic zone between the Moine Thrust (MT) and the Highland Boundary Fault (HBF) characterized by Moine and Dalradian sequences which were deposited over Lewisian basement mainly during Late Precambrian and strongly folded with high grade metamorphism later in the Caledonian orogeny. An early phase of deformation and metamorphism occurred in late Precambrian north of the Great Glen Fault but most of the deformation and

metamorphism occurred in Early Ordovician times especially south of the GGF (Grampian Highlands), Johnstone 1975. There is large scale recumbent folding such as the Loch Tay Nappe. During the Caledonides the Moine was thrust over Lewisian (and Torridonian) basement producing the famous Moine Thrust with displacements up to about 20Km.

The Great Glen Fault (GGF) is a major feature in this area and was recognized as a transcurrent fault by Kennedy (1946) who proposed a sinistral movement of more than 100Km at Old Red Sandstone times (Devonian) based on the separation of two granitic masses (Strontian and Foyers igneous complexes) on NW and SE of the fault. This conclusion has been disputed on the basis of structural differences between the two granites and Garson & Plant (1972) have proposed dextral movement of about 120Km in lower ORS and a further dextral displacement of 30Km during upper Cretaceous. Vertical movements have also occurred as shown by seismic reflection investigations in the Moray Firth basin (Chesher & Bacon 1975) where a normal fault occurred throughout the Mesozoic (SE side downthrown) Another dextral movement of 30Km in the Tertiary was identified by Holgate (1969) starting in Lower Eocene (52 My). The GGF is still active today as indicated by its seismicity.

c) A non-metamorphic zone extending from the Midland Valley to about central England characterized by Lower Palaeozoic sedimentary rocks (Ordovician and Silurian climactically deformed during late Silurian or Devonian) with some ORS and Carboniferous basins in the Midland Valley and northern England. The main feature in this area is the Southern Upland Fault dividing the Midland Valley graben from the Southern Uplands. The crustal movements associated with this fault are not entirely known. A normal displacement of about 2Km has been detected from gravity measurements on the Leadburn Fault (one component of the SUF) with the downthrown side to the NW (Hipkin & Lagios, in preparation).

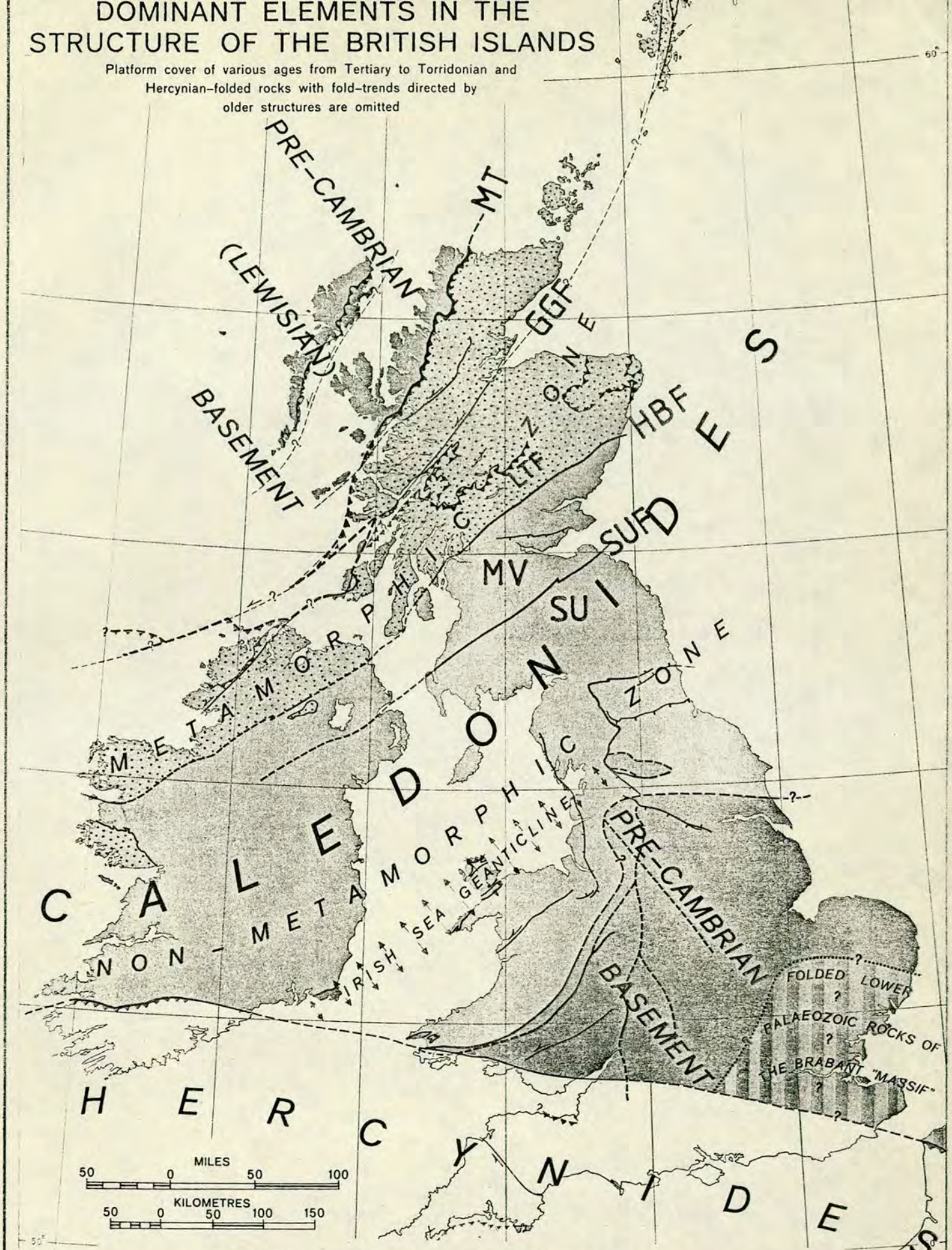

Fig. 1.3 Simplified tectonic map of the British Isles, (from Dunning & Stubblefield 1966).

GGF = Great Glen Fault, HBF = Highland Boundary Fault, LTF = Loch Tay Fault, MT = Moine Thrust, MV = Midland Valley, SU = Southern Uplands, SUF = Southern Upland Fault.

d) Another Precambrian basement at and south of central England down to the Hercynian front.

Mainly on palaeontological basis Wilson (1966) concluded that an ocean (Proto-Atlantic or Iapetus) divided the Scottish Highlands from southern England and Wales during the Precambrian and Lower Palaeozoic. The Highlands of Scotland had been part of an "American" continent and southern England part of the "European" continent. The plate tectonic processes acting on the margins of this ocean (Caledonian orogeny) creating the Midland Valley and Southern Uplands and eventual collision of the two continents are not fully established yet. Many plate tectonic models have been proposed. Dewey (1969) proposed an oceanic lithosphere subducting northwards beneath the Midland Valley and Highlands and another subducting southwards south of the Southern Uplands. Gunn (1973) proposed that the southward dipping Benioff zone was further north at the SUF and the Midland Valley graben was the remnant of an oceanic crust whereas the Southern Uplands would be part of the "European" continental crust. Wright (1976) suggested a series of alternating subductions northwards and southwards (from about 1000 to 450 My) with the creation of island arcs and subsequent collision of the arc with the continent. For example the HBF would mark the collision of an island arc (Midland Valley) with the American continental margin (Highlands). The last subduction on both sides of the ocean would have occurred around Mid Silurian - Early Devonian (450-360 My) causing the final closure of the Iapetus and end of the Caledonian orogen.

Moseley (1977) reviewed most of the proposed tectonic models drawing attention to the geophysical evidence (Powell 1971, and LISPB) that no remnant of oceanic crust exists today either in the Midland Valley or in the Southern Uplands. He suggested that the Proto-Atlantic ocean had closed by late Ordovician (no more faunal distinction) but that true collision

between the two continents occurred in late Silurian to early Devonian causing strong deformation and compression of geosynclinal basins such as the Southern Uplands.

Because of the large number of orogenic events with different ages on either side of the Iapetus the tectonic models have become very complex. Although there is general agreement on the basic ideas of the various tectonic models, details differ however on the number and exact position of the various subduction zones. The suture marking the final collision between the two continents seems to be somewhere near the Southern Uplands but exact location remains uncertain. Smith (1976) pointed out that too much emphasis has been given to plate-tectonics and that perhaps some features of the Caledonian orogen could be explained by alternative models involving vertical crustal movements without subduction zones (such as caused by self heating and partial melting of thick sedimentary basins). Dewey (1976) although emphasizing again the necessity of plate-tectonic models stressed that details of any ancient plate-tectonic orogenic evolution may not be susceptible to complete reconstruction not only because of the enormous complexity of plate boundary evolution but also because much of the evidence is destroyed.

1.3 THE LISPB EXPERIMENT

The Lithospheric Seismic Profile in Britain (LISPB) was a large explosion experiment carried out in July and August 1974 by a combined British-German working group. Full description of the experiment and results can be found in the several papers by the LISPB research group : Bamford et al. 1976, 1977 and 1978, Kaminsky et al. 1976, Nunn et al. 1978 and Faber 1978.

The general objective of the experiment was to determine a detailed cross section of the lithosphere through the British Isles from north to

south. This cross section would provide deep crustal and upper mantle information to help in the discussions of tectonic problems in Britain, in particular of the evolution of the Caledonian orogenic belts.

Sixty 3-component mobile stations (50 German Mars and 10 British Geostore) occupied at different times the four segments ALPHA, BETA, GAMMA and DELTA shown in Fig. 1.4(a). Shots were fired at various shot-points producing a series of reversed and overlapping crustal profiles (to distances of about 200 Km) and long range profiles (up to about 1000 Km). The observation scheme is shown in Fig. 1.4(b) where each line indicates the observed distance range for every particular shot-point. In addition an earthquake (KEQ, Fig. 1.4(a)) of magnitude mb = 3.0 was recorded while the stations were positioned on segments ALPHA and BETA with observed distances in the range 80 to 300 Km.

More than one shot was fired at each shot-point. For example at land shot-point 1 two shots were fired : shot 11 observed on segment BETA and 12 observed on ALPHA. Land shots ranged from 1 to 4 ton depending on the observation distance. At the sea shot-points N2, N1 and S2 a technique was used (Jacob 1975) consisting of firing a string of charges of 0.2 ton each (dispersed shot) all at optimum depth of 95 m instead of a single big charge. This ensured good propagation to long distances as well as the most efficient use of the sea water depths available for the experiment. The number of charges varied from 3 to 9 depending on the observation distance.

1.4 PRINCIPLE RESULTS OF P-WAVE INTERPRETATION (Northern Britain)

The main results for the northern profiles only (ALPHA, BETA and GAMMA) will be presented here as the present study of the S waves was restricted to northern Britain.

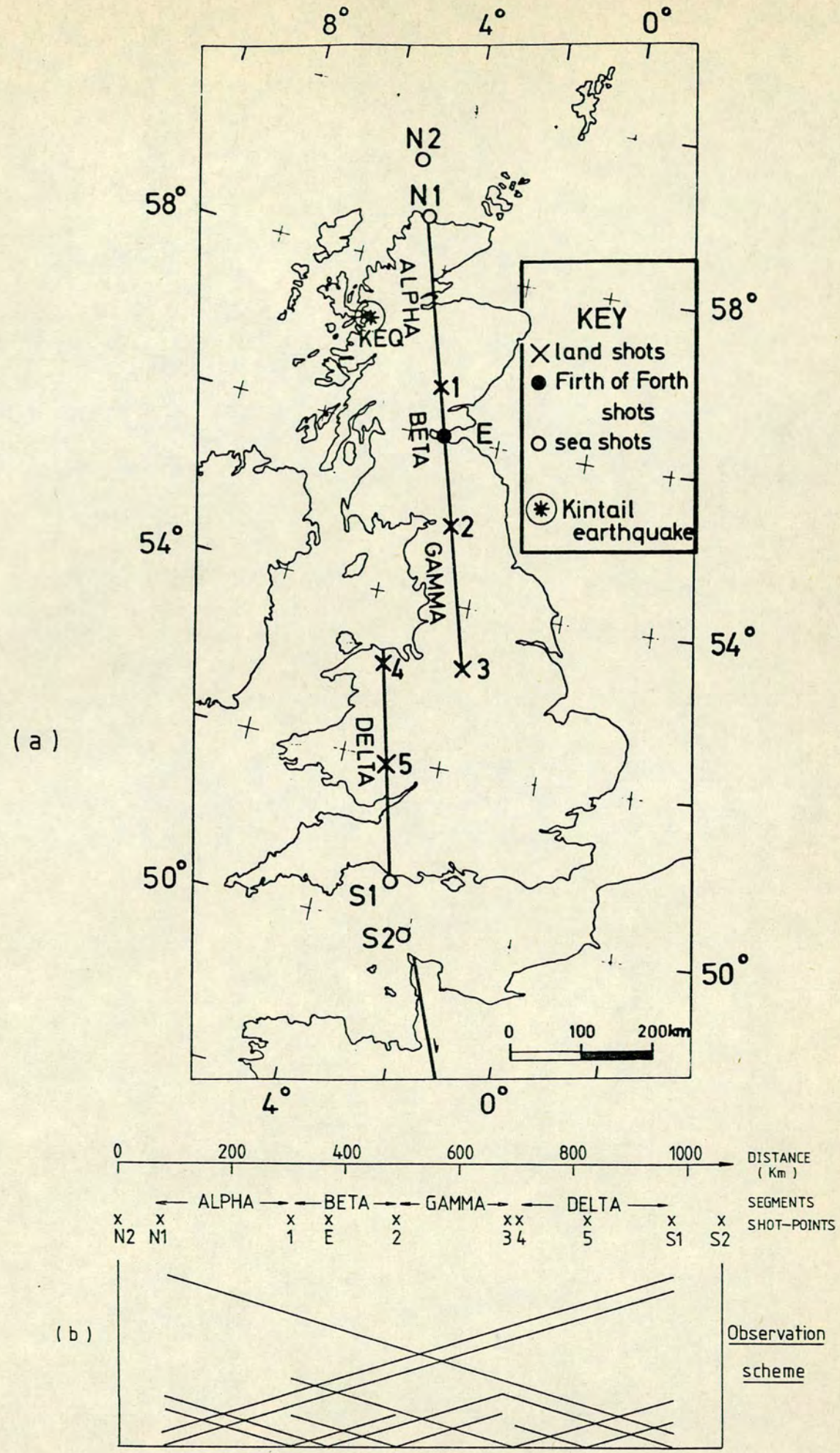

Fig. 1.4 (a) Location of LISPB shots and profiles.
(b) Observation scheme.
(from Bamford et al. 1976)

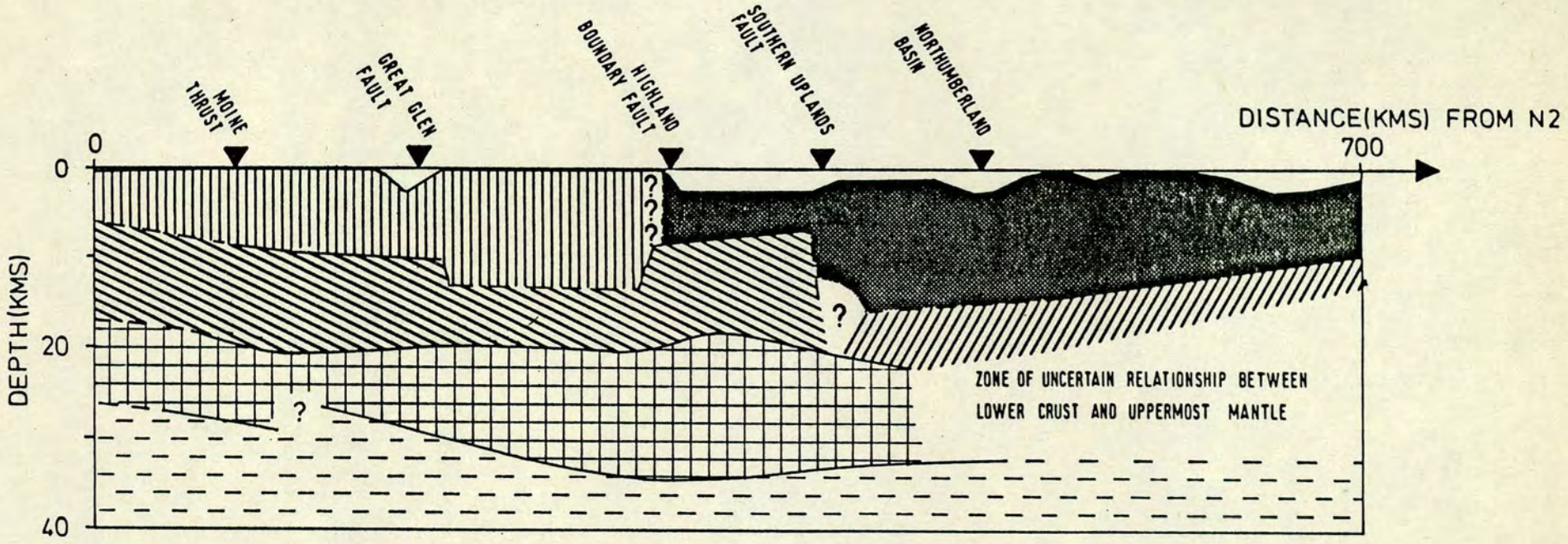

Fig. 1.6 Crustal section of northern Britain from P-wave interpretation (from Bamford et al. 1978).

1.4.1 Correlation of seismic waves.

Interpretation of seismic refraction studies starts with the identification of the various refracted and reflected arrivals returned from the seismic boundaries within the crust and upper mantle. Correlation (= identification of travel time branches) can be very simple as in the case of strong first arrivals or sometimes very difficult and rather subjective as in the case of weak secondary arrivals (Bamford et al. 1977b). To help in the correlation the seismic sections are plotted in various ways such as with true or normalized amplitude, with different band-pass filters and with station corrections to remove effects of near surface inhomogeneities (where good knowledge of near surface geological structure can be of substancial assistance).

The travel time branches found in the LISPB experiment are different for every segment because of the large lateral variation in the structure crossed by the profile. A summary of the travel time branches (= phases) is shown in Fig. 1.5 with the following notation adopted for the various phases :

The 'a' curves are first arrival refractions up to distances of 100 or occasionally 150 Km. The phase 'a_s' is a refraction (or direct) arrival through the uppermost layers, i.e. the sedimentary or low velocity superficial layer, with a velocity of about 4 - 5 Km/s. The phase 'a_o' is a refraction through the uppermost basement (conventionally called Pg) with an apparent velocity varying from 5.8 - 6.0 Km/s (such as the lower palaeozoic sequences of segment BETA) to 6.0 - 6.2 Km/s (such as the metamorphic basement of segment ALPHA). The phase 'a_1' has a higher apparent velocity (>6.2Km/s) and is a refraction from a deeper interface. This phase is not clearly observed on all segments.

At distances greater than about 130-150 Km the first arrivals, phase 'd', have an apparent velocity in the range 7.8 to 8.3 Km/s. This is the

Moho refraction conventionally called Pn.

The main second arrival phases are : 'c', a wide-angle reflection from the Moho transition (sometimes called PmP), and phase 'e' which, in LISPB, has been interpreted as a wide-angle reflection from the top of the lower crust as it is too strong to be a simple continuation of the 'a' refraction and has an apparent velocity too low to be a Moho reflection.

1.4.2 Results

Interpretation of the P waves included techniques such as plus-minus method, time-term analysis, ray-tracing modelling and others and is described by Bamford et al. 1977 and 1978.

The resulting main features of the crust of northern Britain, shown in Fig. 1.6 are :

1) a superficial layer of velocity 4 - 5 Km/s including upper Paleozoic and more recent sediments. Geological information regarding the superficial layer was incorporated in the seismic model as the LISPB experiment was not planned for detailed survey of near surface structure. The main sedimentary basins shown in Fig. 1.6 are : the Old Red Sandstone basin of the Moray Firth (both sides of the Great Glen fault); the Old Red Sandstone and Carboniferous deposits (intermingled with some lava flows) in the Midland Valley between Highland Boundary and Southern Upland Faults; and the lower Carboniferous deposits of Northumberland basin (shot-point 2).

2) an upper crustal layer with velocities varying laterally : north of the Loch Tay Fault the velocity of 6.1 - 6.2 Km/s is mainly related to the Moine formation of the Caledonian metamorphic belt (slightly lower velocity of 6.0Km/s was found south of the GGF perhaps due to the large amounts of granite intrusion in the metamorphic rocks); south of the HBF the velocities of 5.8 - 6.0 Km/s define the lower Paleozoic sequences.

3) a mid crustal layer perhaps defining the pre-Caledonian basement. The

depth of this layer is very variable increasing from about 6 Km at shot point N2 to more than 13 Km at the Loch Tay Fault and shallowing again beneath the Midland Valley to about 7 Km near SUF. There is a relatively large change in depth and velocity across the SUF which indicates that the pre-Caledonian basement is not horizontally continuous along the segments ALPHA and BETA having a possible transition (or discontinuity) near the SUF.

4) a lower crustal layer with velocities around 7 Km/s and depths about 20 Km shallowing slightly northwards and beneath the Midland Valley. This layer may be either absent or simply less well developed to the south.

5) an upper mantle with a uniform velocity close to 8 Km/s. The Moho depth increases southwards with maximum depth beneath the Midland Valley. The Moho does not seem to deepen monotonically towards the south but may have a local dip north at about 150Km south of shot-point N2. The Moho seems to be a sharp transition in segment ALPHA but in BETA the evidences point to a more gradual transition between lower crust and upper mantle.

The different crustal structures north and south of the Southern Uplands will have a considerable implication for further studies of the Caledonides. Some of the early tectonic models had predicted oceanic-type crust either under the Southern Uplands or under the Midland Valley. Clearly this is not the case as shown by Fig. 1.6, although the large structural contrasts between the Midland Valley and Southern Uplands indicate the importance of the Southern Upland Fault in the Caledonian tectonics.

1.5 THE OBJECTIVE OF THE PRESENT WORK

A knowledge of the distribution of Poisson's ratio (or alternatively Vp/Vs) might be expected to add significantly to our understanding of the composition and physical properties of the earth's crust. However most

refraction studies of shear waves are not aimed at determining Poisson's ratio directly but rather at inverting S data to obtain an S velocity-depth distribution independently of the P waves. Although this might have the advantage of providing an independent check on the P-wave derived structure, the uncertainties on the depths of the various crustal interfaces are usually much larger than possible differences between P and S models. In the present work a more direct determination of Poisson's ratio was attempted by treating P and S travel times together (chapter 4). In addition the method developed here takes into account the uncertainties in S (and P) arrival times and can be applied to structures with lateral variations, as the LISPB profile, provided some knowledge of the P velocity structure is available.

CHAPTER 2

OBSERVATION OF S WAVES FROM LISPB EXPLOSIONS

This chapter describes very briefly general aspects of the S waves recorded in the LISPB profiles through Scotland and Northern England such as signal quality, amplitude and frequency. No attempt was made to study these aspects in detail, mainly because that was not essential to the determination of S velocity structure (Chapter 4) where only travel time information was used.

2.1 QUALITY OF OBSERVED S ARRIVALS

Not all the LISPB shots generated good S waves but most shots recorded on profiles ALPHA and BETA produced some shear waves either as upper crustal refractions (shots at 1, E and 2; e.g. Fig. 2.1) or as wide-angle reflections (shots at N2, N1, 1 and E recorded on ALPHA; e.g. Fig. 2.2).

Appendix A contains the seismic sections with the S waves used in this work. The table below shows which S phases had a SNR big enough for S arrivals to be picked with an uncertainty less than or equal to +/- 0.3 s . This table shows all the S phases used in determining Poisson's ratios of the various crustal layers. Phase notation is the same used for the P waves and described in chapter 1 (section 1.4.1).

Table 2.1

	Phase / Profile	a_o	a_1	c	e	d
Optimum depth shots	N2-->ALPHA	⊠		√	√	
	N1-->ALPHA			√		
Firth of Forth shots	E-->BETA+ALPHA	√	√	√		
	E-->BETA+GAMMA		⊠			
Land shots	1-->ALPHA	√	⊠	√		
	1-->BETA	√	√	▨		
	2-->BETA	√	⊠	▨		
	2-->GAMMA			▨		
	3-->GAMMA			▨		

⊠ = neither P or S phase recorded
▨ = very poor P, no S
blank = good P, no S ; √ = P and S .

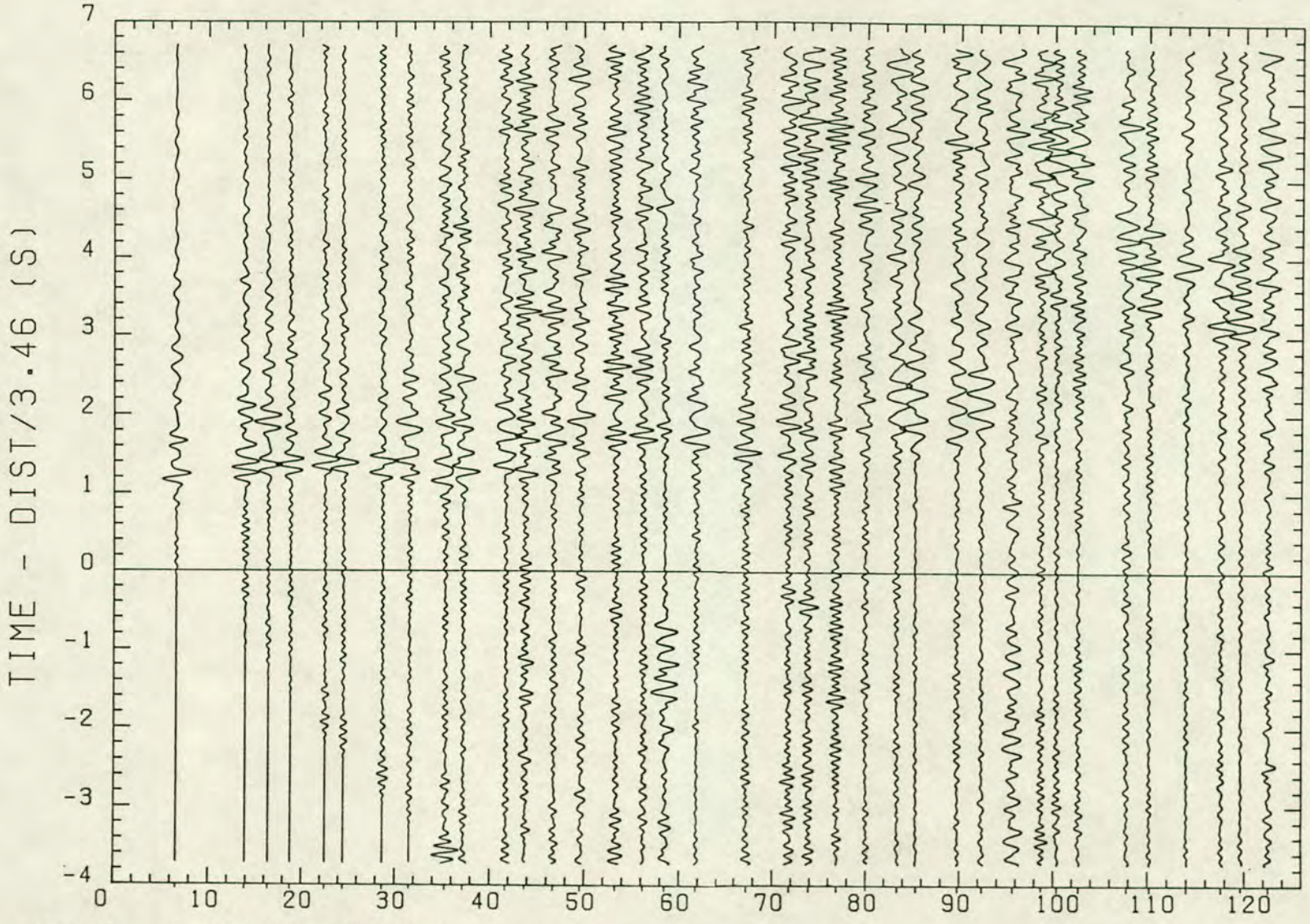

Fig. 2.1 2— BETA (T, 2.5-10. Hz) S waves 'a_o'

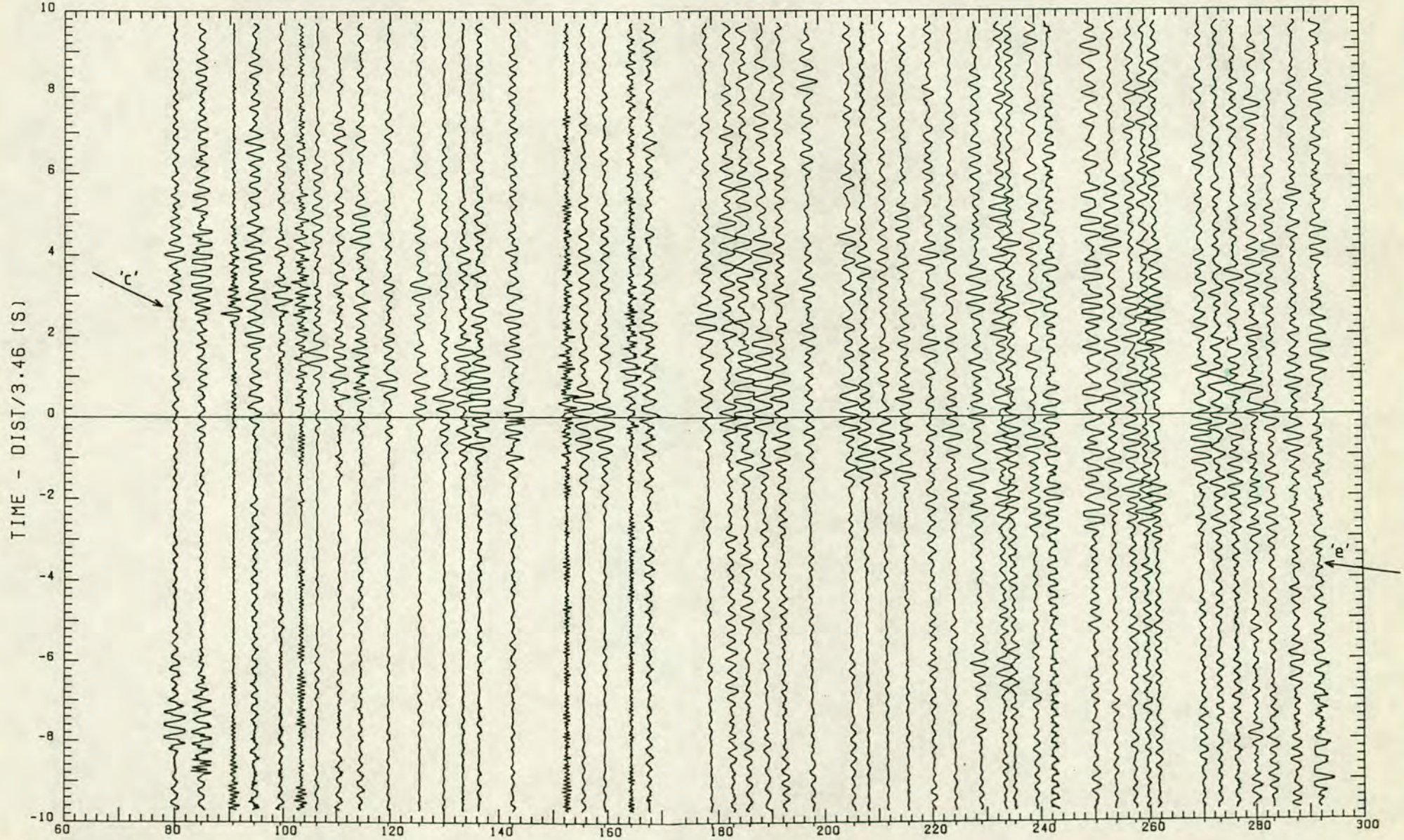

Fig. 2.2 N2—→ALPHA (Z, unfilt.), S waves.

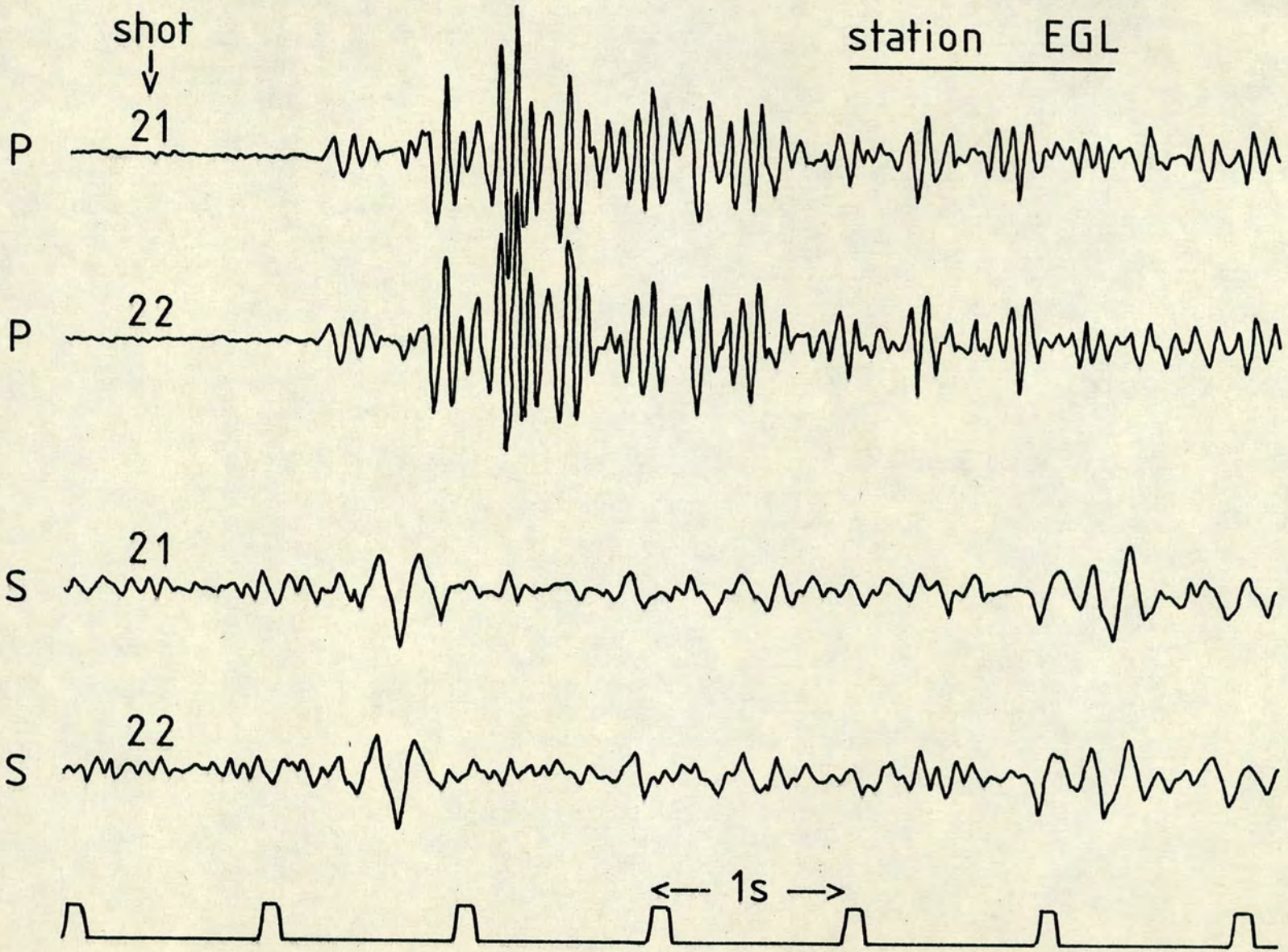

Fig. 2.3(a) Shots 21 and 22 recorded at EGL (Lownet), $\Delta = 87$Km

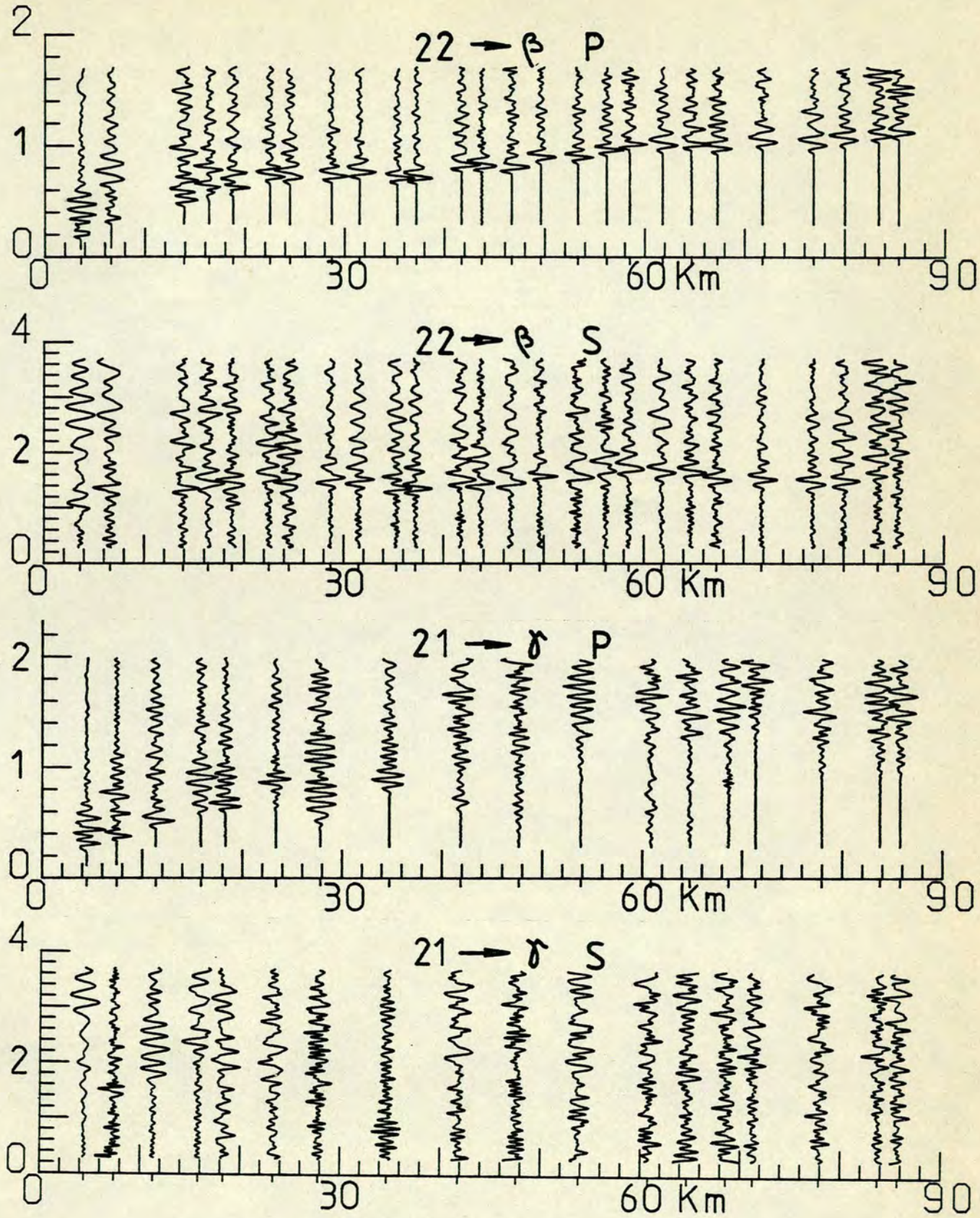

Fig. 2.3(b) Record sections of P and S from profiles 22→ BETA and 21→ GAMMA, phase 'a'. Vert. axis is reduced time in sec. Red. vel. = 6.0 Km/s for P, 3.46 Km/s for S. All vertical components, normalized amplitude.

Not all stations had S waves with amplitudes large enough to be read. For example, out of 102 stations recording P arrivals for upper crustal refractions on profiles E-->BETA+ALPHA, 1-->ALPHA, 1-->BETA and 2-->BETA, about 70% had S arrivals with a SNR large enough that either SV or SH could be picked. Examples of S onsets will be given in the next chapter.

The quality of S waves on segment GAMMA is far inferior to that on ALPHA and BETA, and it seems that a relatively complex structure beneath GAMMA (Bamford et al. 1978) may be responsible. It is difficult to separate effects of the source from effects of velocity structure on the amplitude of crustal shear waves, but it seems that S waves are easily attenuated when propagating through a structure with many velocity discontinuities. This could explain why shot point 2 (Fig. 2.1 and 2.3(b)) produced the best SNR for S waves when observed to the north (BETA), but no S waves when observed to the south (GAMMA). In fact two shots were fired at shot point 2 : shot 21 being observed to the south and shot 22 to the north. Identical shot patterns were used in both cases and the two shots 21 and 22 produced identical records on all LOWNET stations with P and S waves having exactly the same amplitude and waveform, as shown in Fig. 2.3(a). This implies that differences between 21-->GAMMA and 22-->BETA are due to propagation effects rather than source variations. The P waves of 21-->GAMMA at distances greater than 20 Km are very different from those of 22-->BETA, being more "emergent" with energy of first arrivals spread over many cycles (Fig. 2.3(b)). This is a good indication of a complex velocity structure in GAMMA which could also lead to higher attenuation of S waves by scattering or conversion. In addition the reverberation, following the P arrivals, which forms the background noise for the S waves, has greater amplitude (by a factor of 2) in 21-->GAMMA than in 22-->BETA, which would make the S waves even less identifiable in the segment GAMMA.

Similarly a single shot (E2) at E produced reasonably clear S waves to

the north (in the Midland Valley and on ALPHA) to distances of 90 Km whereas to the south the S waves are very poor, perhaps because of complex structure at, and south of, the Southern Uplands Fault.

Absence of clear Moho reflections on both BETA and GAMMA, on the other hand, are very likely due to the anomalous Moho transition identified by Bamford et al. (1978).

No shear refractions from the upper mantle (conventionally called Sn) were detected on any of the crustal profiles. This is probably because the expected amplitude of the Sn head-wave is much smaller than the background noise generated by the preceding P waves.

2.2 AMPLITUDE

Amplitudes of the S phase 'a_o' from shot 22-->BETA were plotted so as to examine amplitude relations between the 3 components. The seismograms were smoothed and the maximum peak-to-trough amplitude in μ/s of each component was measured. The maximum peak-to-trough amplitude during 1 s just before the S onset was taken as the background noise. Results are plotted in Fig. 2.4. There is a large scatter in the amplitude data (due to uncertainties in calibration, station site effects, seismometer planting, etc.) so it was smoothed with Hanning coefficients [$y_n=(y_{n-1}+2y_n + y_{n+1})/4$]. Fig. 2.4 shows that all three components have about the same amplitude. Between 20 and 40 Km the transverse component (T), and between 40 and 80 Km the vertical component (Z), has the best SNR.

Amplitude data for shot 12-->ALPHA is shown in Fig. 2.5. Again there is not a marked difference in amplitudes between the 3 components for the 'a_o' refraction, with the transverse only slightly better than the other two. For phase 'c' on the other hand the vertical component has amplitudes smaller than the two horizontals by a factor of about 2, with no significant difference between the two horizontals.

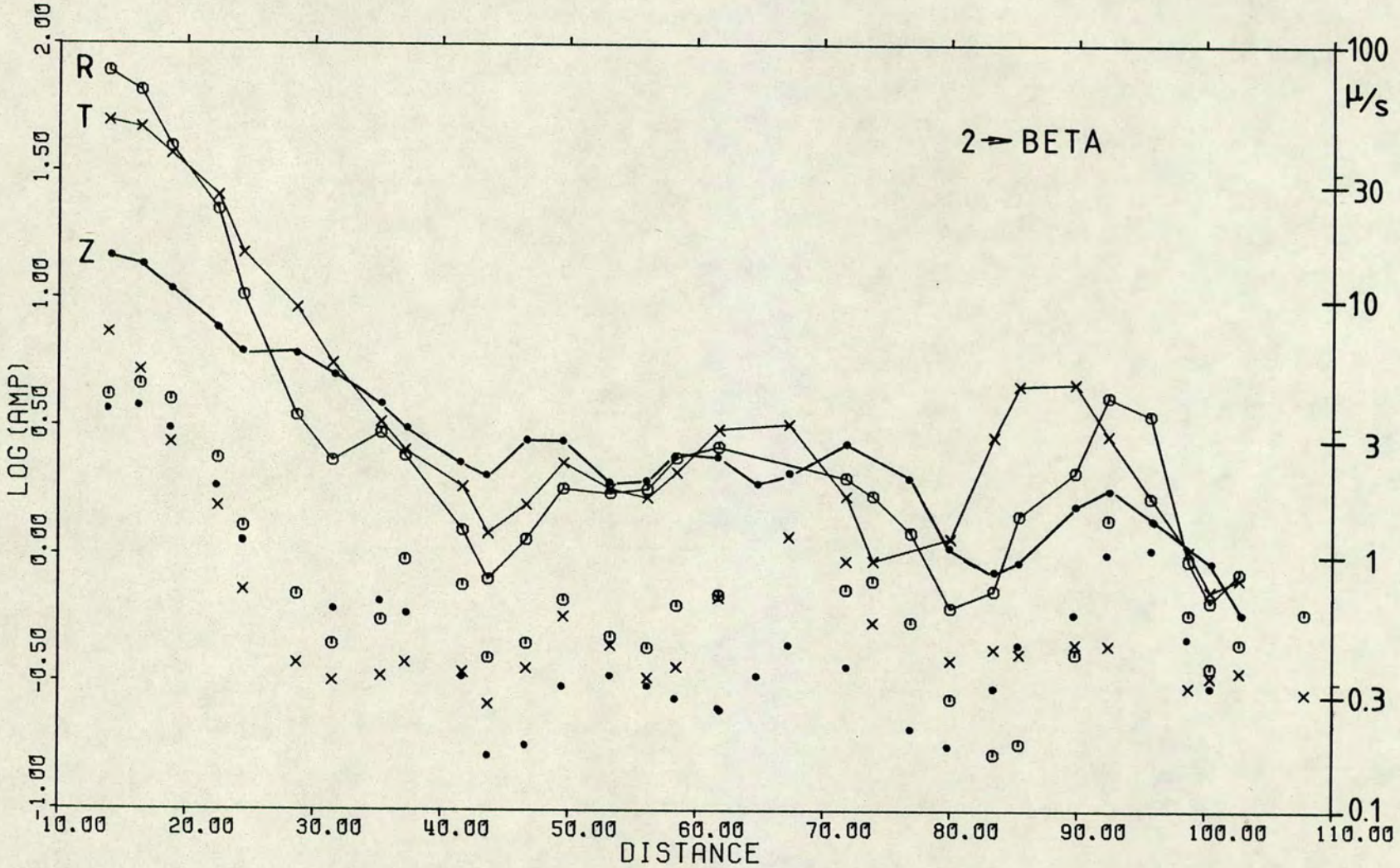

Fig. 2.4 Peak-to-peak amplitude of S phase 'a_o' (2→BETA). R,T,Z are radial, transverse and vertical components. Continuous line = signal, points = background noise.

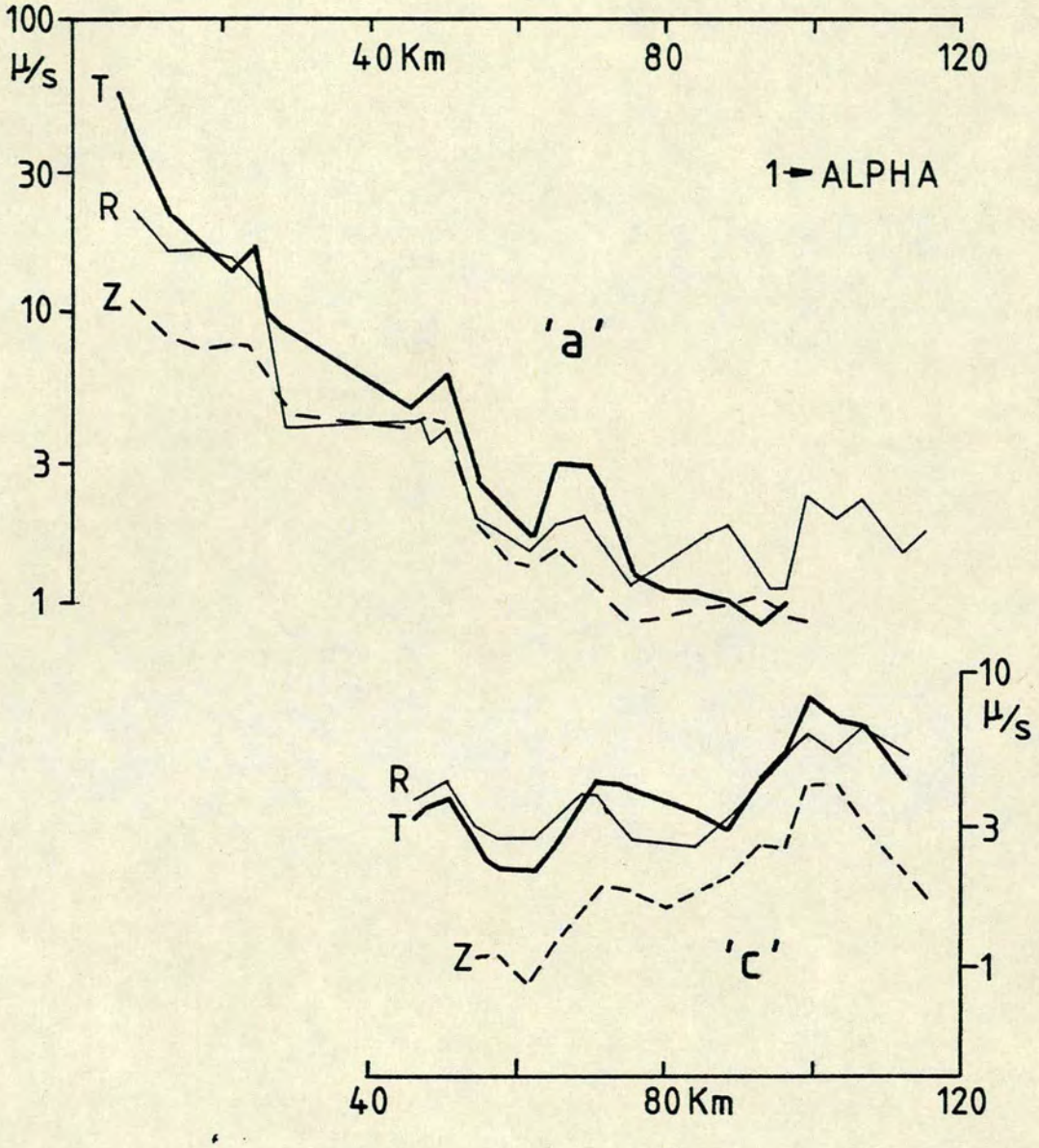

Fig. 2.5 Peak-to-peak amplitude of S phases 'a' and 'c' from 1→ ALPHA.

Sea shot-points N2 and N1 in many cases also show lower amplitude on the vertical component for the S Moho reflection 'c', but no significant difference between the two horizontals. Lower amplitudes in the vertical component of 'c' phases could probably be accounted for by their steeper angles of incidence.

In conclusion it can be said that there is at least as much S energy in the horizontal transverse components as in the horizontal radial components. This means either 1) that as much SH as SV is generated by the explosive source, or 2) that the crust, far from being horizontally homogeneous in the scale of about 1 Km, does not allow complete decoupling of SH from SV, that is to say, the polarization angle of S waves could change dramatically as they refract through highly heterogeneous material. Velocity anisotropy in the crust (due to orientated cracks or bandings) could also be an explanation for the appearance of SH.

No attempt was made at distinguishing between these explanations as probably all of them contribute to the complexity of the S waves in the seismograms.

2.3 FREQUENCY

Some spectral analyses were performed for S and P waves of shot-point 1 and optimum depth sea shot-point N2 with the aim of comparing the main frequencies of P and S waves. The spectra of P and S signals will of course depend on reverberations in the near surface structure at the stations but such effects should be partly averaged out if several stations are used.

Choice of stations was restricted to those with reasonable S and P signals on the same component. For this reason only vertical components were used. No corrections for instrumental response were made as they are all supposed to be flat above 2Hz, i.e. for all frequencies of interest.

2.3.1 Land shot 12

This shot consisted of a total charge of 1.37 ton spread in six boreholes 46 m deep and 30 m apart. Data lengths of 1 s were used for P and S first arrivals (phase 'a_o'). Fig. 2.6 shows some results, the shaded peaks denoting the main frequency of the signal. Peaks of higher frequency are probably due to signal-generated noise (scattered waves) and reverberations near the stations. Table 2.2 shows the results for land shot 12. The average frequency of P waves is about 7.9 Hz and that of S waves about 5.2 Hz (excluding values in parenthesis), which gives a ratio of 7.9/5.2 = 1.5 +/-0.3 .

Table 2.2 Main P and S frequencies of shot 12-->ALPHA.

Station	Dist. (km)	P freq. (Hz)	S freq. (Hz)
A48	47.3	(5.8)*	4.3
A47	50.9	7.6	(8.6)*
A46	54.4	8.0	5.2
A45	57.6	8.0	6.4
A43	65.4	8.8	6.2
A42	69.4	7.0	4.6
A41	71.2	8.2	4.3
Average freq.		7.9	5.2

* Not used to calculate average.

2.3.2 Sea shots N21 and N22

The shots N21 and N22 consisted of 1.2 tons of explosive dispersed in 6 equal parts of 0.2 ton and detonated at an optimum depth (for the 0.2 ton charge) of 95 m in water 115 m deep. Three stations were analysed for the phase 'a_1' and three for phase 'c'. Record lengths of 2.4 s for 'a_1' and 2.0 s for 'c' were used. Table 2.3 shows the results. In spite of the low signal to noise ratio of the S 'a_1' phase it can be seen that P and S waves from shot-point N2 have the same main frequency. The theoretical bubble pulse frequency of a 0.2 ton charge at a depth of 95 m is 3.9 Hz (e.g. Wielandt 1975). The observed 3.2 Hz is a result of the frequency filter produced by the reverberations in the 115 m of water (O'Brien 1967b, Faber 1978).

Table 2.3 Main P and S frequencies of N2-->ALPHA

Station	Dist. (Km)	P freq. (Hz)	S freq. (Hz)
phase 'a_1'			
A00	80.1	3.1	2.7
A01	81.6	3.1	3.0
A05	94.6	3.2	3.1
phase 'c'			
A00	80.1	3.1	3.2
A01	81.6	3.2	3.1
A06	99.5	3.3	3.3
Average freq.		3.2	3.1

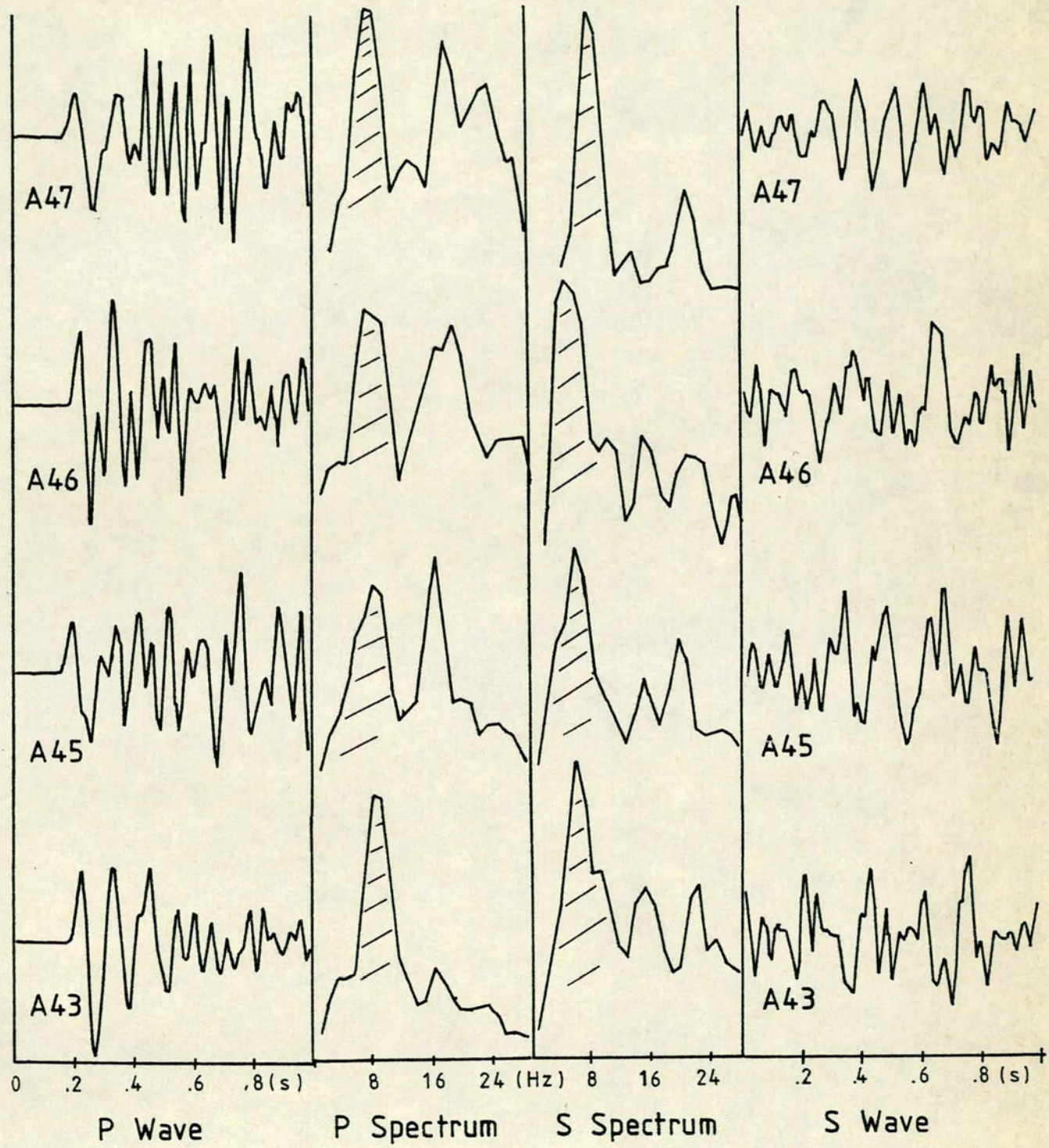

Fig. 2.6 Spectra of phase 'a_o' from land shot 12. Stippled peaks indicate 'main' frequencies. Arbitrary vertical scales.

2.3.3 Discussion

The contrast in the P to S frequency ratios for land and sea shots can be very qualitatively and simplistically explained as follows. The radiation of seismic waves in land shots is partly controled by the size of the cavity produced in the rock so that the emitted P and S wavelengths will be about the same (O'Brien 1967a). In this case the predominant frequency of P waves will be higher than S and the ratio should approach the Vp/Vs ratio at the source which is usually around 1.7 - 2.0 (i.e. σ = 0.25 - 0.33). In optimum depth shots the S waves are probably generated by conversions from P waves at the bottom (either water/sediment or sediment/basement interface). The predominant frequency in optimum depth shots is not determined by the duration of the initial shock wave, but by the "pressing" of the sea bottom by the successive pressure waves from the bubble oscillations enhanced by the water reverberation. The period of P and S waves will then be equal to the period of these oscillations (in a way similar to forced vibrations).

These qualitative results are further illustrated by shot-point E (Firth of Forth: single charge of 0.6 ton, depth of 24m in 34m deep water) The bubble of gases from the explosion would not oscillate as in the case of optimum depth shots because of interference of the sea bottom, Wielandt 1975 (the theoretical maximum bubble radius was about 10m). In this case it is not unreasonble to expect that the main frequencies radiated would be partly controlled by the size of the bottom area unelastically affected. No spectral analysis were made but rough estimates of predominant frequencies are: P about 6 to 8 Hz, S about 3 to 5 Hz, which would give a ratio of 1.5 to 2.0, more in agreement with land shots than optimum depth sea shots.

CHAPTER 3

DETERMINATION OF ONSETS

3.1 P WAVES

P wave first arrivals in LISPB are usually very clear as the experiment produced on the whole good quality records. The quality of secondary arrivals, on the other hand, varies a lot and seems to depend to some extent on the crustal structure itself. For example, a sharply defined Moho usually produces clear high amplitude 'c' reflections (Braile & Smith 1975), so that the absence of a clear 'c' phase has been interpreted (Bamford et al.1978) as evidence of gradational Moho.

The P wave secondary arrivals used in the determination of Poisson's ratio (Chapter 4) were: wide angle reflections from the Moho ('c') observed from shot-points N2, N1, 1 and E, and the wide angle reflection from the lower crust (phase 'e') from N2, all on profile ALPHA. This last reflection (N2-->ALPHA) was very clear and its P arrivals were picked with an estimated uncertainty of +/-.05 s by simple visual examination. Afterwards these arrivals were checked with particle-motion plots and general agreement was found. For the other reflections ('c') the onsets were picked as explained below.

3.1.1 Correlation and sum of seismograms - CORSUM

For the phases 'c' from N2, N1 and E (but not from 1 as explained later), a processing consisting of correlation and sum of seismograms (here called CORSUM) was employed, so that P onsets could be picked on the summed seismogram with better SNR than the individual records. This process assumes that the signal does not change its shape in the range of stations used. For this reason only stations beyond the critical distance were used

to avoid the rapid changes in phase occurring around the critical reflection (Richards 1961) and interference with the Pn head wave (Cerverny 1961; Cerverny & Hron 1961). Also stations near the cross-over between phases 'c' and 'e' were avoided because of interference problems. Another obvious criterion is that the stations should have approximately similar waveforms, that is, it should be possible to follow peaks and troughs across the seismic section. In this way only a small range of distances was available: 20 Km for N2 with 6 stations, 15 Km for N1 with 5 stations and 12 Km for E with 6 stations. In actual fact one should expect a small phase change in the signal across such distances. Nevertheless estimates of phase changes based on geometrical seismics (Richards 1961) and also finite frequency calculations (Cerverny & Hron 1961) show that errors in travel time should be around +/- 0.02 s if such phase changes are ignored. Synthetic seismograms were calculated confirming that phase shifts are of the order of +/- 0.02 s. As these errors are smaller than the final error in the 'c' onsets (around +/- 0.05) such phase changes were ignored and perfect coherence in the signal was assumed. In addition the periods of the P waves are long enough (about 3 Hz for N2 and N1, and 7 Hz for E) that differences between phase correlation and group correlation (Giese 1976) can probably be neglected, i.e., the fine structure of the lower crust should not affect the signal shape very much.

The CORSUM procedure was as follows: a window containing the first few cycles of the signal was used for correlations. One record was chosen as reference and all others were cross-correlated with it for various time-shifts. In this way the signal delay between the various stations was determined. The seismograms were then summed after shifting with the appropriate delay. This sum with improved SNR was then used as the reference record and the process was repeated to find better values for the delays. Two iterations were sufficient for convergence. In the summation

each record was weighted with the square of its SNR so that the sum would be likely to have the best SNR. Sometimes the SNR itself, instead of its square, was tried as weight in an attempt to get slightly better SNR in the sum.

Seismograms that could not be used in CORSUM had their onsets picked by "visual examination" using the normal criteria of change in amplitude and frequency whilst also taking into account the approximate expected wave form of the signal.

3.1.2 Results

Fig. 3.1 to 3.3 show the 'c' waves from N2, N1 and E . Figs.(a) show which stations were used in CORSUM as well as the sum of the vertical (and radial components if not noisy or oversaturated) and Figs.(b) show record sections with a line drawn through the picked onsets. For N2, Fig. 3.1(a), smoothing of the records was necessary to increase the signal coherence across the stations. In Fig. 3.1(b) and 3.2(b) some seismograms are offset to make the first arrivals ('a_1' for N2, 'a_0' for N1) lie on a straight line - this facilitates the correlation of peaks and troughs of the 'c' signal in the seismic section.

Land shot 12-->ALPHA was not suitable for CORSUM because of the high frequency of the 'c' waves, around 10 Hz , which made the signal lose coherence from one station to another. Fig. 3.4 shows a seismic section of smoothed vertical components with a line through the 'c' picks. Profiles 1, E and 2-->BETA did not have good P 'c' arrivals (nor good S 'c') probably due to gradational Moho (Bamford et al. 1978).

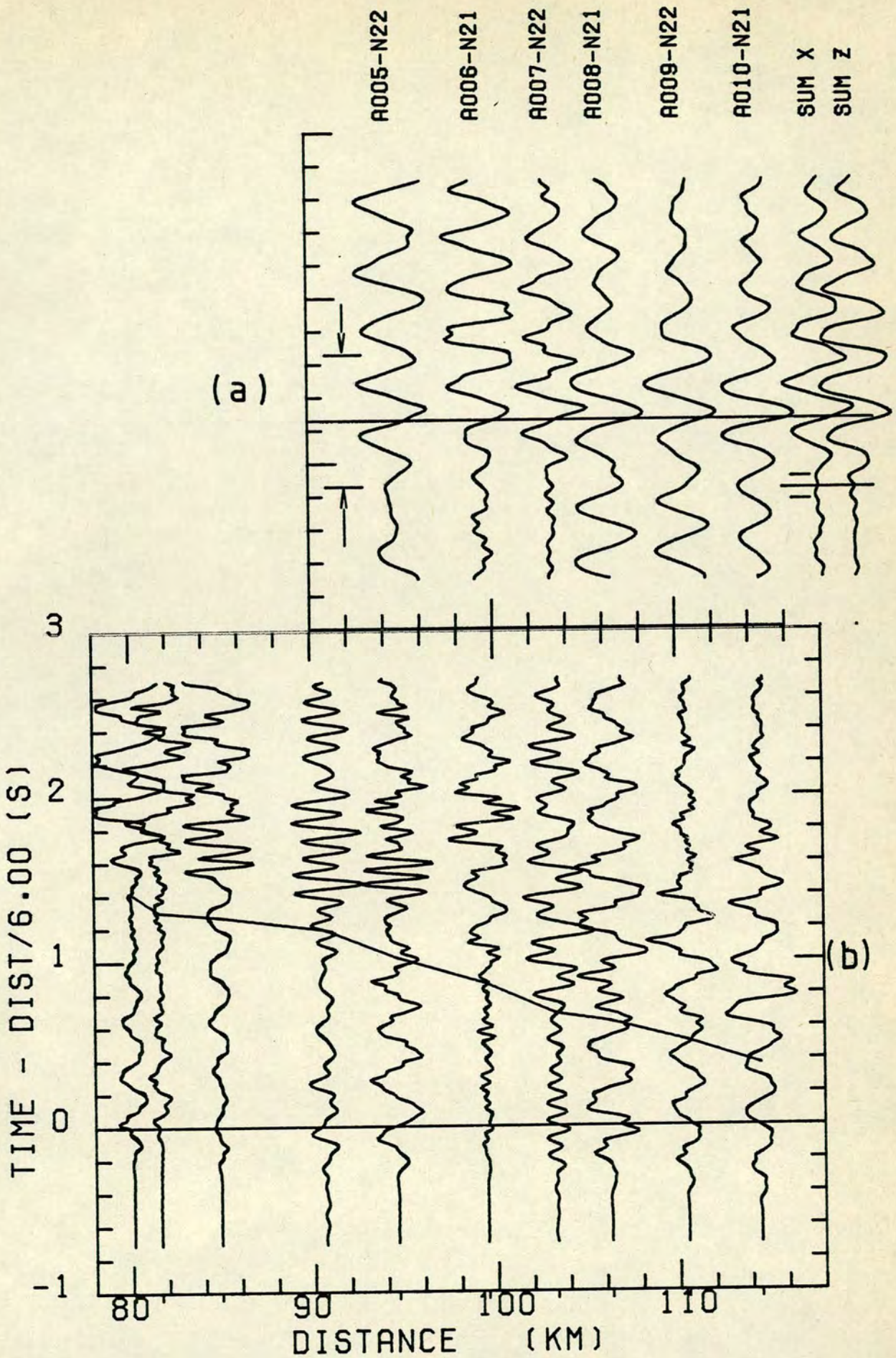

Fig. 3.1 N2→ ALPHA, P, 'c'. (a) aligned records (radial) used for summation; SUM X = sum of radials, SUM Z = sum of verticals; arrows indicate correlation window. (b) record section of vertical component with line joining the picked onsets.

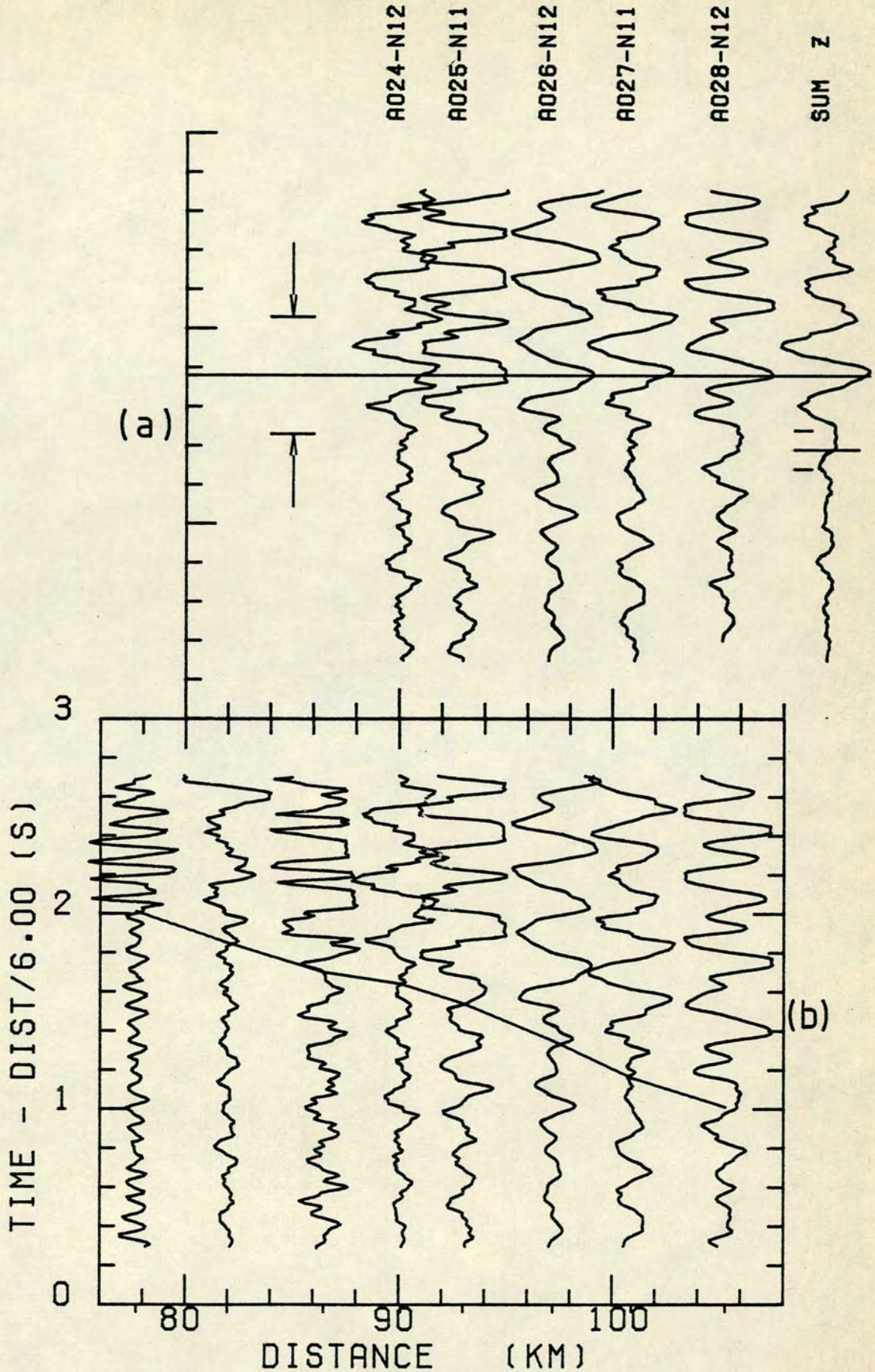

Fig. 3.2 N1→ ALPHA, P, 'c'. (a) aligned vertical records.
(b) seismic section of vertical comp. with joined picks.

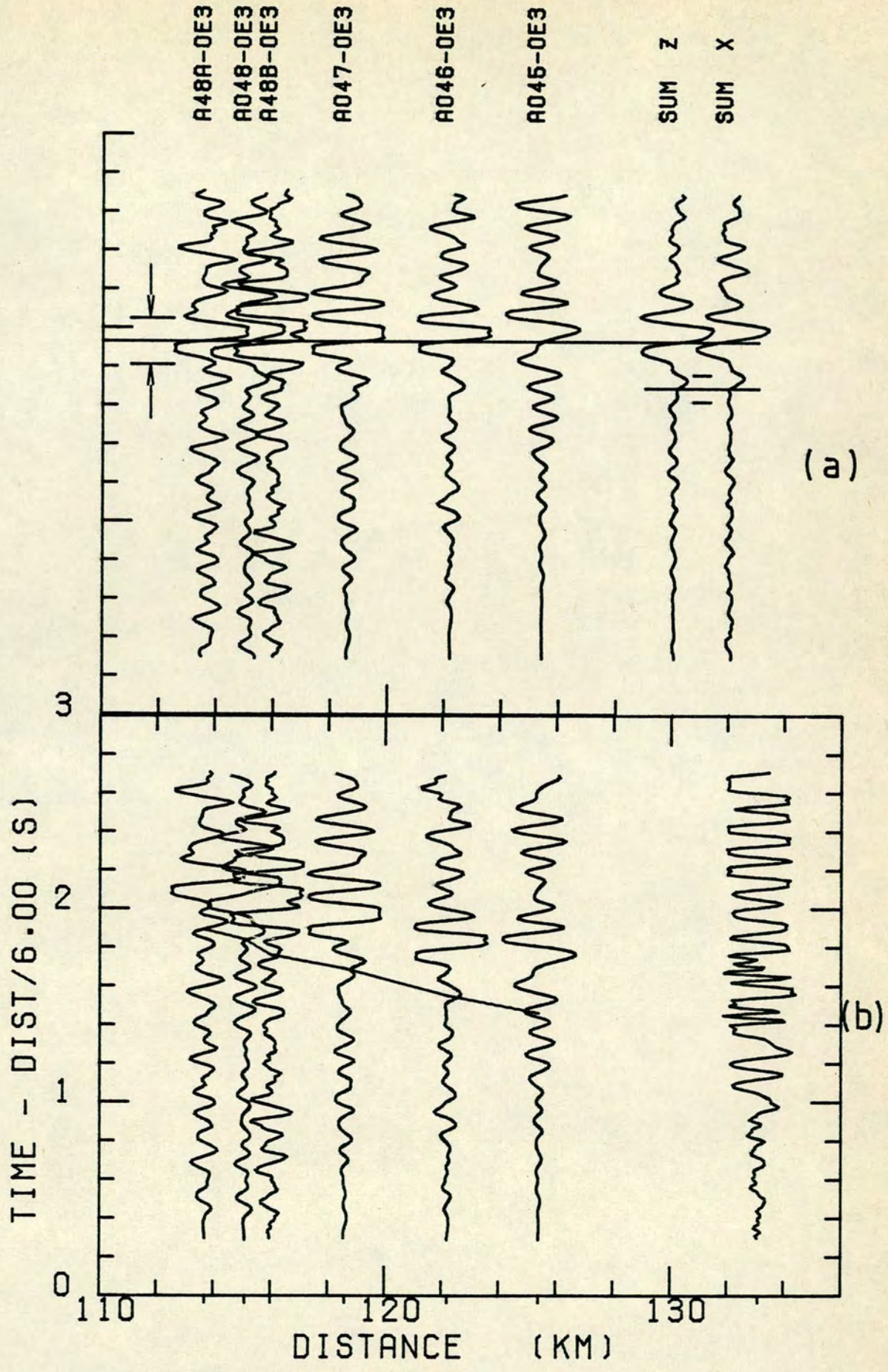

Fig. 3.3 E→ALPHA, P, 'c'. (a) aligned vertical records. (b) seismic section of vertical components.

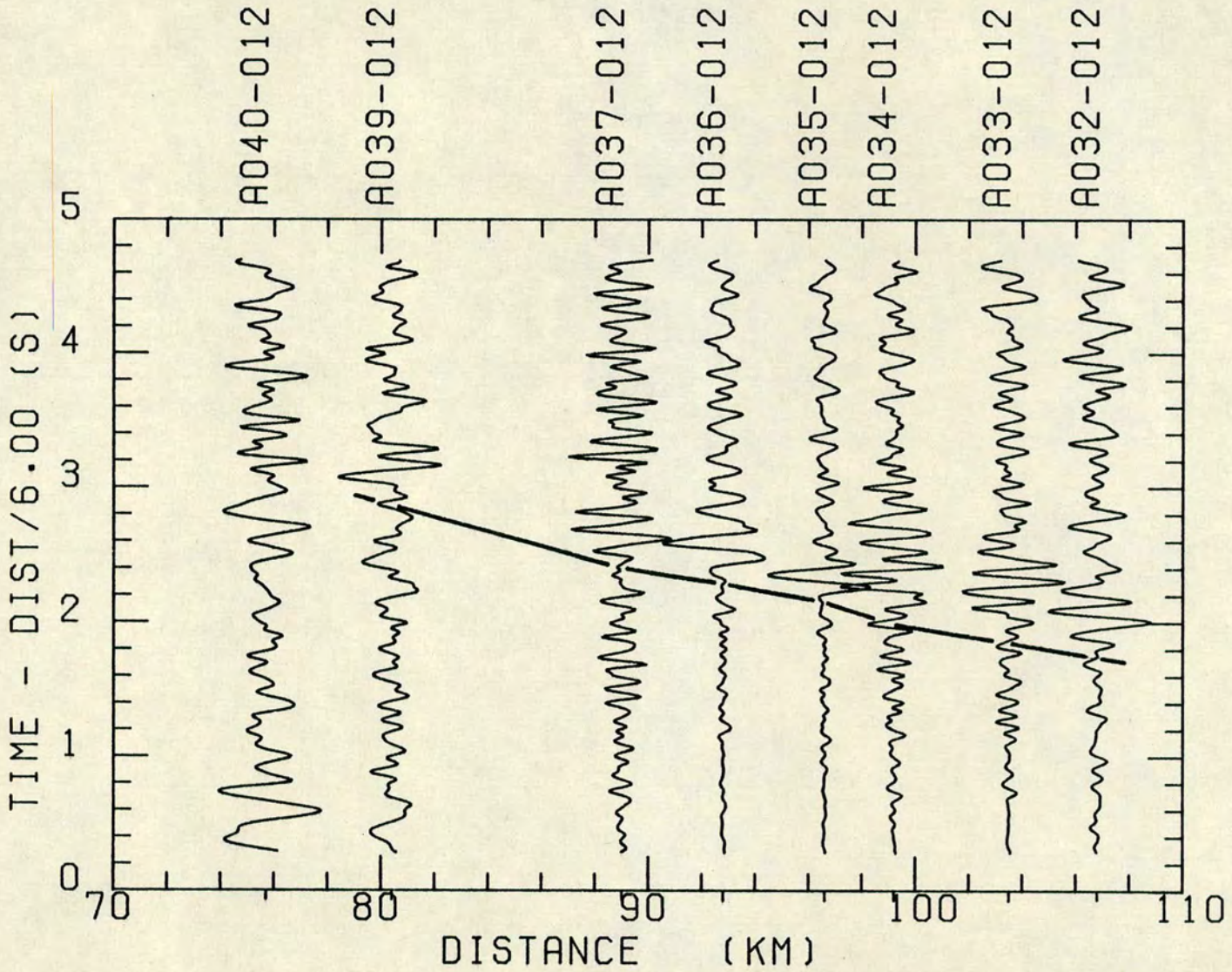

Fig. 3.4 1→ ALPHA, P, 'c'. Seismic section of vertical components (smoothed) with line joining picked onsets.

3.2 S WAVES

Determination of shear wave arrivals is a major difficulty in refraction work and is the main reason why relatively little use is made of S waves in crustal investigations. This is so mainly because S waves are secondary arrivals and will always have a background of noise generated by the P waves, and because of P precursors (S converted to P near the stations) which obscure the true S onset.

In this work the initial identification of S phases was made based on travel times using the P correlations as a reference and assuming average Poisson's ratio around 0.25 . Two methods were then tried to determine S onsets: multiplication of radial and vertical components and analysis of particle-motion diagrams.

3.2.1 R*Z product and particle-motion plots

Multiplication of the radial horizontal (R) and vertical (Z) components has been used sometimes to help identify S onsets (e.g. Sutton & Pomeroy 1963; Griffiths et al. 1971) and is based on the principle that P and SV waves should have opposite polarities. It seems at first an attractive technique to be used in large seismic sections because of its simplicity, as compared to detailed examination of the whole particle-motion which is very time consuming.

Fig. 3.5 shows one example of this method for the S Moho reflection (phase 'c') from N2. Only those stations with good records were used (i.e., not oversaturated, no high frequency noise or electronic problems) and smoothing was applied before multiplication. In the record section of Fig. 3.5 some seismograms were offset to align the first arrival ('a_1') and make the 'c' arrivals more easily identifiable in the record section. The offsets for the S waves were those of the P multiplied by $\sqrt{3}$.

It can be seen that whereas the P product has a constant positive

polarity that of the S waves is very variable and can oscillate as in the case of stations A08 , A09 and A10. This indicates that the S particle-motion for those stations is not linear, i.e., about at right angles to the P but is elliptical with a phase difference between radial and vertical components of around 90^{o} instead of 180^{o} .

Particle motion diagrams of S 'c' phase for these three stations are plotted in Fig. 3.6 and show elliptical prograde motion. In those diagrams the two horizontal components were rotated to realign the R component along the actual direction of arrival. (It is assumed that the true direction of arrival of the S waves is approximately the same as that of the P waves (say, less than 10^{o} difference) so that the actual radial and transverse components of S can be determined using the observed azimuth of the P waves).

Further examples of R*Z products are shown in Fig. 3.7 for the phase 'a_o' of shot 22-->BETA. Offsets were also applied to the record section as before. Fig. 3.8 shows the particle-motion plots for some of the stations, and it is seen that non-linear motion is also present, for example stations B50 (31.5 Km) and B34 (80 Km).

3.2.2 Theoretical results for a homogeneous half-space

It is known theoretically that the S wave ground motion in a homogeneous half-space is not always linear but can be elliptical for shallow angles of emergence (e) at the surface (e.g. Nuttli 1961, Meissner 1965). For example, SV is elliptical with 90^{o}phase difference between R and Z for emergence angles, e, (measured from the horizontal) less than $e=54.7^{o}$ or 57.7^{o} for Poisson's ratios 0.25 or 0.30 respectively. The motion is retrograde for e between this critical angle and 45^{o},and prograde for $e<45^{o}$. This result is not basically different if a thin low velocity layer is present at the surface (Haskell 1962).

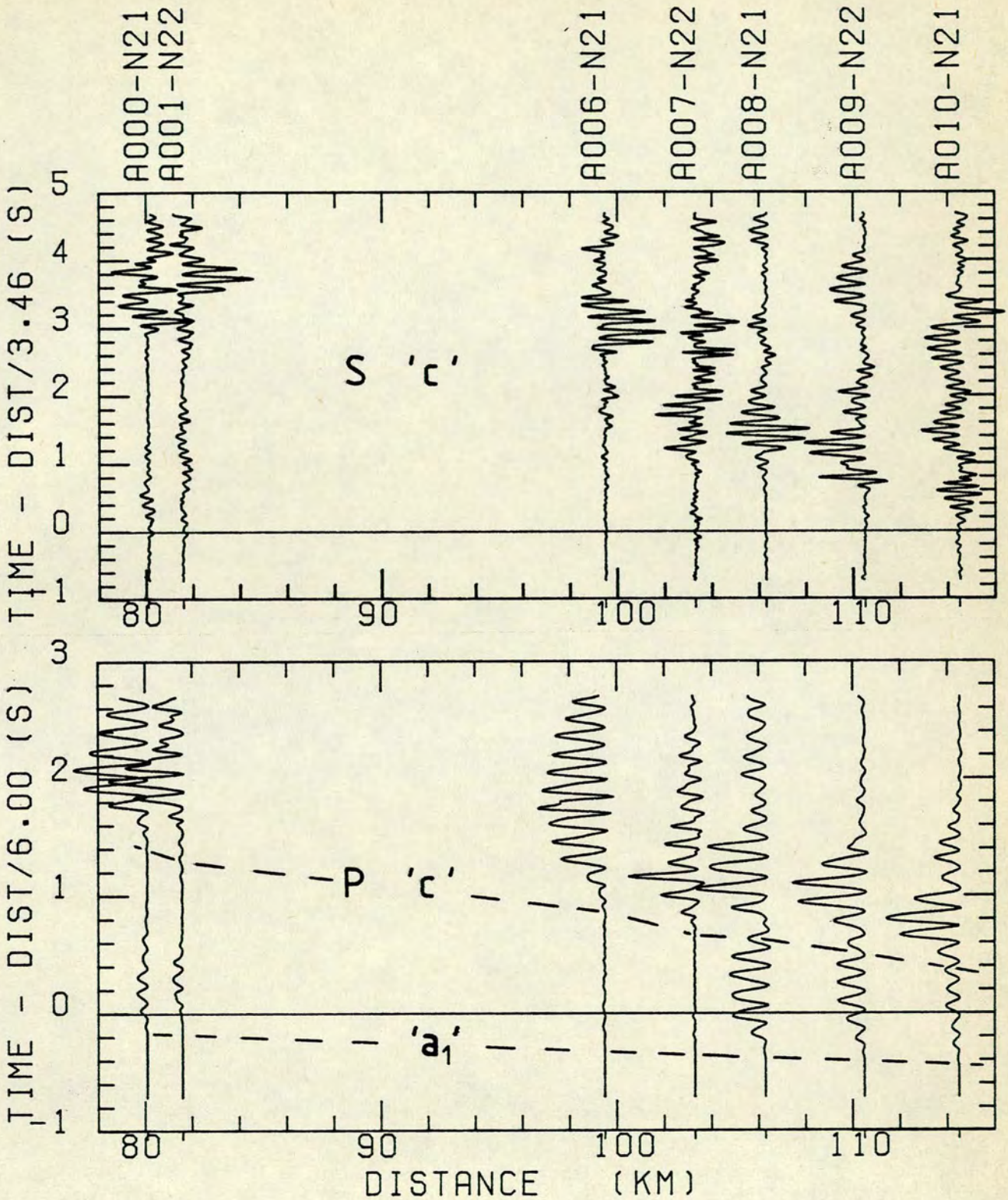

Fig. 3.5 N2→ ALPHA, 'c'. Product of radial and vertical.

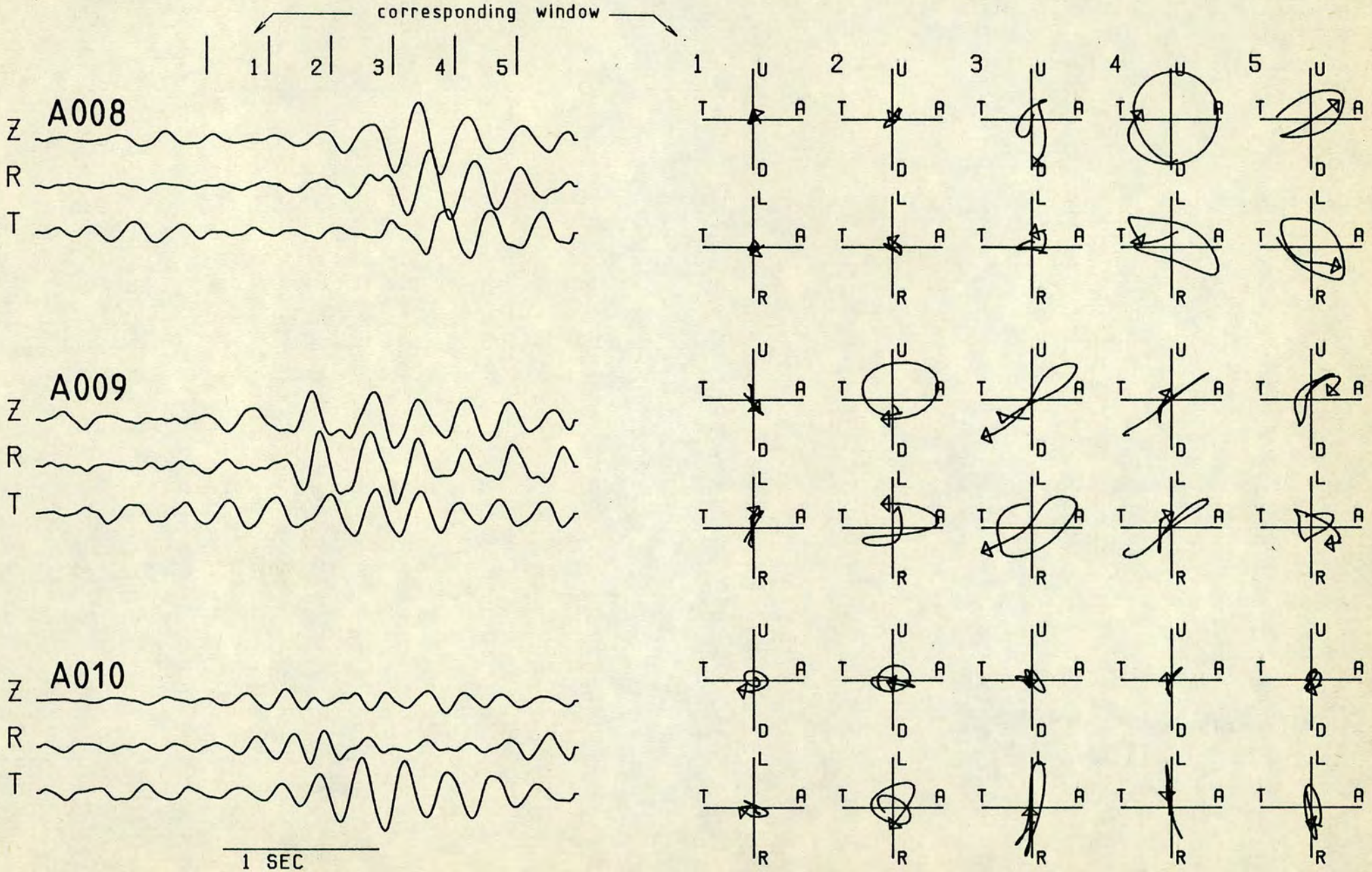

FIG. 3.6 N2-ALPHA S 'C'

U=Up ; Down ; Away from, Towards the shot ; Left ; Right .

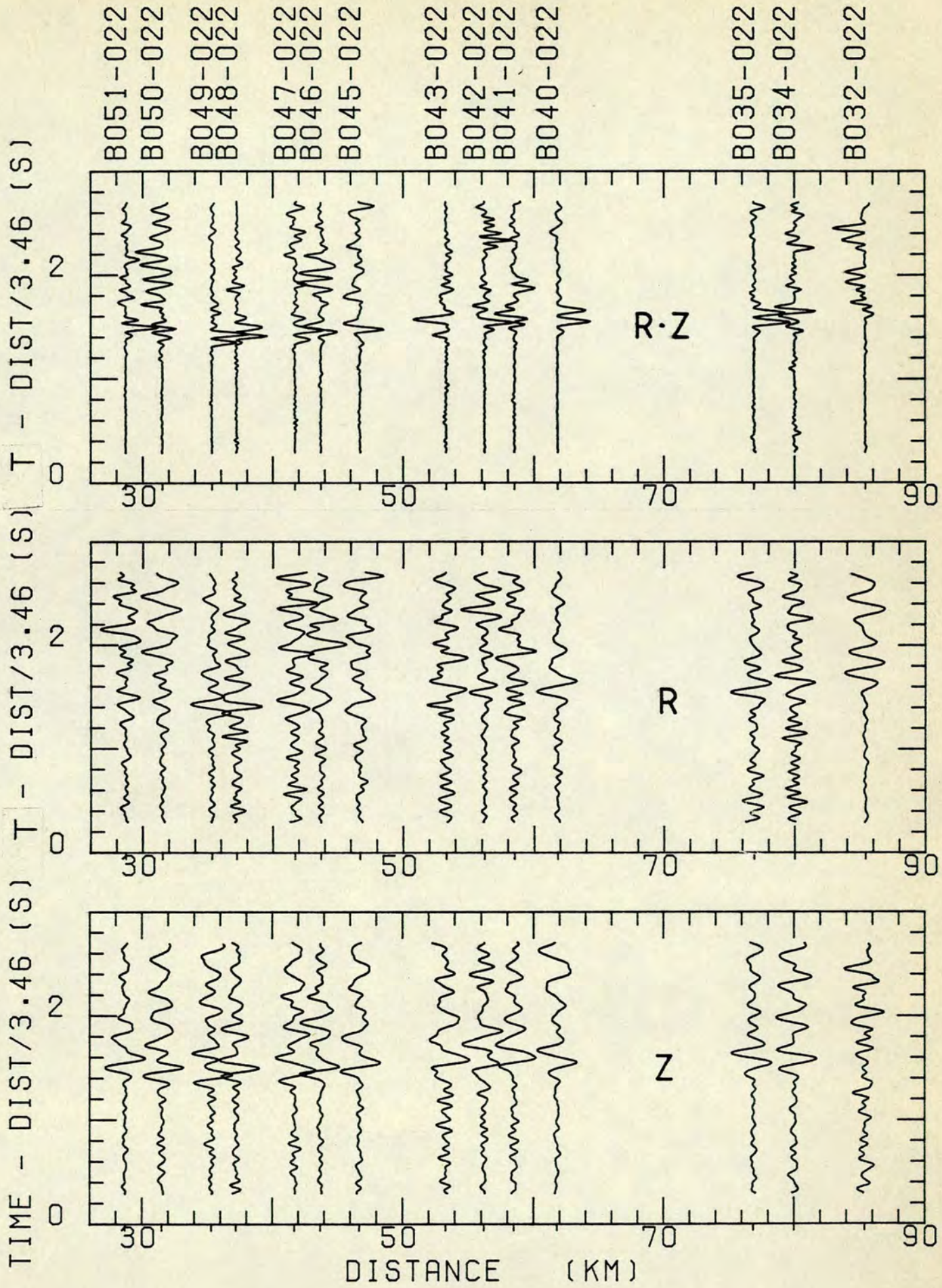

Fig. 3.7 2→BETA, S, 'a_o'. Radial (R) and vertical (Z) are smoothed.

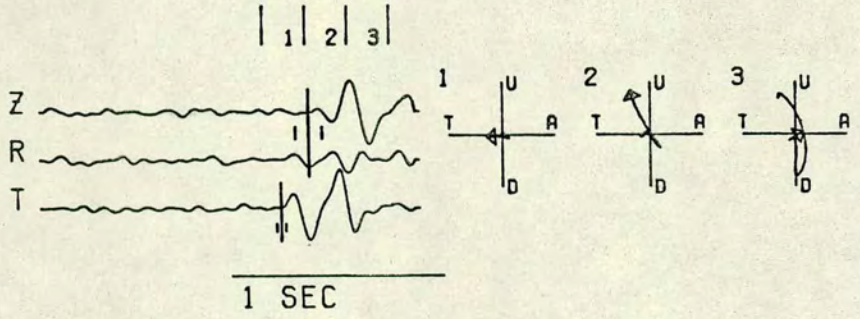

2-B51 SG 28.7KM

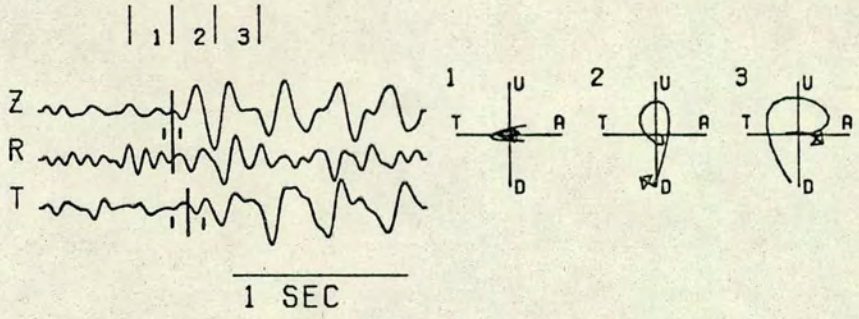

2-B34 SG 80.0KM

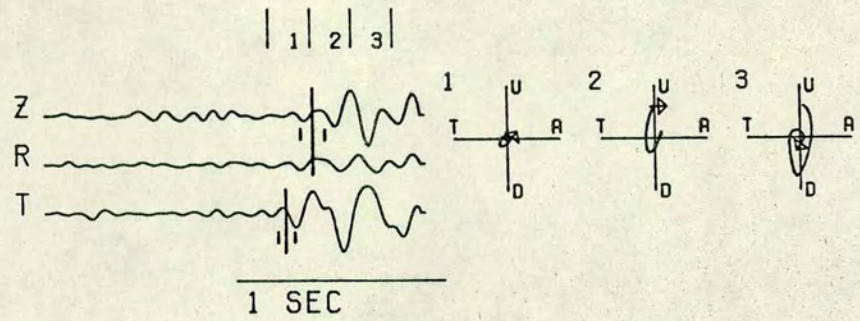

2-B50 SG 31.5KM

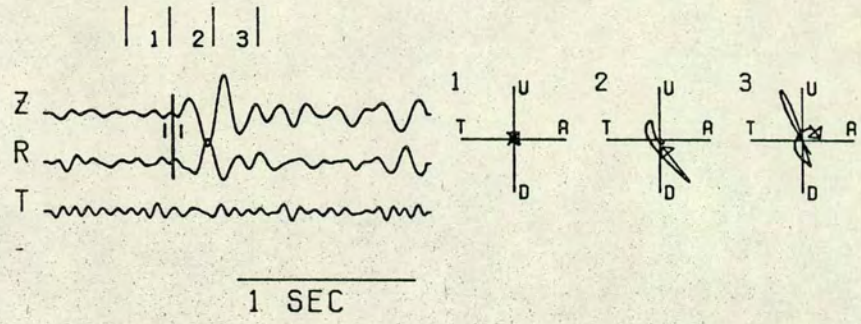

2-B35 SG 76.9KM

Fig. 3.8 2→ BETA, 'a_o'

It is very important then to know the emergence angle of the various crustal phases before proper use is made of the R*Z product. However this is extremely difficult because the effective angle of emergence of the S waves (wavelengths <1 Km) will depend on the velocities in the top 1 Km of the crust which may vary enormously from station to station. For example, the phase 'c' at a distance of 80 Km, for a 3-layered crust (P vel. = 6.0, 6.4, 7.0 and PR=0.25) has e=42° and prograde motion should be expected. But if the top 1 Km of the crust beneath the station had a P velocity of 4.5 Km/s (and PR = 0.25) instead of 6.0 Km/s, e=56° and linear motion would be expected. The fact that near the surface the velocity structure is far from a stack of horizontal homogeneous layers complicates things even further.

Thus it is clear that although the R*Z product may be used to determine roughly where the whole S wave train is in the seismogram, it cannot be relied upon to pick the very onset of any S phase with an accuracy better than a few periods of the S signal.

Quite often the ground motion of the S waves is even more complicated than the examples shown in Figs. 3.6 and 3.8. The character of the SV and SH ground motion sometimes changes completely between adjacent stations indicating that it is strongly affected by the near surface structure (1 or 2 Km beneath the station) as was also found by O'Brien (1967c). For this reason no special processing could be applied to pick or enhance the S waves such as polarization filters (e.g. Montalbetti & Kanasewich 1970) or CORSUM, where the same kind of ground motion would have to be assumed for all stations.

A rough attempt was made to correlate the kind of ground motion (whether linear or elliptical) with the geology of the station (whether sedimentary or igneous). Table 3.1 lists those stations for which the SV particle-motion was clearly linear or clearly elliptical. It seems there is a slight tendency for linear motion to occur in stations overlying

sedimentary rocks (lower velocity) and elliptical motion to occur on igneous or metamorphic rocks (higher velocity). This is to be expected on the basis that lower velocity near the surface implies steeper angles of emergence which tend to give linear ground motion. Nevertheless, this relationship is not very clear, as shown by Table 3.1, probably because the geology (and consequently the velocity structure) can be very complex near the surface so that conclusions from horizontal plane layer models are not always applicable.

Table 3.1 Geology of stations showing clear particle-motion

	Shot-Station	Phase	geological formation(*)	
linear	N2 - A32	e	sedimentary	Old Red Sandstone(54)
	N2 - A34	e	sedimentary	O.R.S.(54)
	N1 - A26	c	sedimentary	O.R.S.(54)
	1 - B11	a_o	igneous	lava(23)
	1 - B1?	a_1	sedimentary	limestone(57)
	1 - A55	a_o	metamorphic	Dalradian(44)
	E - A45	c	metamorphic	Moine(31)
	2 - B49	a_o	sedimentary	Silurian(50)
	2 - B47	a_o	sedimentary	Silurian(50)
	2 - B40	a_o	sedimentary	Silurian(50)
	2 - B35	a_o	sedimentary	Ordovician(49)
prograde	N2 - A08	c	metamorphic	Moine(33)
	N2 - A09	c	metamorphic	Moine(33)
	N2 - A10	c	metamorphic	Moine(33)
	E - B13	a_o	igneous	lava(23)
	E - B12	a_o	igneous	lava(23)
	E - B02	a_1	metamorphic	Dalradian(44)
	E - A46	c	metamorphic	Moine(31)
	2 - B34	a_o	sedimentary	Ordovician(49)
retrog.	1 - B02	a_o	metamorphic	Dalradian(44)
	2 - B46	a_o	sedimentary	Silurian(50)
	2 - B45	a_o	sedimentary	Silurian(50)
	KEQ - A28	a_1	sedimentary	O.R.S.(54)

(*) Numbers refer to index in Geol. Map of G.Britain ("10 mile",1957)

3.2.3 Picking procedure

The following procedure was used to pick S waves using particle-motion diagrams.

A time window of a few seconds and including the suspected S arrival was selected for each station. The ground motion was plotted in the sagittal plane (R.Z) and in the horizontal plane (R.T). For this purpose the original records were filtered with a low-pass Hanning window (i.e. were smoothed) instead of a band-pass. This reduces the high frequency noise without diffusing the onsets with the "ringing" often caused by narrow band-pass filters.

An SV onset was picked from the vertical and radial components and an independent SH onset was picked from the transverse. Together with the usual criteria of change in amplitude and frequency any motion with a phase difference between R and Z ranging from 180° (linear motion) to +/- 90° (elliptical) was regarded as SV.

Some knowledge of the "impulsiveness" of the signal also helped when picking phases ("impulsiveness" here defined as the number of cycles between the onset and the maximum amplitude in the signal). For example land shots tend to be quite impulsive whereas optimum depth sea shots are more emergent with the highest amplitude in the third or fifth peak (counting troughs as peaks), Fig. 3.9 . Of course the signal shape will depend on the structure along the path, attenuation, response of the site and seismometer, etc., but as a first approximation it seems that P and S in explosions have the same "impulsiveness".

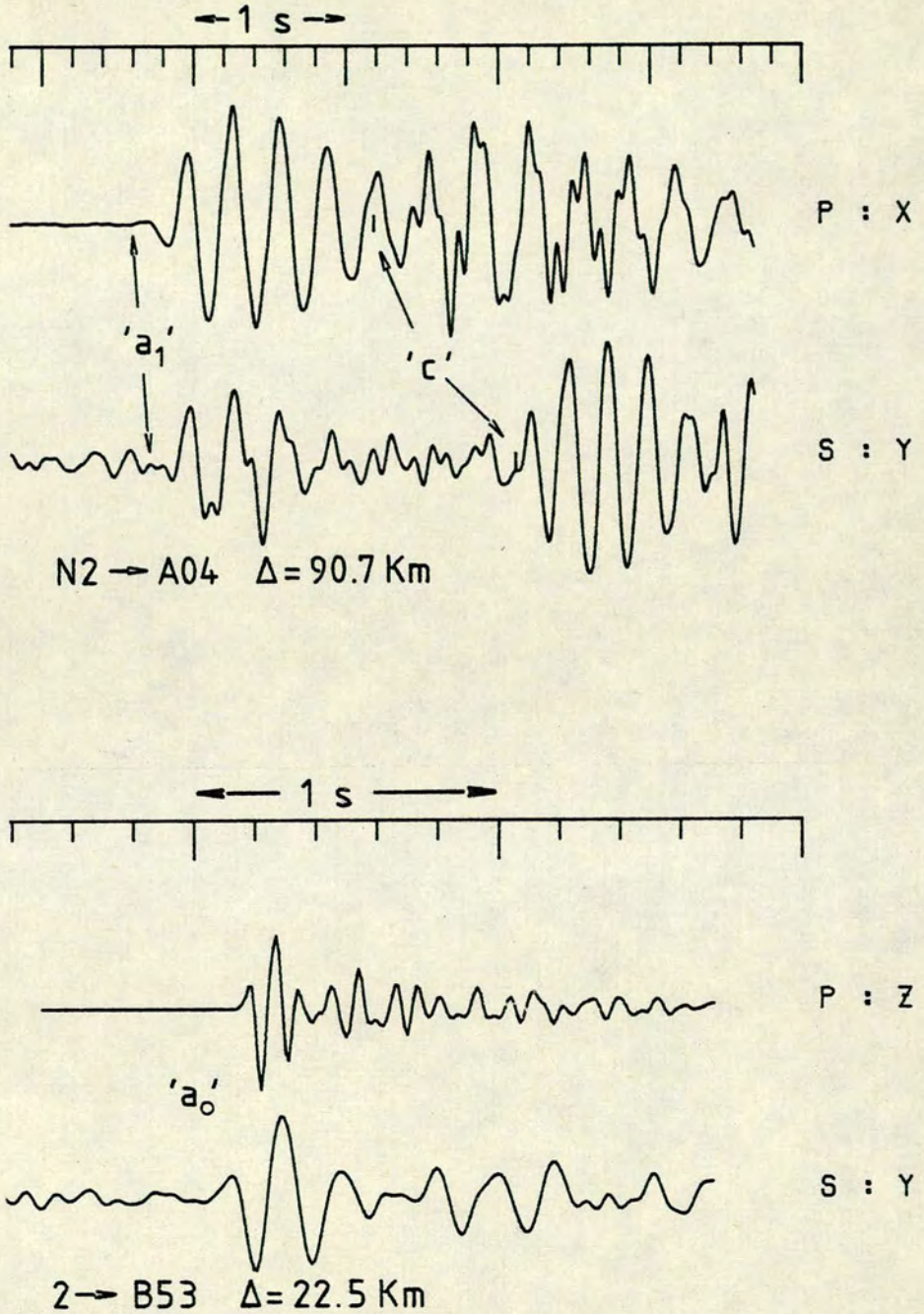

Fig. 3.9 Two examples of P and S signal with the same "impulsiveness". X, Y and Z are radial, transverse and vertical components.

3.3 CONCLUSION

No completely objective procedure was found to pick S onsets mainly because the S signal is very variable and depends to a large extent on the structure right beneath the station. The only alternative was careful examination of particle motion diagrams and assignment of an uncertainty to each pick depending mainly on the signal to noise ratio. P precursors were avoided by using particle-motion plots (as they would be for R*Z products too).

The uncertainties of the S onsets vary approximately from +/- T/4 (good SNR) to +/- T (poor SNR), where T is the main period of the signal. Thus land shot arrivals for upper crustal phases (e.g. Fig. 2.1) can have onsets determined with a precision of about +/- 0.05 to +/- 0.10 s whereas those from deeper penetrating arrivals from sea shots (e.g. Fig.2.2) can be determined to within +/- 0.1 to +/- 0.3 s. Stations with uncertainties greater than +/- 0.3 s were not used in the determination of Poisson's ratio.

Appendix B contains particle-motion diagrams (sagittal plane only for simplicity) of most of the S waves used in this study.

Subjectivity in picking S onsets was not completely eliminated, but it is believed that the uncertainties assigned to each pick are large enough to include the "true" S onset in most cases.

Appendix C lists all arrival times used to determine Poisson's ratios, as described in the following chapter.

CHAPTER 4

DETERMINATION OF POISSON'S RATIO

4.1 INTRODUCTION

It was not possible to use only the S wave data to get an independent model of crustal structure, especially depths of boundaries, because of the incompleteness of the S refraction data. For example shot-point N1 did not produce a clear S refraction in the upper crust (phase 'a_o') so that no measurement of S velocity or Poisson's ratio was possible for layer 1 north of the Great Glen Fault (see Fig 4.1 for shot positions and layer numbers). Also S sedimentary phases 'a_s' from 1, E and 2 are either very weak or very emergent so that no reliable direct measurement of S velocity in the near surface layers was possible. No S mantle refraction (phase 'd') was observed.

Analysis of the S wave data was made using the layered crustal structure as obtained from the P wave data and inserting S velocities, or more exactly Poisson's ratios, to fit the observed S travel times. Poisson's ratio was chosen as the parameter to be determined directly instead of S velocities because in this way the P velocities were automatically taken into account. The observed quantity used in the inversion was the ratio of S travel time (ts) to P travel time (tp). This has the advantage that scatter in travel times due to small lateral variations near the surface (e.g. thickness of superficial layer) is reduced in the ts/tp ratio because these heterogeneities tend to affect the S wave by an amount proportional to that of the P wave.

The crustal layers were divided into blocks with constant P (and S) velocity. The inversion then consisted of finding Poisson's ratio in each of these blocks (keeping the P velocities fixed) in order to fit the

observed ts/tp data. This was done in two stages: 1) an initial model was found in a detailed trial and error search, and 2) the initial model of Poisson's ratios was improved iteratively by a least-squares procedure. Theoretical travel times for the ts/tp ratios were calculated using average horizontal plane layer models with different layerings allowed under the shot-point and under each station.

The advantage of this method for calculating Poisson's ratios is that it is not critically dependent on the P velocities. Thus P velocities could be wrong by +/- 0.1 Km/s without affecting the theoretical ts/tp values at all. In this way Poisson's ratios can be determined, particularly in the upper crust, with greater accuracy than by simply calculating P and S velocities independently and forming the ratio of the two.

However two assumptions have been made in order to determine Poisson's ratio structure. These are:

(i) That the Poisson's ratio, as a first approximation, is constant with depth within each crustal block. This means that the PR value determined by a refraction which travels in the uppermost part of the refractor layer can be used as representative of the whole layer. For layer 1 under the Midland Valley (between shot points 1 and E) this is a reasonable assumption as PR is only slightly affected by changes in confining pressure and temperature for depths grater than about 4Km. For a change in confining pressure from about 1 Kb (depth around 4 Km), PR usually increases by less than 0.005 (Simmons 1964; Christensen 1965, 1966). An increase in PR of 0.005 from the top to the bottom of layer 1 would produce an increase in ts/tp for refractions in layer 2 of only 0.001 (in terms of Poisson's ratio) at distances around 50 Km . Temperature has little effect on PR and a temperature difference of the order of 50°C between depths of 4 and 8 Km would produce a change in PR of less than 0.001 (Birch 1969, Fielitz 1976). These values are much less than the measurement errors due to travel time

inaccuracies. On the other hand, between the Great Glen Fault and shot point 1, Fig. 4.1, PR may not be constant throughout the whole depth of layer 1 . From 2 Km depth (probable depth of penetration of phase 'a_o') where pressure is about 0.5 Kb down to 12 Km where pressure is about 3 Kb, Poisson's ratio could increase by as much as 0.01 (Simmons 1964; Christensen 1965,1966).

(ii) That an average Poisson's ratio over a crustal block tens of kilometers long (or even more than a hundred kilometers long) is a good representation, as a first approximation, of the actual distribution of PR along the block. This hypothesis can only be tested by checking how well the theoretical ts/tp curves fit the observed data.

4.2 THE P VELOCITY MODEL

4.2.1 Improving the lower crust in segment ALPHA

As explained in section 4.1 (Introduction) a P velocity model was necessary as a reference to determine Poisson's ratio. However calculation of the whole P velocity structure was not completed yet when inversion of Poisson's ratio started. Modelling of the upper crust had already been finished by Bamford et al. (1977) using mainly plus-minus methods (Hagedoorn 1959) and ray-tracing techniques. For the lower crust on the other hand only schematic features were known based on horizontal plane layer fits to each record section, so that an improvement in the lower crust was desirable.

This improvement in the P velocity lower crustal model was made in two stages:

1) Using ray tracing methods with the reflected phases 'e', 'c' and 'd', middle/lower crust and Moho interfaces were adjusted by trial-and-error so that better fits to the observed travel times were obtained. First the bottom of layer 2 (Fig. 4.1) was modelled using phase 'e' from shots N2, N1

and 1 recorded in ALPHA. Afterwards the Moho transition was improved using Moho reflections and upper mantle refractions of those same shots. In this stage velocities were held constant and only interfaces were changed. Fig. 4.1 shows the initial P velocity model inferred from the horizontal plane-layer fits (called model 0) and the intermediate model (model 1) after adjustments with ray-tracing, as well as the final model to be explained below.

2) In a second stage using model 1 above as a starting model the travel times were linearized with respect to certain parameters in the model (velocity, depth and dip of interfaces) and normal least-squares methods were used in an iterative procedure.

The travel times to each station were linearized with a Taylor's series expansion (first order only) such as

$$T(h+\Delta h, v+\Delta v) = T(h,v) + \Delta h(dT/dh) + \Delta v(dT/dv)$$

where h, v are two parameters

T(h,v) is the travel-time for the starting model

Δh, Δv are parameter variations to be found by least-squares

Because lateral variation is one of the main features of the crustal structure under investigation, there was no suitable analytical formula to calculate the time derivatives. These had to be calculated by running the ray-tracing program twice: once with the starting model and again with the model perturbed in one of its parameters.

The choice of parameters was very important. It was found that dips had less effect on the travel times than either velocity or depth and for this reason dips were often held constant.

A more detailed explanation of the method of linearization and least-squares, with an example, is given in appendix D.

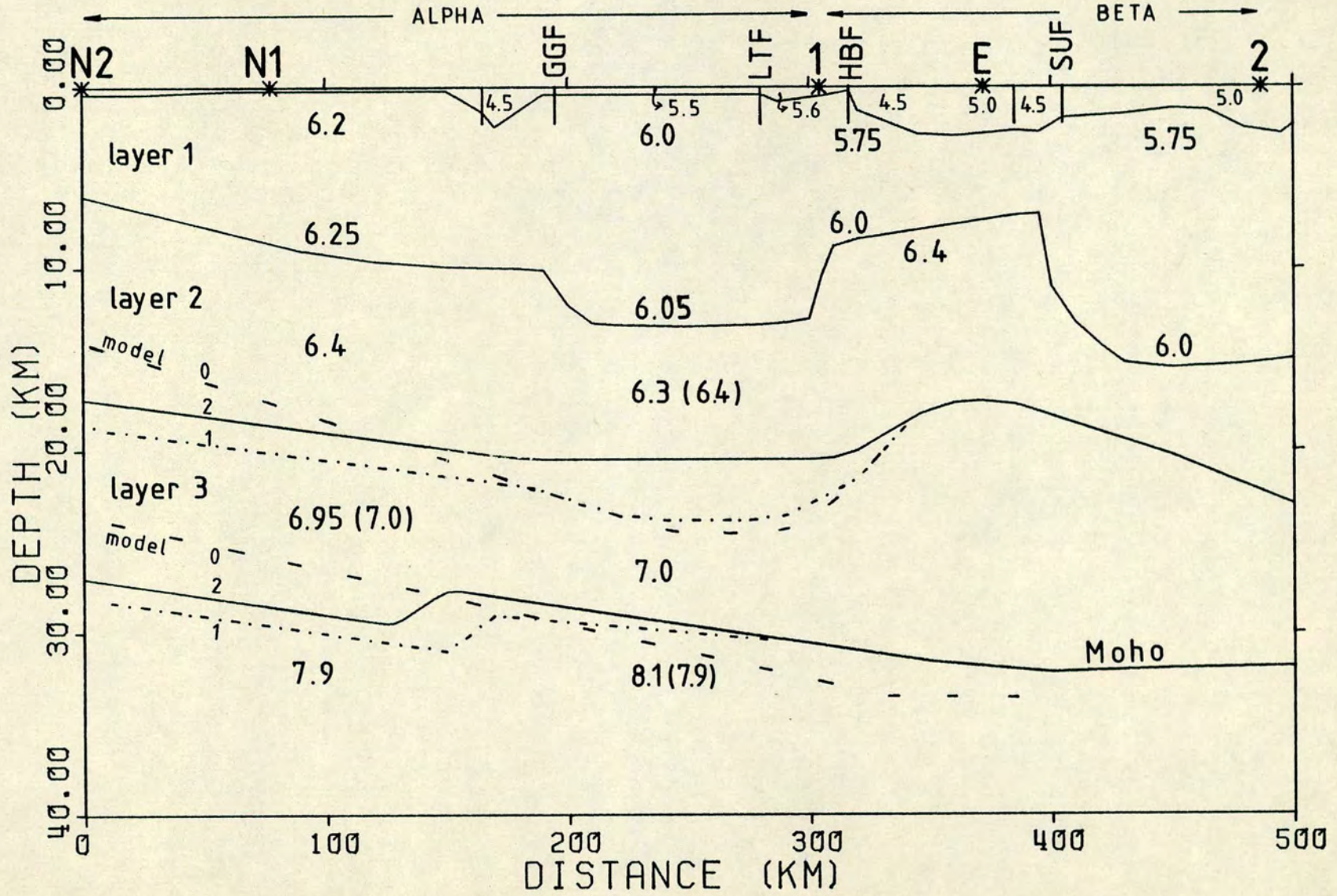

Fig. 4.1 P velocity models. Numbers are P velocities in Km/s. Values in () are those of models 0 and 1 if different from model 2. Model 2 is the reference P model.

Phase 'e' from shot-points N2 and N1 were used to determine the bottom velocity and bottom depth of layer 2 from horizontal coordinate 70 to 190 Km. Phase 'e' from shot-point 1 was used to determine the velocity and bottom depth of layer 2 from 200 to 260 Km . For layer 3 phase 'c' from N2 and N1 together with phase 'd' (Pn) from N2 were used to determine velocity of layer 3, Moho depth and upper mantle velocity from about 30 to 120 Km.

For the Moho from about 120 to 270 Km all phases sampling that part of the crust were used, that is, Pn from N2, N1 and 1, and Moho reflection from shot-point 1. Velocity of layer 3, Moho depths and upper mantle velocity were the parameters chosen. However very little improvement was possible in this part of the model.

Table 4.1 shows the results of the P velocity model 2, Fig. 4.1, as compared to the starting model 1. Model 2 is the reference crustal model used in the inversion of Poisson's ratio. The general features of this model agree well with the results of Bamford et al. 1978. For example layer 2 between Great Glen and Highland Boundary faults was found to be thinner with a P velocity slightly lower than 6.4 Km/s in good agreement with Bamford et al. 1978. Slight differences between the two models (such as topography of the lower crust and Moho depths) are not really significant. Our two Pn velocities of 7.9 and 8.1 Km/s are probably not significantly different from their constant 8.0 Km/s along the whole profile.

Table 4.1 P Travel time residuals

Shot	Phase	r.m.s residual (s) Starting model 1	model 2
N2	e	0.09	0.07
N1	e	0.14	0.12
1	e	0.31	0.17
E	e	0.18	0.08
N2	c	0.14	0.09
N1	c	0.12	0.05
N2	d	0.07	0.07
(Δ=30 to 120 Km)			
N2,N1,1	d	0.34	0.21
(Δ=120 to 270 Km)			

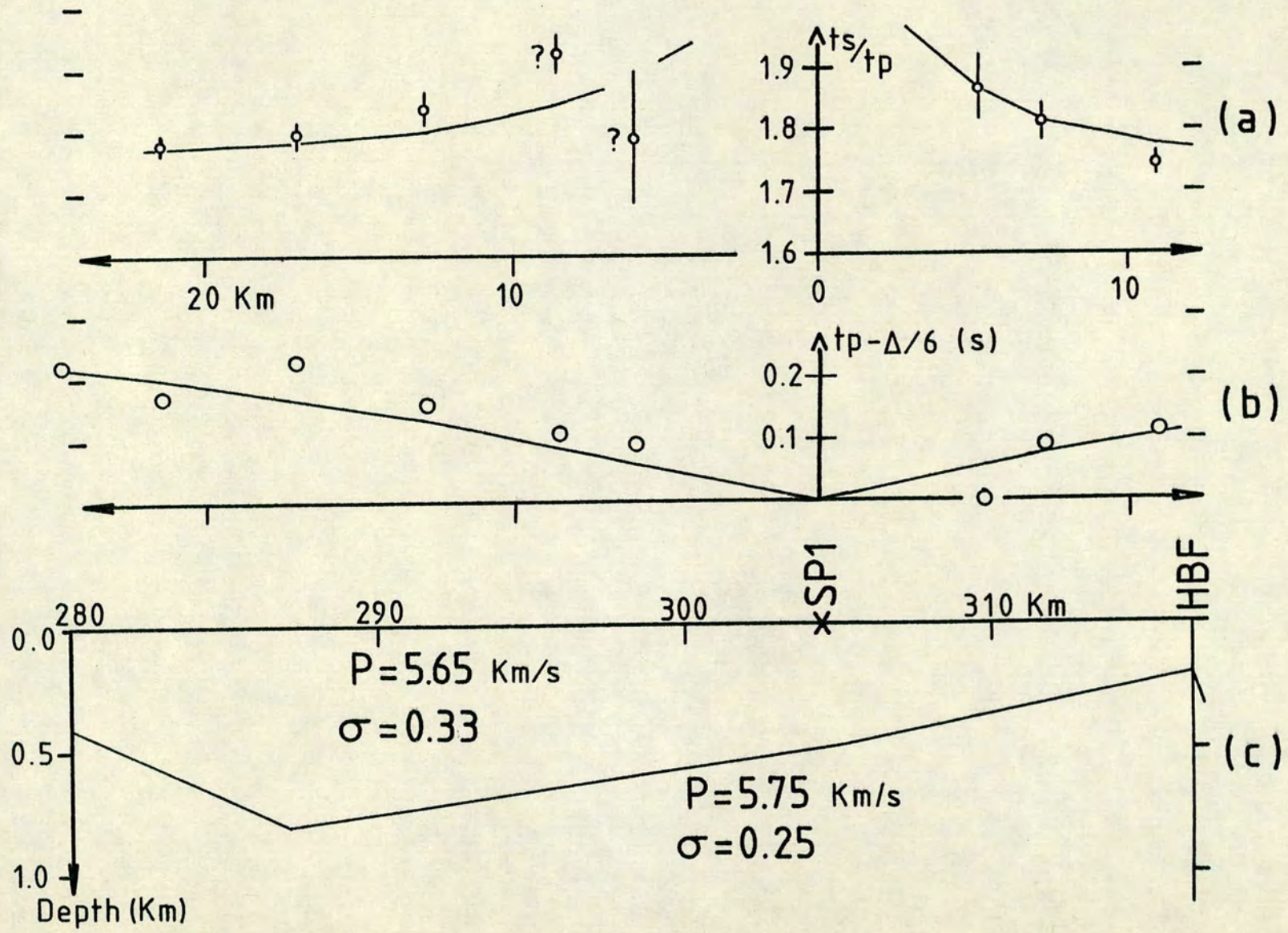

Fig. 4.2 Surface layer at shot-point 1. Theoretical curves in (a) and (b) are calculated with the model shown in (c).

4.2.2 Surface layer at shot-point 1

One small modification was made on the original P velocity model of Bamford et al. 1977. Under shot-point 1 the superficial layer of velocity 5.0 Km/s and 0.2 Km thickness was substituted by one dipping north with P velocity 5.65 Km/s and thickness 0.5 Km (beneath shot-point 1), Fig. 4.2. This is not in contradiction to the model of Bamford et al. because the scale of the LISPB experiment does not allow resolution of such details. Both models are equivalent in that they give about the same P travel time for stations near shot-point 1. Such modification was made in order to account for the ts/tp ratios of stations within about 15 Km either side of shot 1 . As shown by Fig. 4.2(a) the ts/tp ratio decreases more rapidly with distance south than north of the shot-point. This was tentatively modelled by a surface layer with high PR ($\sim$0.33) thicker to the north of shot 1 and thinner to the south. Detailed determination of near surface structure is not possible with station spacings of a few kilometers. S arrivals with high relative uncertainties do not help decrease the non-uniqueness of the modelling. Only very coarse models are possible. In the case of shot-point 1 a thicker higher velocity superficial layer accounted slightly better for the ts/tp ratios.

4.3 TRAVEL TIME RATIOS

4.3.1 Observed data

Travel time ratios ts/tp were plotted against distance from the shot. These ts/tp curves are shown in Figs. 4.3 to 4.5 In these plots two horizontal lines were drawn at those values of ts/tp equivalent to PR = 0.26 and 0.24. The curves through the data points are the fitted theoretical curves from the final model to be explained below. SV and SH picks are indicated by squares and triangles respectively.

It is believed that the uncertainty assigned to each S onset is large

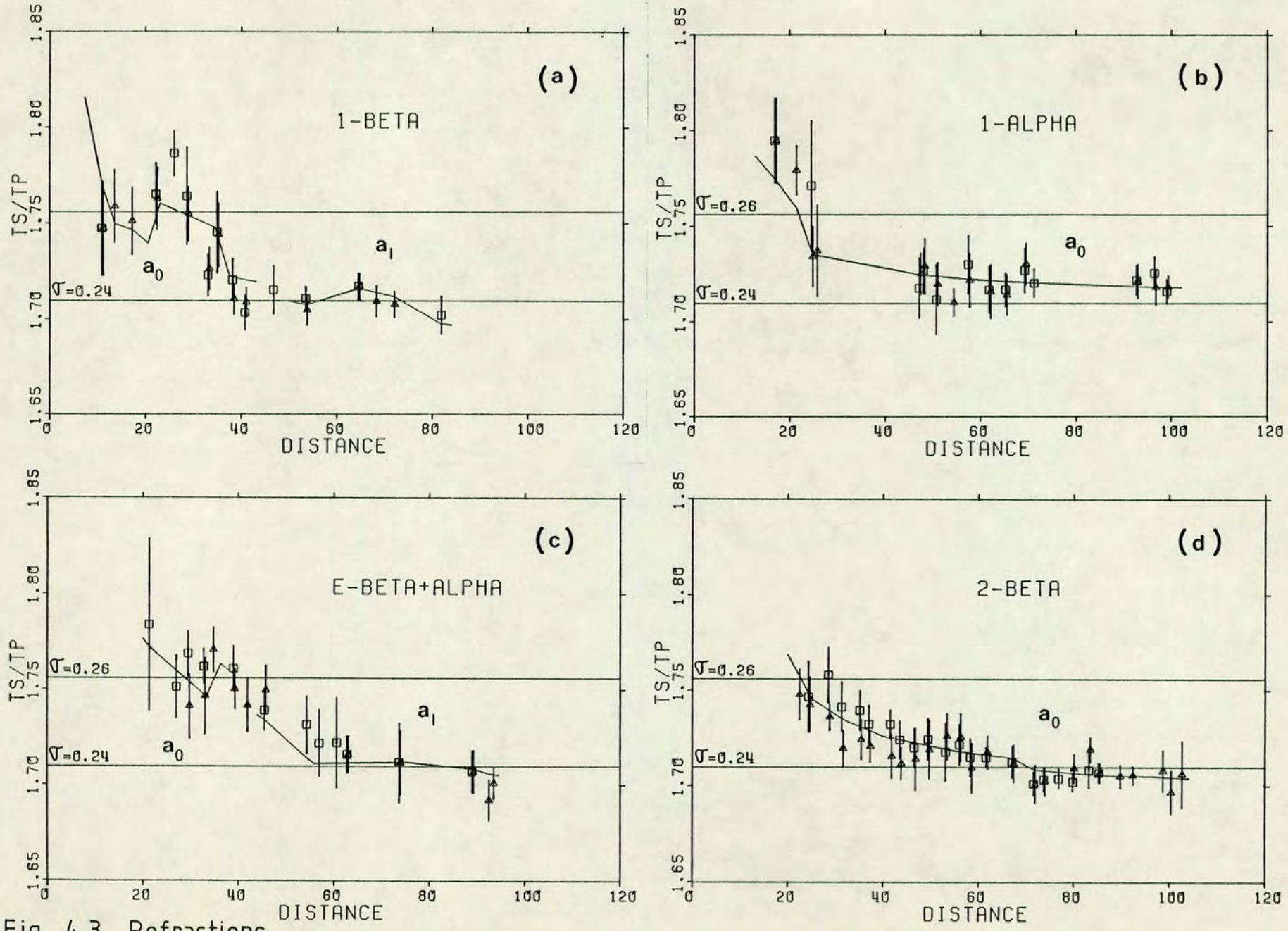

Fig. 4.3 Refractions

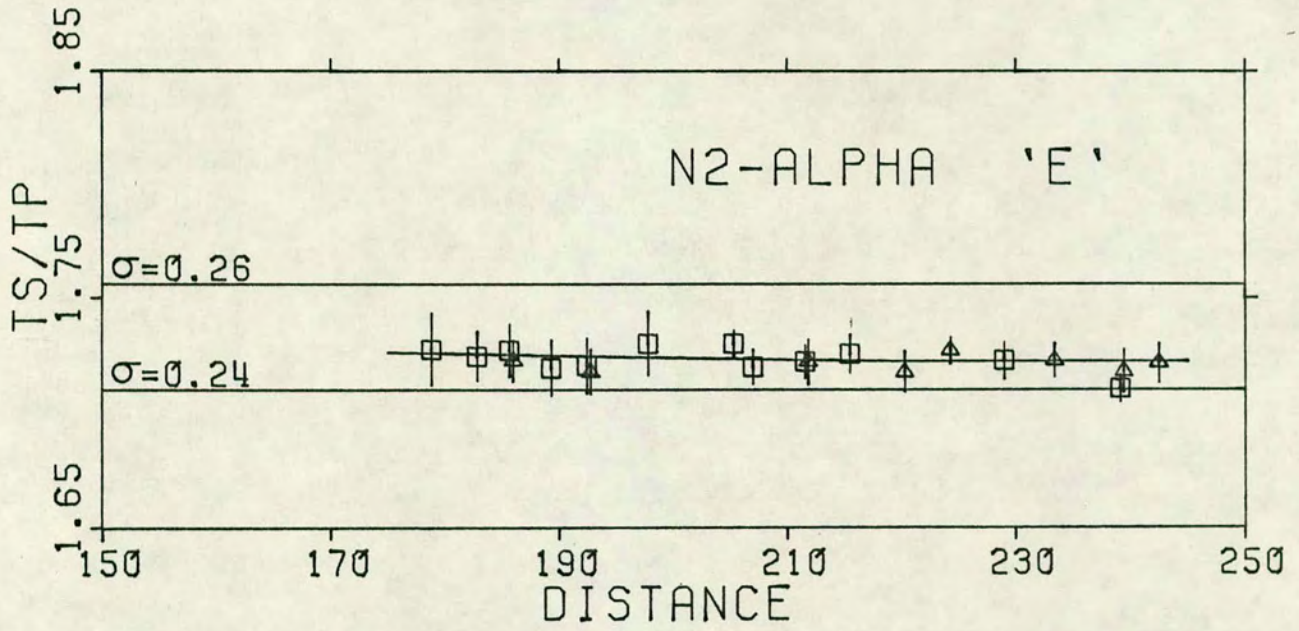

Fig. 4.4 t_s/t_p of wide-angle reflection from the bottom of layer 2, phase 'e'.

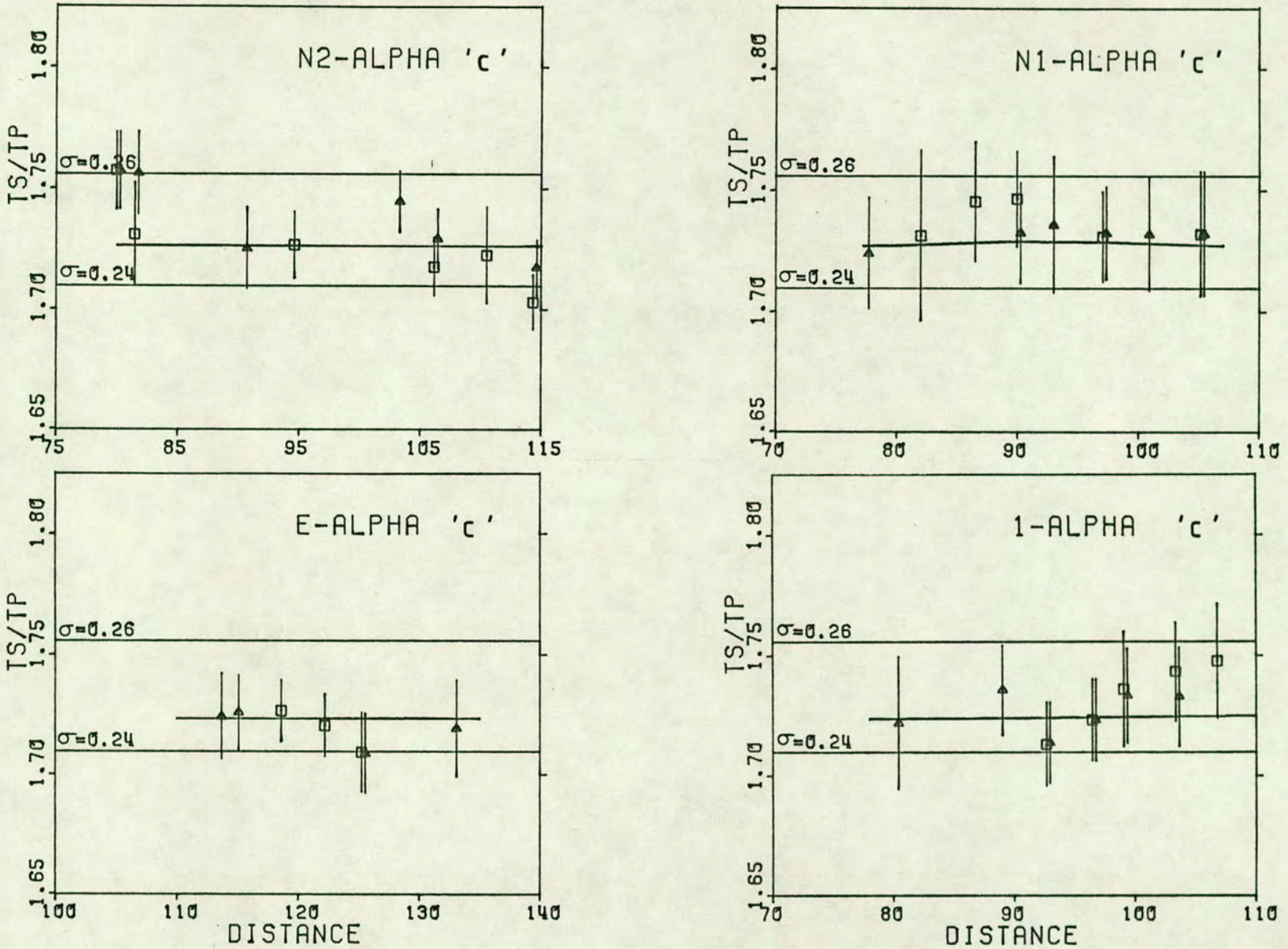

Fig. 4.5 t_s/t_p of Moho reflections, phase 'c'

enough to include the true S onset in most cases. For this reason these uncertainties were regarded as being equivalent to one standard deviation in the inversion procedure used to determine Poisson's ratio. As can be seen from the ts/tp plots the uncertainties, or "standard deviations", are consistent with the scatter of the points around the theoretical curves.

Fig. 4.3 shows all upper crustal refractions 'a_o' and 'a_1'. All profiles have the same general trend of high ts/tp near the shot, decreasing with distance. This is explained by high values of PR near the surface, especially in sedimentary basins like the Midland Valley and Northumberland basin (shot point 2). Near the shot ts/tp is largely affected by the high PR of sediments, but as the waves travel longer distances in the refractor, below the sediments, the final ts/tp approaches the P to S velocity ratio of the refractor which is lower than that of the sediments.

Fig. 4.4 shows ts/tp data for phase 'e' from N2 (wide angle reflection from the top of the lower crust). Fig.4.5 shows ts/tp for Moho reflections.

4.3.2 The forward problem

In order to calculate theoretical values of ts/tp two programs were written, one for refractions and another for reflections, basically similar except for the subroutine to calculate travel times. The programs accepted as input a layered structure under the shot and different layered structures under each station. For each layer including the refractor a P velocity and a range of PR were specified. For every distance minimum and maximum values of ts/tp were also given as input. For every possible combination of PR in the various layers tp and ts were calculated and the ts/tp ratio tested against the specified bounds for each station. The combinations of PR that passed the test for all stations were listed. From this list maximum and minimum values of PR for each layer were found. Figs.

PROGRAM SIGREFRA

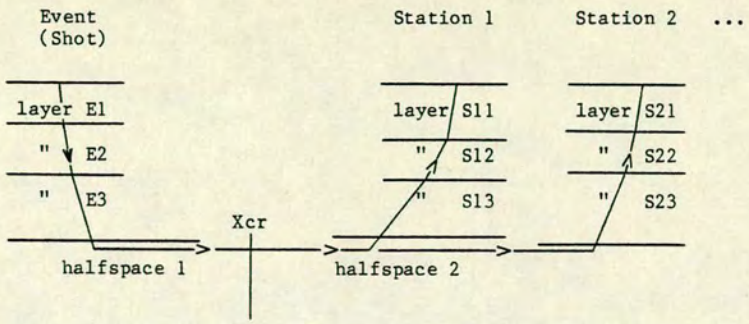

INPUT: P vel.,thickness and range of Poisson's ratio (PR) in each layer. (For the stations PR of layer S11 = PR of S21 = PR of S31, etc., but P velocities and thicknesses are different for each station).
P vel. and PR range for the two half-spaces separated at Xcr.
Distance, minimum and maximum ts/tp for each station.

CALCULATION: For every combination of PR ts/tp is calculated for each station and checked against its specified range of ts/tp.

OUTPUT: A list of all combinations of PR that produced ts/tp within the range specified for each station. Fom this list the range of allowed PR in each layer can easily be found.

Fig. 4.6 SIGREFRA

PROGRAM SIGREFLE

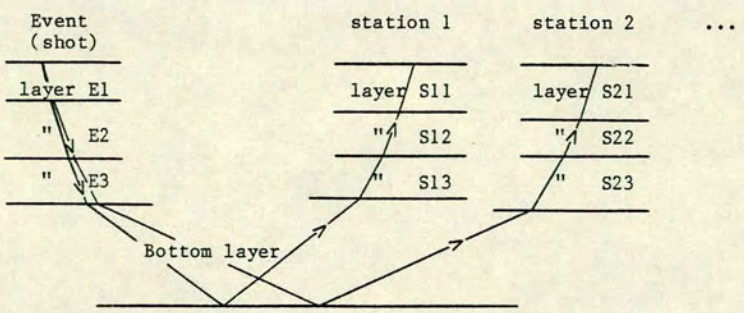

INPUT: P vel., thickness and range of PR in each layer. (For the stations PR of layer S11 = PR of layer S21 = PR of S31, etc., but P vel. and thicknesses are different for each station).
P vel., thickness and range of PR for the Bottom layer inside which reflection will occur.
Distance, minimum and maximum ts/tp for each station.

CALCULATION: For every combination of PR ts/tp is calculated for each station and checked against its specified range of ts/tp.

OUTPUT: A list of all combinations of PR that produced ts/tp within the range specified for each station. From this list the range of allowed PR in each layer can easily be found.

Fig. 4.7 SIGREFLE

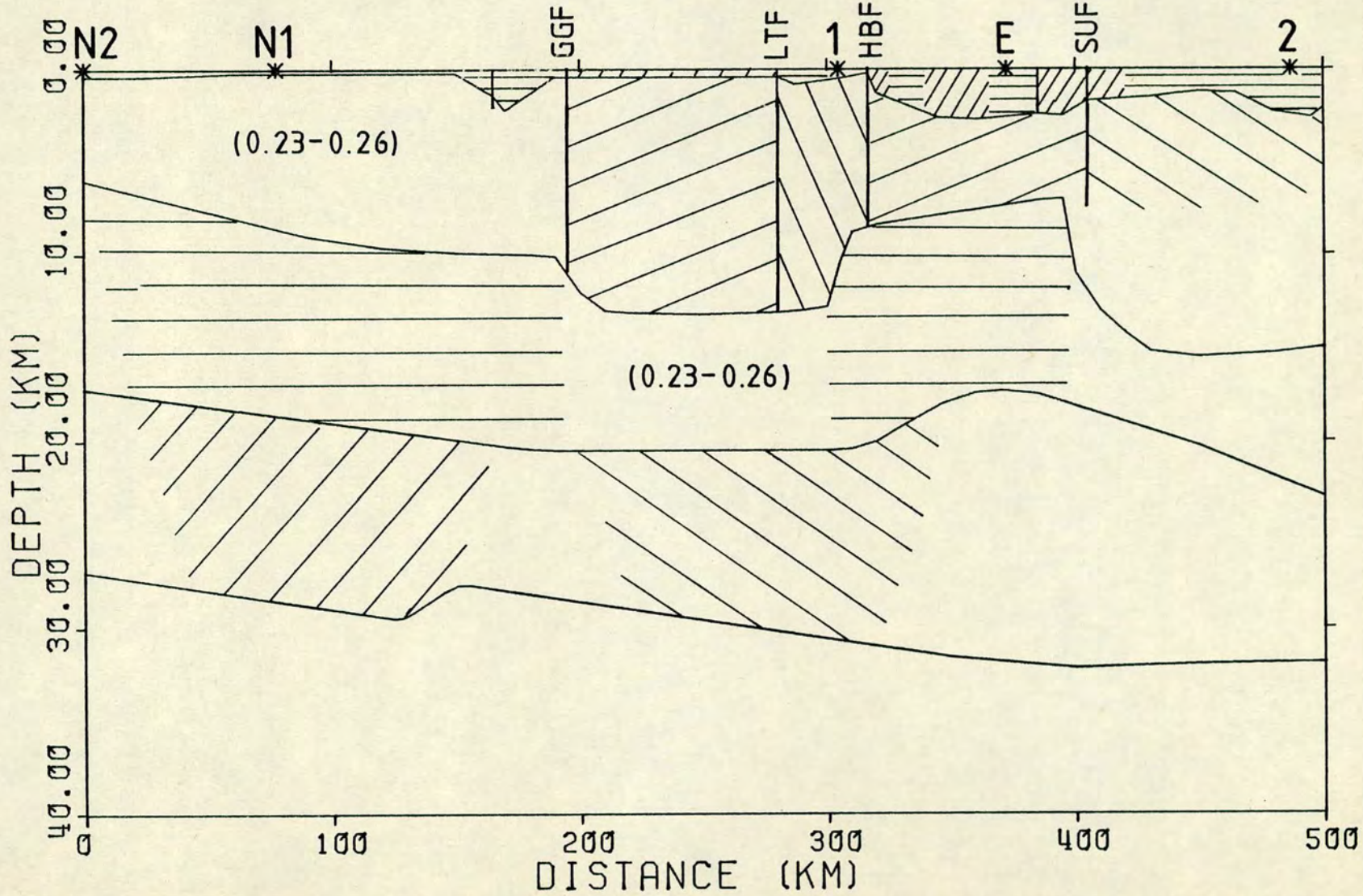

Fig. 4.8 The crustal blocks where Poisson's ratios were determined. Constant σ assumed in each block. Values in () are assumed range of σ where no direct determination was possible.

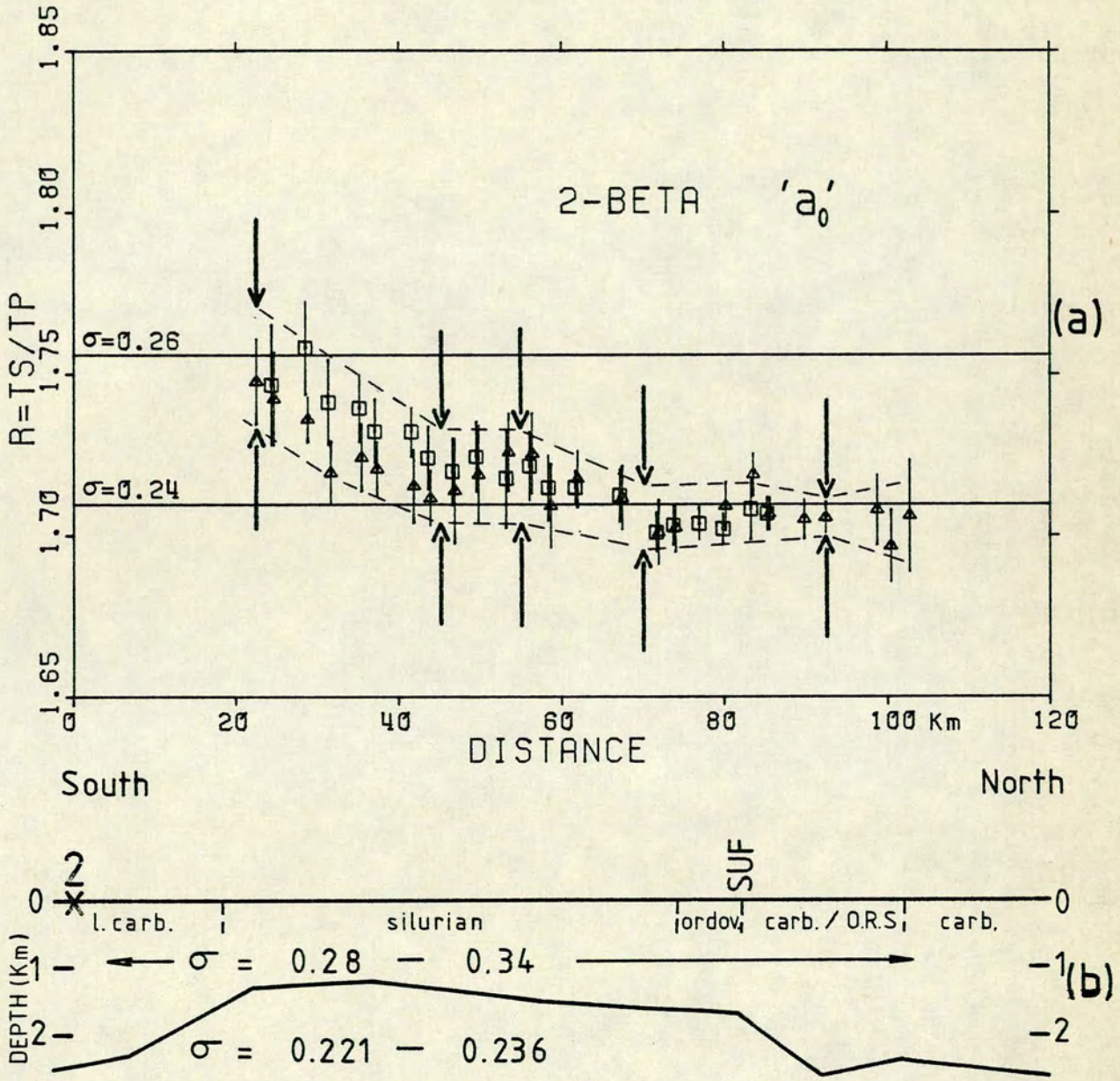

Fig. 4.9 (a) Envelopes around t_s/t_p data of 2→BETA, 'a_o'. Arrows indicate limiting values used in the program SIGREFRA.

(b) Resultant range of the two σ parameters in the upper crustal model of segment BETA.

4.6 and 4.7 explain schematically those two programs.

These programs were run for each shot and phase, as explained below, in order to have a preliminary idea of the Poisson's ratio structure: i.e., approximate bounds for the PR in each block were determined and from these an initial model was chosen for the linearized least-squares inversion.

4.4 INVERSION METHOD

4.4.1 Finding a starting model

As explained before the determination of Poisson's ratio structure was made in two stages: 1) an initial preliminary model was found on a trial and error basis, and 2) the problem was linearized and an iterative least-square procedure was applied.

The crustal structure was divided into blocks as shown in Fig. 4.8. The size and extent of these blocks were determined partly on geophysical grounds (P velocity, faults) and partly on the coverage offered by the seismic profiles: Poisson's ratio in each of these blocks was assumed to be constant. Where no direct measurement of PR was possible (i.e. neither refraction nor reflection ts/tp data was available), PR was assumed to lie in the range 0.23 to 0.26, as shown in brackets in Fig.4.8.

The initial model was found as follows. For every phase two "envelopes" were drawn in the ts/tp plot containing all data points and most of the uncertainty bars. From these envelopes lower and upper limits of ts/tp were taken for a few stations spread along the observed distance range for that particular phase. These limits were used with the programs described in the last section to find a range of possible values of Poisson's ratio for each of the blocks sampled by that phase.

Fig. 4.9(a) shows an example of limits on the ts/tp ratios for phase 'a_o' of profile 2-->BETA. The arrows indicate the upper and lower bounds on ts/tp used in the program SIGREFRA. The results for that phase, assuming

the same PR for the whole superficial layer, Fig. 4.9(b), are :

Poisson's ratio of superficial layer = 0.28 to 0.34

Poisson's ratio of basement = 0.221 to 0.236

All phases of all ts/tp plots were treated in a similar way. As a result a range of Poisson's ratio for each block was found, and from within the range the initial model was chosen, shown in Fig 4.11 .

No statistical criteria was used to draw those envelopes, but this is not important as only an approximate preliminary model was required.

4.4.2 The superficial layer

The superficial layer is here defined as the plane layer above the basement and the basement by the refractor of phase 'a_o' . This is, of course, a very simplified model of the actual structure near the surface, but the scale of the LISPB experiment (station spacing about 3 to 4 Km) does not allow any finer detail to be modelled. The superficial layer in some places is about 2 Km thick consisting mainly of low velocity sedimentary rocks like the Old Red Sandstone basin of the Moray Firth (near the Great Glen Fault) and the upper paleozoic sedimentary sequences of the Midland Valley and Northumberland basin (shot point 2). In other parts (e.g. north of the Highland Boundary Fault) the superficial layer is a thin layer (<0.5Km) of mainly metamorphic rocks where the P velocity (about 5.5 Km/s) is lower than the basement (6.0 to 6.2 Km/s) because of weathering, open pore spaces and cracks.

Shear wave sedimentary phases (distances < 10Km) did not have onsets sharp enough to define the average Poisson's ratio for the superficial layer with good resolution. The number of stations in that range was also very limited. This means that no direct measurement of PR in the superficial layer was possible and indirect estimates had to be made with the ts/tp data of phase 'a_o'. For example phase 'a_o' of shot 2-->BETA (Fig.

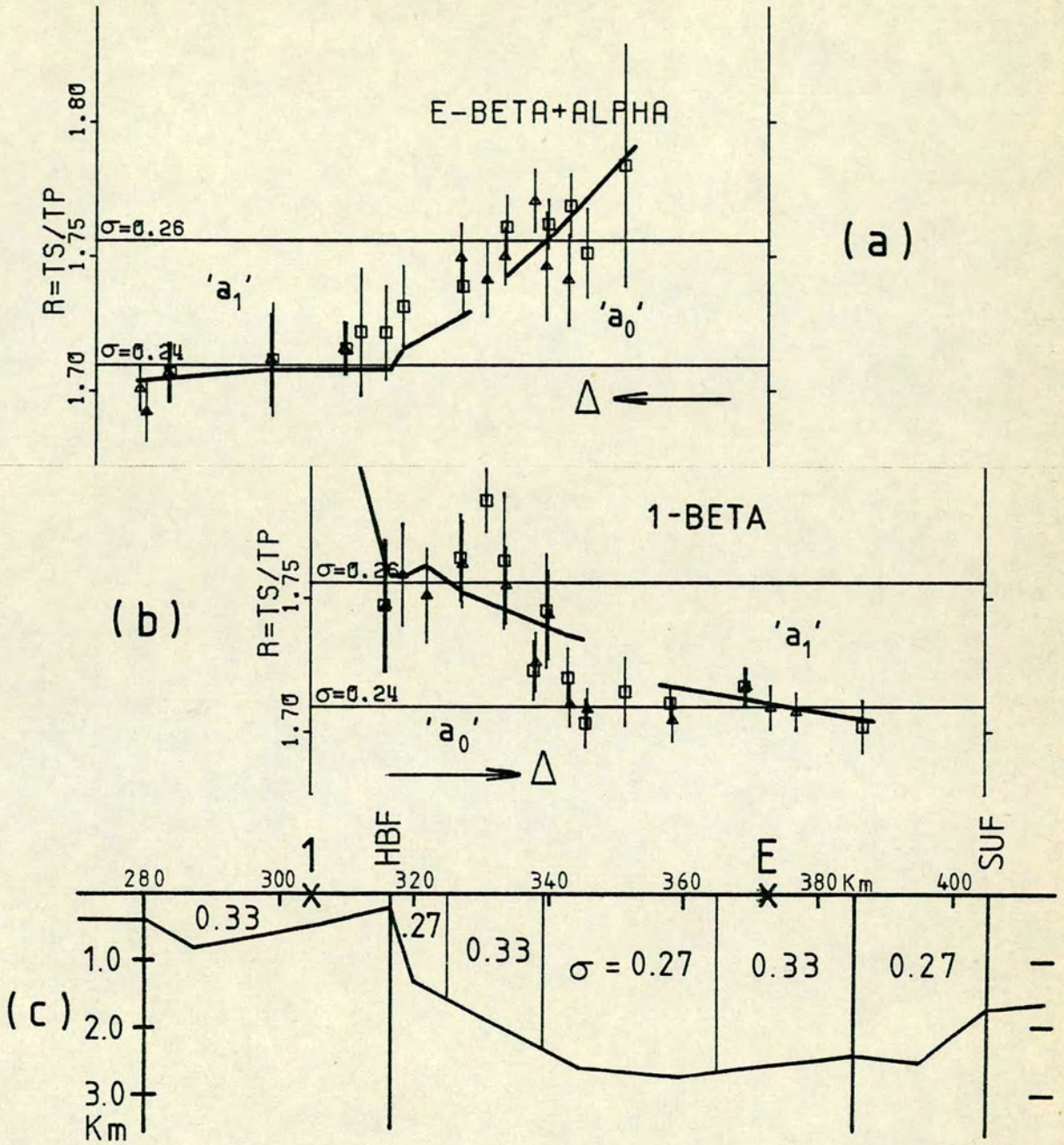

Fig. 4.10 (a) and (b) ts/tp in Midland Valley; thick lines calculated with PR = 0.31 constant for whole sedimentary layer.
(c) Blocks of high (0.33) and low (0.27) PR to account for relative highs and lows in ts/tp data.

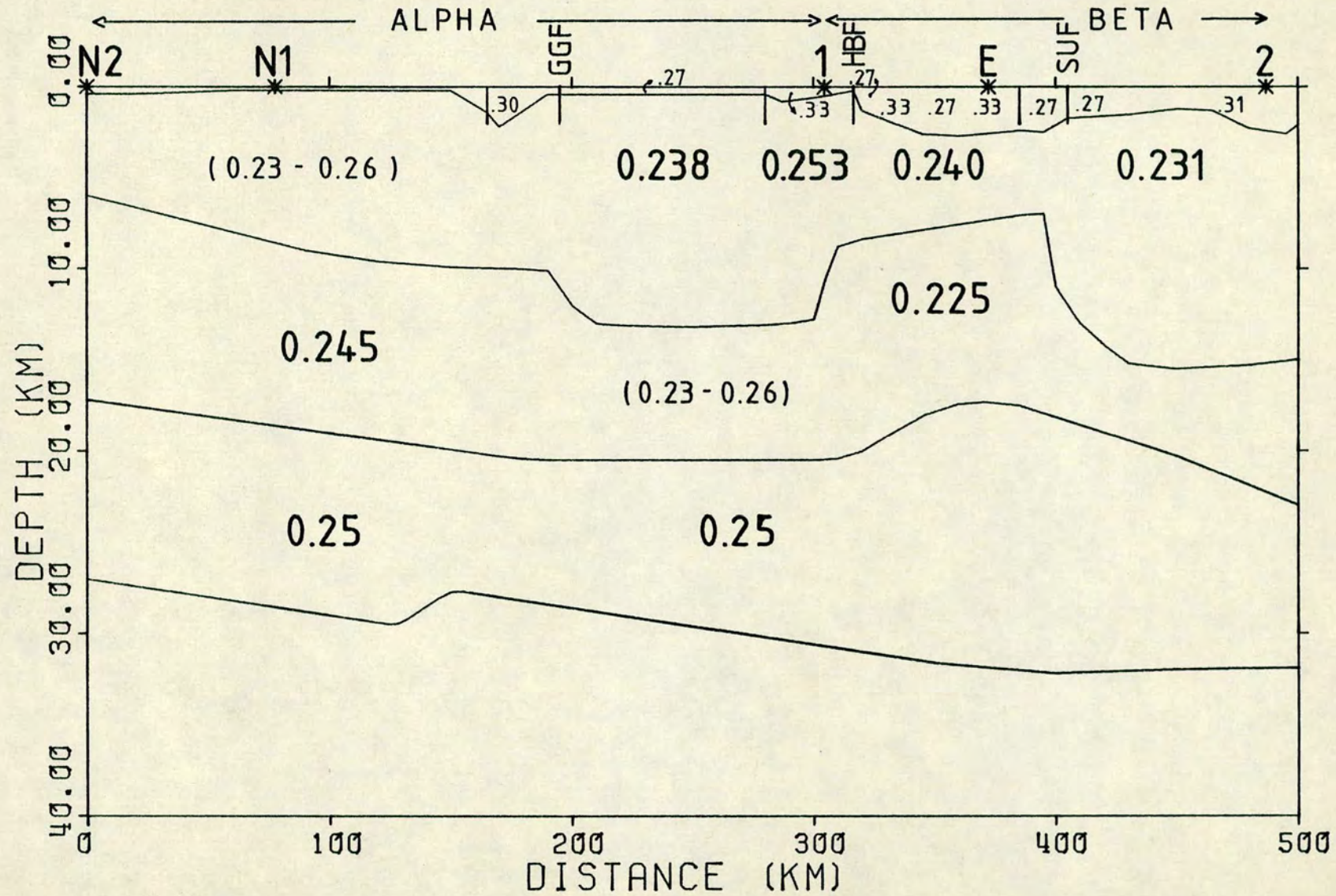

Fig. 4.11 Initial model of Poisson's ratio.

4.9) indicates that the average PR of that superficial layer lies between 0.28 and 0.34 (that is, assuming PR constant all along the superficial layer). Similarly several runs of the program SIGREFRA (section 4.3.2) with shots 1 and E indicate that the average PR of the Midland Valley superficial layer lies roughly between 0.30 and 0.36.

The assumption of a constant value of Poisson's ratio for the sedimentary layer (e.g. PR=0.31) in the Midland Valley (between HBF and SUF) does not seem appropriate as indicated by the thick line drawn through the ts/tp data from shots 1-->BETA and E-->BETA+ALPHA in Fig. 4.10(a),(b). Those ts/tp data indicate that we can separate the stations in the Midland Valley into two sets: one with higher values of PR, and the other with lower values. These values were chosen as 0.33 and 0.27 from within the range given by the program SIGREFRA. The several blocks in the sedimentary layer of Fig. 4.11(c) were chosen so as to account for the relative highs and lows in the ts/tp observations. These blocks are rather arbitrary in their boundaries and should only be interpreted as an attempt to better fit the ts/tp data with 2 Poisson's ratio parameters (0.33 and 0.27) instead of only one PR parameter for the whole superficial layer. For this reason there is not a clear correlation between these superficial blocks and the surface geology, with only a slight indication that blocks with lower Poisson's ratio (0.27) have a large amount of igneous rocks as opposed to blocks with higher PR (0.33) which are mainly sandstones.

High values of Poisson's ratio in the sediments, or generally near the surface, is the rule rather than the exception, as indicated by many field measurements like those of Jolly(1956); Erickson et al.(1968); Geyer & Martner(1969); Tatham & Stoffa(1976) and Scarascia et al.(1976).

Laboratory measurements of Poisson's ratio in dry sandstones and limestones have a very wide range (e.g. King 1966; Gregory 1976) and are usually less than 0.25. However rocks are usually porous and when specimens

are filled with fluid, which is probably closer to the average condition in the field, then PR can increase significantly (King 1966, Gregory 1976). A small proportion of soft and unconsolidated sediments near the surface will also contribute to high average values of PR (Scarascia et al.1976; Gregory 1976). Thus Poisson's ratios as high as 0.33 near the surface as required by ts/tp data are in general agreement with laboratory and field measurements.

4.4.3 Linearization and least-squares

After a preliminary model was obtained, Fig. 4.11, the Poisson's ratio structure was determined by means of linearization of that initial model and least-squares fitting to all ts/tp data.

The theoretical ts/tp value for each station/shot pair was linearized in a first order Taylor series with respect to the Poisson's ratio of the various blocks, σ_1 , σ_2 , σ_3 ,... Calling ts/tp = R

$$R(i, \Delta\sigma_1 , \Delta\sigma_2 ,...) = R_o(i,\text{in. model}) + \Delta\sigma_1 \frac{\partial R}{\partial \sigma_1} + \Delta\sigma_2 \frac{\partial R}{\partial \sigma_2} +$$

where $R_o(i)$ is the theoretical ts/tp given by the initial model for station/shot pair i , and

$\Delta\sigma_1$, $\Delta\sigma_2$,... are variations in the parameters σ_1 , σ_2 ,...

Normal least-squares procedure yields the required variations in the Poisson's ratios. This is of course an iterative procedure with results of the first iteration being the new initial model for the second iteration.

The difficulty in this method is that the derivatives $dR/d\sigma$ cannot be expressed in a simple formula because of the inhomogeneous nature of the structure, especially when data from various shots and phases are inverted simultaneously. For this reason those derivatives were calculated by running the programs SIGREFRA, or SIGREFLE, with two close values of PR for

each PR parameter to be determined. In practice it is not necessary to calculate those derivatives for all stations of each profile but only for a few stations (key stations) spread along the observed distance range - values can then be interpolated for the rest of the stations. A program was written, called CURFIT, to solve the least-squares equations using as input the observed ts/tp data with its standard deviations, and theoretical values at those key stations for the initial model and for the perturbed initial model. This program is explained in more detail in appendix D.

The expansion of ts/tp ratio in a Taylor series is a good aproximation for variations of Poisson's ratio up to +/- 0.02 . This was enough to assure convergence in only two iterations. Poisson's ratio of the final model differed by less than 0.01 from the values of the preliminary model.

4.5 RESULTS

4.5.1 The superficial layer

The Poisson's ratios of the sedimentary layers were not well constrained by the data, as explained before, and this led to some instability in the least-squares solution. For this reason PR in the superficial layers were constrained to the values of the preliminary model. Uncertainties in these Poisson's ratios were nevertheless taken into account. Based on results of the program SIGREFRA and also on reported field measurements of Poisson's ratio it was assumed that the maximum range of possible values of PR for the superficial layer was +/- 0.03 : this means, for example, that σ =.33 (Fig. 4.11, between HBF and SUF) could in fact range from 0.30 to 0.36 and σ =.27 could range from 0.24 to 0.30. (This range was treated as if it were equivalent to a 95% confidence limit).

The important point is that this uncertainty of +/- 0.03 does not significantly affect the determination of Poisson's ratio for the lower refractors 'a_o' and 'a_1'. For example, if under shot-point E (Fig. 4.11) PR

was decreased by 0.03, PR for the 'a_o' refractor (layer 1) would need to be increased by only 0.007 to give the same ts/tp at a distance of 40Km. The various values of PR in the superficial layers should thus be interpreted as mere "sedimentary" corrections, or a kind of weathering correction in terms of Poisson's ratio.

For shot point 2 (Northumberland basin) however it was possible to find the PR of the sedimentary layer with the least-squares program. This was because the S onsets are sharper (smaller uncertainties) than for shot-points 1 and E, and also because the range of phase 'a_o' is from about 20 to 100 Km (as opposed to 20 to 40Km for the Midland Valley), which gives good stability for the PR solutions of the sedimentary layer (0.31+/-.025) and refractor basement (0.231+/-.005).

4.5.2 Northumberland Basin - Southern Uplands

Fig. 4.12 shows the PR parameters used in the least-squares fitting of ts/tp data from shot 2-->BETA, phase 'a_o'. The inclusion of two different parameters for the superficial layer seems justified in view of the drop in ts/tp at a distance of 70 Km in Fig. 4.3(d), which would be very difficult to explain otherwise. This extra parameter, nevertheless, had to be fixed at 0.27 with the usual maximum uncertainty of +/- 0.03 taken into account.

The solution for the least-squares fitting was identical to that obtained by the program SIGREFRA, that is PR = 0.31 for the sedimentary layer (constant up to 50 Km distance) and PR = 0.231 for the basement.The uncertainties in the first two parameters were obtained by summing the standard deviation of the least-squares fit with the deviation in the solution caused by a variation of +/- 0.03 in the fixed (3rd) parameter.

Table 4.2 shows the resulting standard deviations. For example, parameter 1 (PR of the sedimentary layer), had a least-squares solution of 0.307 +/- 0.011 when parameter 3 was fixed at 0.27. If σ_3 were decreased by

0.03 (σ_3 = 0.24) the solution for σ_1 would be 0.314 (= 0.307+0.007). If σ_3 were increased by 0.03 then σ_1 would be lower by 0.007. That means the maximum allowed range of +/-0.03 in the fixed parameter introduces a maximum uncertainty of +/- 0.007 in the solution of σ_1 . The final uncertainty of parameter 1 (shown in the 3rd line of Table 4.2) is then 0.011 + 0.007 = 0.018. This was interpreted as roughly equivalent to a "95% confidence limit". Straight summation of uncertainties was used instead of summation of variances because the allowed range of the fixed parameters are not exactly statistical uncertainties but simple probable maximum limits of Poisson's ratio.

4.5.3 Midland Valley to Great Glen

Fig. 4.13 shows the various blocks with their Poisson's ratio parameters. Phases 'a_o' and 'a_1' of shots E-->BETA+ALPHA, 1-->BETA and 1-->ALPHA, together with the Moho reflections from 1-->ALPHA and E-->ALPHA were used in the least-squares fitting with resulting theoretical ts/tp curves shown in Figs. 4.3 and 4.5.

Poisson's ratios of the superficial layer were restrained as explained before. Also in layer 2 between horizontal coordinates 200 and 300 Km Poisson's ratio had to be fixed as no direct measurement was possible (i.e., neither S phase 'a_1' nor 'e' were well recorded from that part of the crust). A value of 0.245 was chosen (based on similar results of the preliminary model for that same layer further north) and a maximum range of +/-0.015 was assumed. In view of the preliminary results for the surrounding blocks, Fig. 4.11, this range of 0.23 to 0.26 was considered adequate to represent the maximum probable uncertainty of PR in that block.

Table 4.3 presents the resulting Poisson's ratio parameters together with their uncertainties. The first line contains the starting values given by the preliminary model of Fig. 4.11. The second line contains the

solutions of the least-squares fit and the third line shows two standard deviations of these solutions. The remaining lines are the contributions to the final uncertainty from the assumed range of PR of the fixed parameters.

It can be seen that in most cases the uncertainties in the fixed parameters contribute little, less than 0.01, to the final uncertainties of the Poisson's ratios. The one exception is the PR of layer 1 at the Midland Valley. Because of the large thickness of the sedimentary layer at the Midland Valley (2Km) and the short range of phase 'a_o' from 20 to 40 Km only, the +/-0.03 range of the two fixed PR in the sedimentary layer affect o (Fig. 4.13) by +/- 0.014. An interesting effect on the other hand is the relative insensitivity of PR of layer 2 beneath the Midland Valley (σ =0.224) to the large uncertainties of the upper layers.

LISPB shot-point 1 was well observed by most of the stations of the permanent Lowland Seismic Network (LOWNET), especially by the Edinburgh 3-component station (EDI). The S and P 'a_1' phase of shot 1-->EDI (dist. = 81.7Km) gave travel times of 23.98+/-.05 and 14.04+/-.02 seconds respectivelly. This data was not used in the determination of the Poisson's ratio structure and so can be used as a slight check on the model. The observed ts/tp ratio of 1.708+/-.006 (=23.98/14.04) is in general agreement with the theoretical ts/tp ratio of 1.698+/-.014 (this uncertainty is a minimum estimate caused by the uncertainty of σ_4=0.224+/-.012 in Fig.4.13). LISPB shot E was only about 14Km away from EDI so that the S phase is not well separated from other close arrivals (the same happens with those LISPB stations at similar distances) and so cannot be used to check the PR model. Shot 2 was about 100Km away and the first S arrival, being too poor, is not useful either.

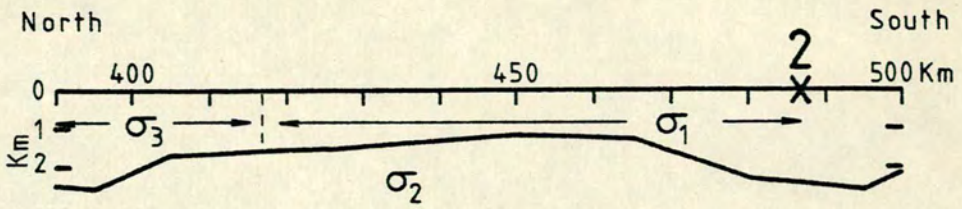

Fig. 4.12 2—BETA. Poisson's ratio parameters used in the least-square fit.

TABLE 4.2 Uncertainties from least-squares and from range of fixed parameters. Shot 2--> BETA, 'a_o'.

least-sq. solution	σ_1 = 0.307	σ_2 =0.231
+/- 2 st. dev.	± .011	± .003
fixed parameter σ_3 = 0.27 ± .03	± .007	± .002
final uncertainty	± .018	± .005

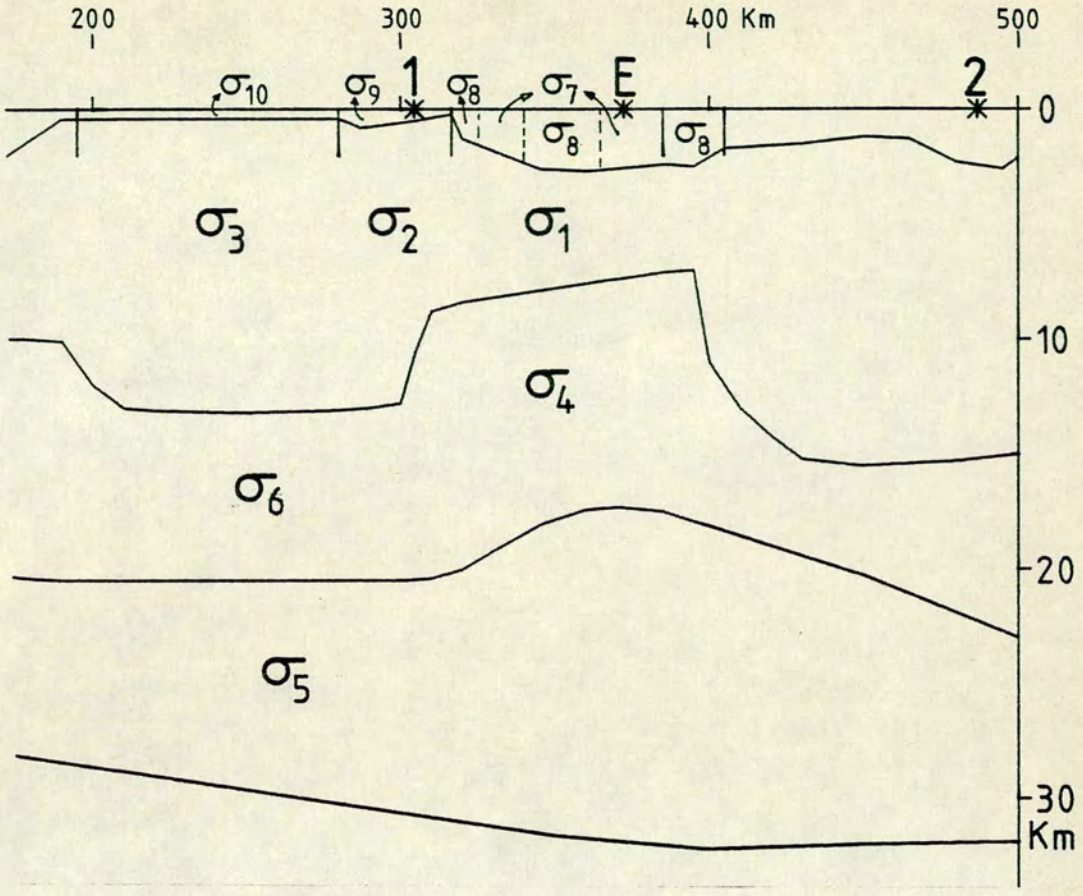

Fig. 4.13 σ parameters for the least-squares fit of ts/tp from shots 1, E → ALPHA and BETA.

TABLE 4.3 Uncertainties from least-squares and range of fixed parameters. Shots 1,E --> ALPHA & BETA; phases 'a_o', 'a_1' and 'c'.

	σ_1	σ_2	σ_3	σ_4	σ_5
least-sq. solution	0.2326	0.2440	0.2407	0.2243	0.2490
+/- 2 st. dev.	±.0045	±.0048	±.0038	±.0050	±.0088
fixed parameters					
σ_6 = 0.245 ±.015	±.0002	±.0003	±.0001	±.0002	±.0057
σ_7 = 0.33 .03	.0090	.0016	.0007	.0036	.0014
σ_8 = 0.27 .03	.0055	.0006	.0003	.0013	.0001
σ_9 = 0.33 .03	.0002	.0058	.0016	.0015	.0003
σ_{10} = 0.27 .03	.0002	.0005	.0006	.0001	.0003
final uncertainty	±.020	±.014	±.007	±.012	±.017

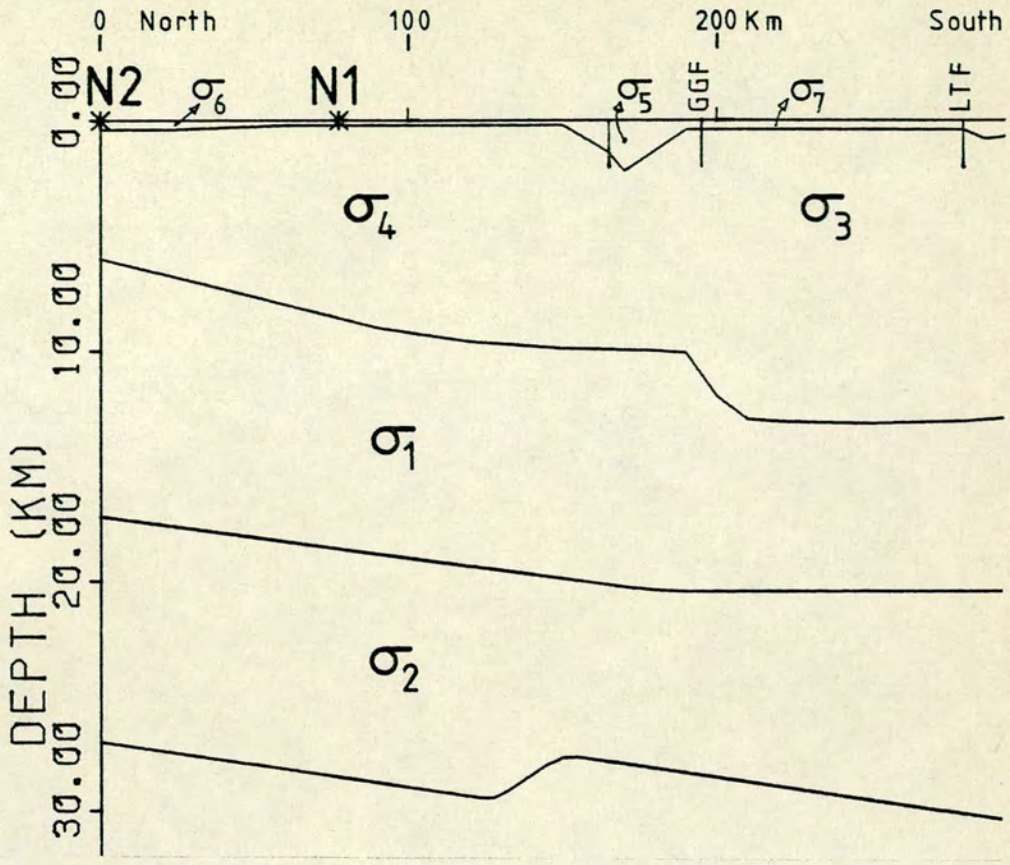

Fig. 4.14 σ parameters for the least-squares fit of ts/tp from profiles N2, N1→ALPHA.

TABLE 4.4 Uncertainties from least-squares and range of fixed parameter. Shots N2,N1--> ALPHA phases 'c' and 'e'.

	σ_1	σ_2
least-sq. solution	0.2458	0.2482
+/- 2 st. dev.	± .0022	± .0070
fixed parameters		
σ_3 = 0.241 ± .007	± .0007	± .0006
σ_4 = 0.245 .015	.0029	.0066
σ_5 = 0.30 .03	.0002	.0010
σ_6 = 0.30 .03	.0003	.0012
σ_7 = 0.27 .03	.0001	.0001
final uncertainty	± .006	± .017

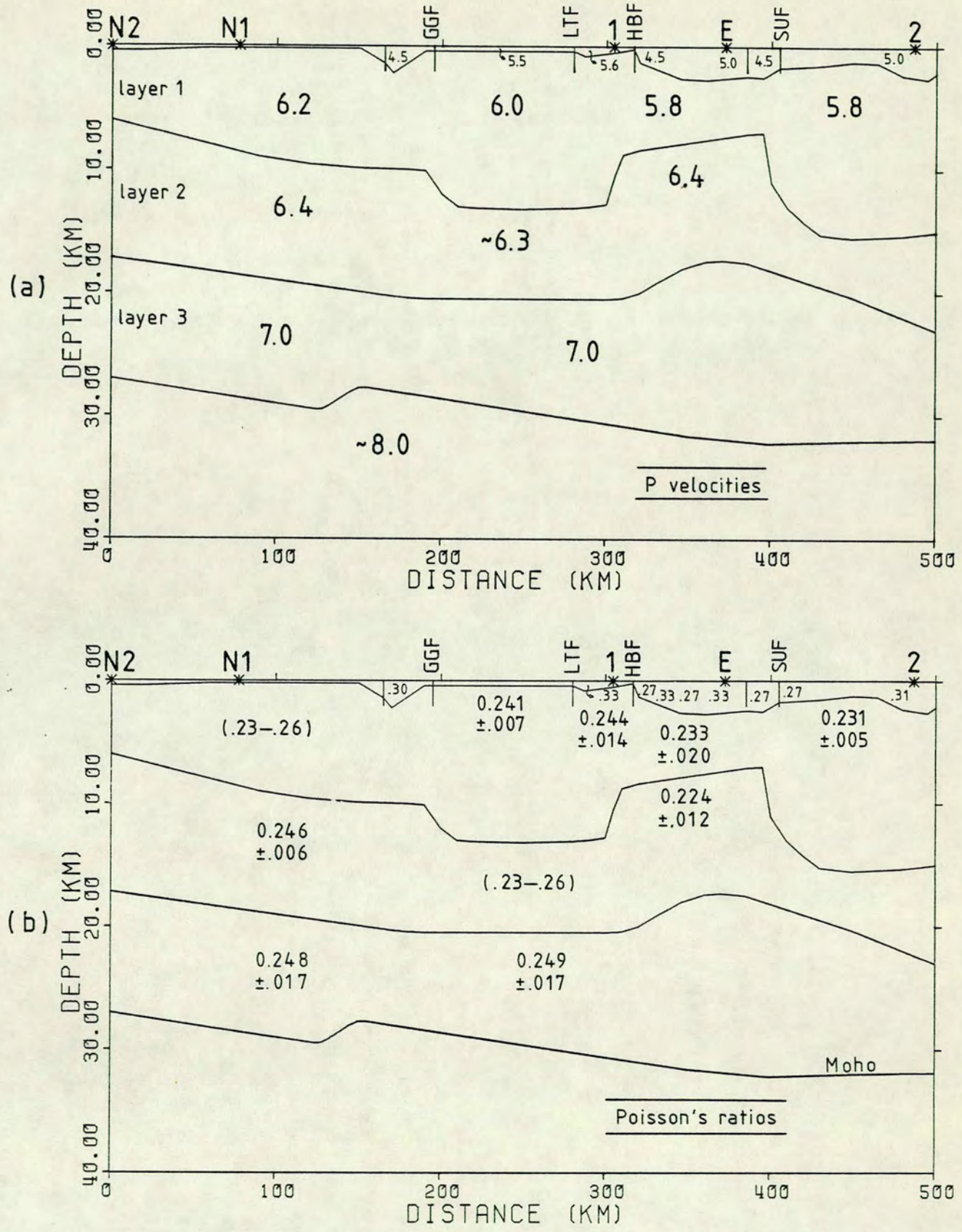

Fig. 4.15 Crustal structure of segments ALPHA and BETA.

(a) P velocities in Km/s.

(b) Poisson's ratios. Values in () are assumed range of σ. Uncertainties correspond to 2 standard deviations.

4.5.4 North of Great Glen Fault

For the northernmost part of profile ALPHA only reflected phases were used, that is, phase 'e' from N2 and 'c' from N2 and N1. No well recorded refraction 'a_o' or 'a_1' was available so that PR for layer 1 had to be fixed in the range 0.23 to 0.26. Poisson's ratio of the superficial layer were also fixed at 0.30 with the usual range of +/-0.03.

Fig. 4.14 shows the Poisson's ratio parameters determined by least-squares.

Phase 'e' (reflection from the bottom of layer 2) was recorded mainly south of the Great Glen Fault. As the data from the reflections of shots N2 and N1 have no control on the PR of layer 1 south of GGF, PR on that block had to be fixed. The value used of course was the result of the previous section, PR = 0.241 with the maximum allowed variation of +/- 0.007 (Table 4.3).

Table 4.4 shows the results with their uncertainties. It can be seen in this case that the ts/tp data itself and the uncertainty of the fixed parameter in layer 1 contribute equally to the final standard deviation of the two solutions, with the PR of the superficial layer having negligible effect. Figs. 4.4 and 4.5 show the ts/tp data for the phases used here with the theoretical curves from the solution of Table 4.4.

4.6 CONCLUSION

4.6.1 Inversion method

The method used in this chapter to obtain Poisson's ratios from ts/tp data is rather laborious. This was because of the lateral variation in the structure which gives different sub-surface structure beneath each station and shot-point. Ideally it would be desirable (for the linearization procedure) to write a program that would calculate the ts/tp derivatives automatically (see section 4.4.3), although this is not a straightforward

task.

Secondly Poisson's ratio is not the most appropriate parameter in the least-squares linearized inversion. It would have been better if K = Vp/Vs (= ratio of P to S velocities) had been chosen instead. The travel time ratio ts/tp is more linearly dependent on K than on Poisson's ratio . It is probable that no specially calculated initial model would be necessary had K been the parameter. That means it should be possible to start from Poisson's ratio = 0.25 (i.e. K = Vp/Vs = $\sqrt{3}$) in all blocks and arrive at the final model after only 2 iterations, even if the final model differed considerably from the conventional Vp/Vs=$\sqrt{3}$.

4.6.2 Discussion of results

Fig. 4.15 shows the final Poisson's ratio structure together with the P velocity model for profiles ALPHA and BETA. Except for the sedimentary layer Poisson's ratios are generally close to the conventional 0.25. The biggest deviations are found in the basement in the Southern Uplands (PR=0.231) and in layer 2 beneath the Midland Valley (PR=0.224). The upper crust seems to have Poisson's ratios less than 0.24 south of the Highland Boundary Fault and greater than 0.24 north of it.

It is known that Poisson's ratio depends on many factors such as mineral constituency (e.g. Christensen & Fountain 1975), crack and porosity (e.g. O'Connell & Budiansky 1977), fluid saturation and pore fluid pressure (e.g. Nur 1972). In the superficial layer mineralogy is much less important than the other factors. For depths greater than about 2 Km chemical constitution starts to be important but porosity and pore pressure can still affect Poisson's ratio very much. In layer 2, on the other hand, most of the cracks and pore spaces are closed and Poisson's ratio should depend more on mineral composition than on porosity and cracks.

Layer 2 with P velocity of 6.4 Km/s has been interpreted as a

continuation of the Lewisian granulite formation of NW Scotland (Smith & Bott 1975, Hall & Al-Haddad 1976 and Bamford et al. 1977). The Poisson's ratio of layer 2 (0.246+/-.006) north of the Great Glen Fault is consistent with this interpretation in the sense that it agrees with the value calculated from the ratio of apparent velocities determined by Smith & Bott (1975) for the same layer further north on a profile between Cape Wrath and Shetland. Their P and S velocities of 6.40+/-.09 and 3.76+/-.05 give PR = 0.236+/-.015 . On the other hand, beneath the Midland Valley the PR (0.224+/-.012) seems definetly lower than the value north of the Great Glen. This difference (about 2.7% in terms of S velocity) is likely to imply different petrological composition between these two parts of layer 2. One possible petrological model to explain such a difference is a higher content of quartz beneath the Midland Valley which would decrease the Poisson's ratio (Christensen 1965, Christensen & Fountain 1975). The last two authors showed that the lower crust composition can be modelled in terms of granulite-facies rocks and calculated seismic velocities and Poisson's ratios for four major three-component mineral assemblages typical of granulite-facies rocks. Out of these four mineralogical models only one (quartz+plagioclase+pyroxene) can give the P velocity and Poisson's ratio for layer 2 as shown below :

P vel. = 6.4 Km/s, σ = 0.246 (north of Great Glen)

27% quartz, 69% plagioclase(29%An) and 4% bronzite(pyroxene)

P vel. = 6.4 Km/s, σ = 0.224 (Midland Valley)

38% quartz, 56% plagioclase(29%An) and 6% bronzite(pyroxene)

The absolute percentages above are not very reliable because of uncertainties in the method used to calculate aggregate velocities from

single crystal data and also because of uncertainties in extrapolating single crystal velocities to high pressures (Christensen & Fountain 1975). Nevertheless these uncertainties are less important when only changes in mineralogy (rather than actual mineral composition) are considered. Although other different mineral assemblages not considered by Christensen & Fountain may also reproduce the LISPB results, measurements of PR by Christensen (1966) on metamorphic rocks also indicate that a higher percentage of quartz is necessary to give the values of PR = 0.224. This means that an increase of 10% in quartz in the Midland Valley is a reasonably good explanation for the lower Poisson's ratio, although other petrological models different from granulite facies may be possible. It is not clear if such difference in Poisson's ratio implies that the pre-Caledonian basement in the Midland Valley has a different origin from the one further north or whether it has the same origin but has been subjected to different grades of metamorphism and transformation during the Caledonides.

It is clear from the discussion above that the Poisson's ratios determined for the LISPB profiles will considerably reduce the number of petrological interpretations possible for the crust in Northern Britain.

Two applications were made of the Poisson's ratio structure determined in this chapter : a study of the PmS Moho reflection from shot-point N1 (chapter 5) and calculation of accurate epicentres for the Kintail earthquake series of August 1974 using P and S arrivals (chapter 6).

CHAPTER 5

PS MOHO REFLECTION AND LOWER CRUSTAL STRUCTURE

5.1 INTRODUCTION

PS reflections from the Moho are seldom observed in seismic refractions for two main reasons: a) PS amplitudes are very much reduced if the Moho is a gradational transition between lower crust and upper mantle (Fuchs 1975), and b) PS amplitudes are largest on the radial-horizontal component and very weak on the vertical (Jacob & Booth 1977). (The simplified notation PS and PP from Fuchs 1975 is adopted instead of the more explicit PmS and PmP).

A clear PS reflection was observed in the LISPB experiment from shot-point N1 recorded in section ALPHA (Fig. 5.1). It was observed only on the radial component. Fig. 5.2 is a record section where PP (or 'c') and PS Moho reflections are indicated. The PS phase is recognized as such by having about the expected travel time and apparent velocity and by the particle motion (Fig. 5.3) which shows that it arrives as S waves. The ground motion of the PS phase is linear because of its steep angle of incidence. It is assumed that the signal observed is a true Moho reflection and not a PPS mantle headwave as that is usually at least one order of magnitude smaller than the reflection proper (Fuchs 1975).

The observation of a PS phase is an indication of a very sharp Moho transition. If the Moho transition zone is assumed to be at most 1/4 of the P wavelength so that reasonably high PS amplitudes can be observed (Fig. 8 of Fuchs 1975) then the transition zone should be less than 0.5 Km thick (PS frequency of 3.2 Hz and lower crust P velocity of 6.7 Km/s). The amplitudes observed here were too scattered for a more direct determination of Moho thickness. The observed ratio of average PP amplitude (vert.) to

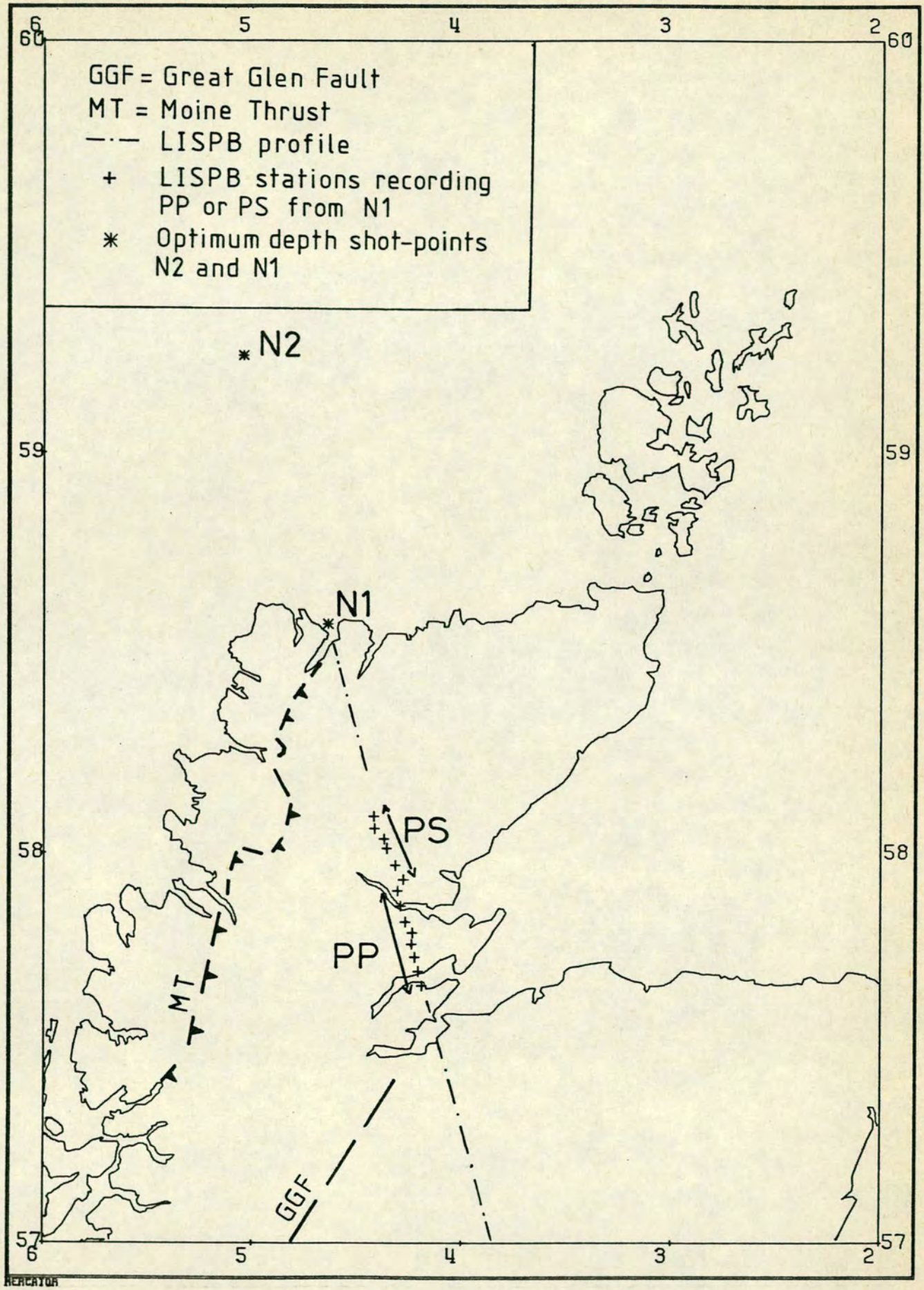

Fig. 5.1 Location of stations and shot-points.

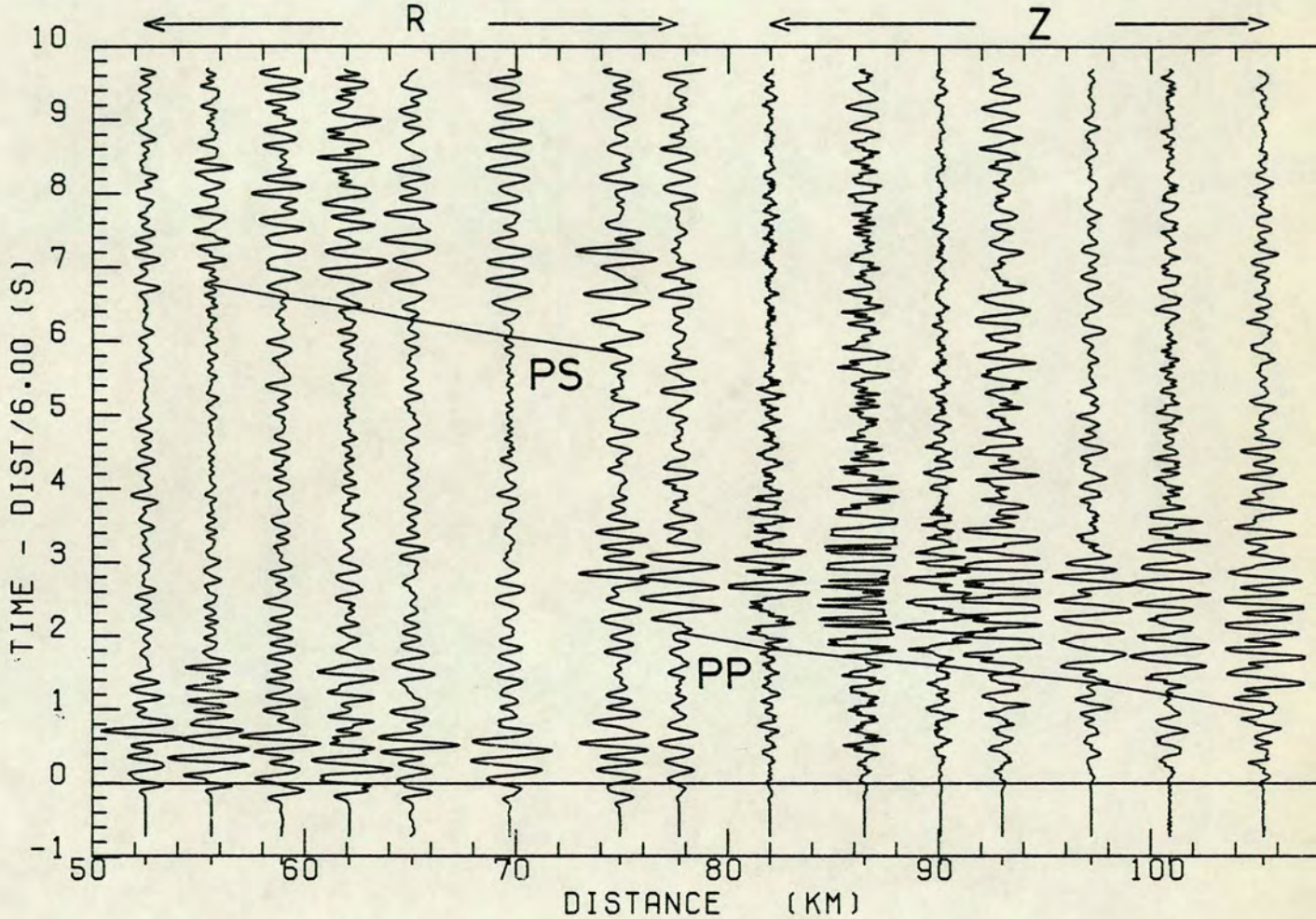

Fig. 5.2 Record section showing PS and PP Moho reflections from shot-point N1. Radial-horizontal component up to 78 Km (slightly low-pass filtered). Unfiltered vertical component from 82 to 105 Km. The curves show the picked onsets. Normalized amplitudes.

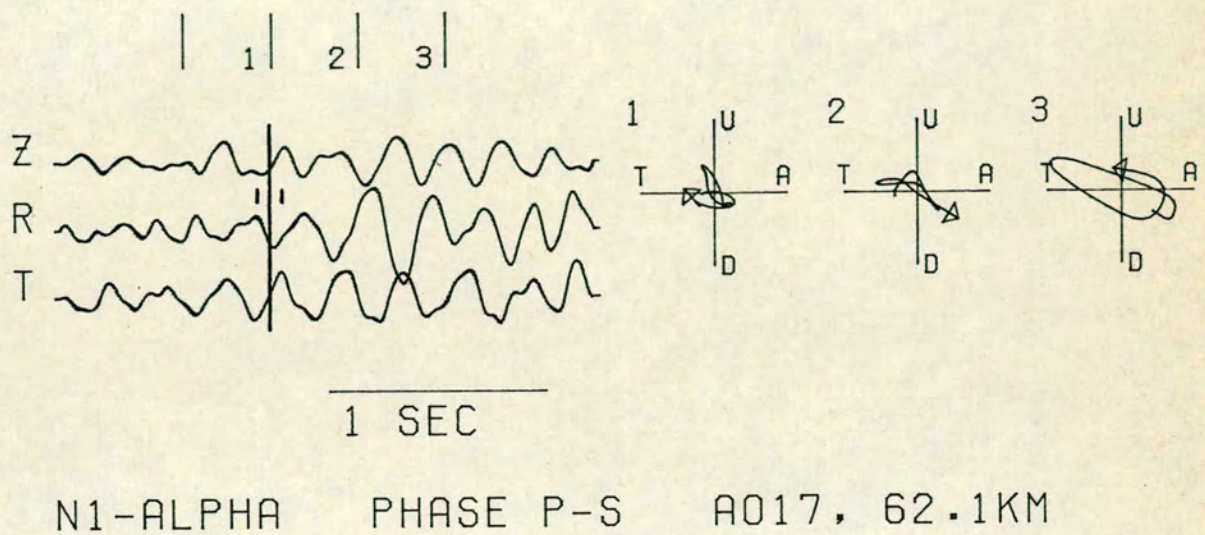

Fig. 5.3 Three components and particle-motion of the PS wave recorded by station A17 at 62.1 Km distance. Numbers on the top left of the particle-motion diagrams refer to the time windows on top of the seismograms. Z = vertical, R = horizontal-radial, T = horizontal-transverse, U = Up, D = Down, T = Towards, A = Away from the shot.

average PS amplitude (hor.) was 3.7 (+/- a factor of 2).

The crustal structure in the area has already been studied (Bamford et al. 1977, 78; and chapter 4) although the lower crust is only known schematically. Travel times of PS and PP reflections were here analysed together to investigate details of the lower crust.

5.2 PS AND PP ARRIVAL TIME

The stations recording the PS phase were situated directly on metamorphic and igneous rocks (siliceous granulites of the Moine series with granite and granodiorite intrusions) not covered by any low velocity sedimentary layer. It was observed that the PS signal correlated well across the record section (Fig. 5.2) and this was probably due to the absence of sedimentary layers that might change the waveform by reverberations and also to the periodicity of the source signal from an optimum depth shot. The apparent PS wave-length was 2.6 Km and the station spacings varied from 3.0 to 5.2 Km.

Arrival times of the PS phase were picked after summing the records, with appropriate delays between each station, to improve the signal-to-noise ratio (Fig. 5.4), i.e., the CORSUM method described in section 3.1.1 was used. The delays between the stations were initially found by correlating the first two cycles of each record with a reference record (chosen as the one at 62.1 Km distance) and summing all records with weights proportional to their signal-to-noise ratio. The process was repeated to get better delays using the previous sum as reference for correlations. The new delays were identical to those of the first iteration.

Phase changes in the PS signal occur upon reflection at the Moho particularly near the critical angle. Nevertheless the distance range of the observed PS waves was short enough (20 Km) for relative differences in

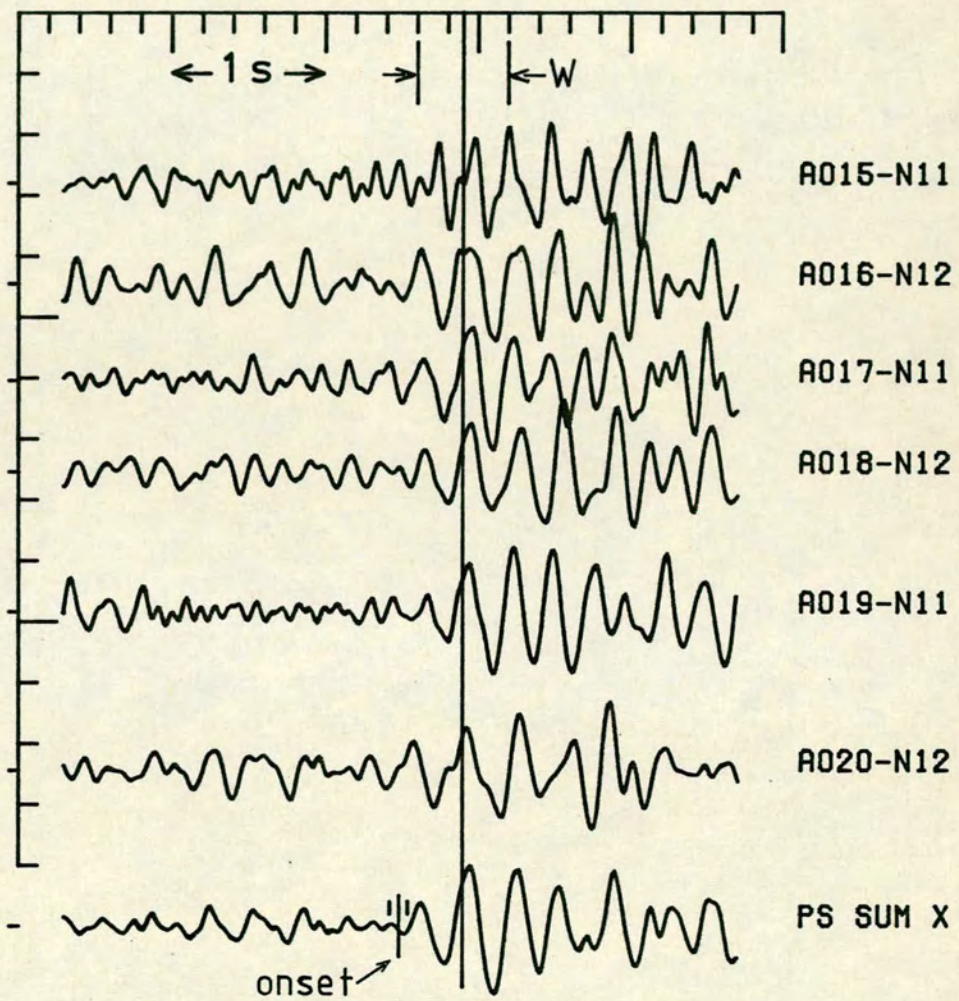

Fig. 5.4 Aligned PS records, radial components. Delays for alignment were obtained by correlating the first two cycles with the window W. The summed record is shown in the bottom with the two small lines on each side of the onset indicating its estimated uncertainty of $\pm$ 0.06 s .

such phase changes to be neglected. Computation of synthetic seismograms showed that errors in travel times introduced by neglecting those phase changes and assuming perfect coherence of the signal across the observed distance range were smaller than +/- 0.03s which is less than the estimated error in the PS onsets of +/- 0.06s (Fig. 5.4). Summation of seismograms (CORSUM) was also used with some of the PP records (from 90 to 105 Km, Fig. 3.2). The others were picked by simple visual examination. Again there are phase changes in the PP signal because of near critical reflection, but they are not important compared with the estimated uncertainties of +/-0.1s for all PP onsets.

5.3 TRAVEL TIME MODELLING

PP reflections recorded at distances of 78 to 105 Km come from the same part of the Moho as the PS reflections recorded at 55 to 75 Km. So both phases could be used together to model the lower crust structure in that specific area.

The 3-layered crustal structure determined by Bamford et al. (1977, 1978) was used as a starting model for P waves (Fig. 5.5). Poisson's ratios given in chapter 4, Fig. 4.15(b) were used. The two upper layers were assumed to be correct and only the lower crust was changed to find a model which best fitted the PP and PS times. Travel times were calculated with ray-tracing using a program written by I. Psencik based on the method of Cerveny et al.(1974). The travel time for each station was linearized with respect to the parameters in the initial model and a new model was determined by mormal least squares, using the program CURFIT described in appendix D. An iterative procedure was followed with two iterations only being enough for convergence.

Initially the Moho was taken to be horizontal and P velocity for the bottom layer (α) and Moho depth (h) were determined. The obtained model,

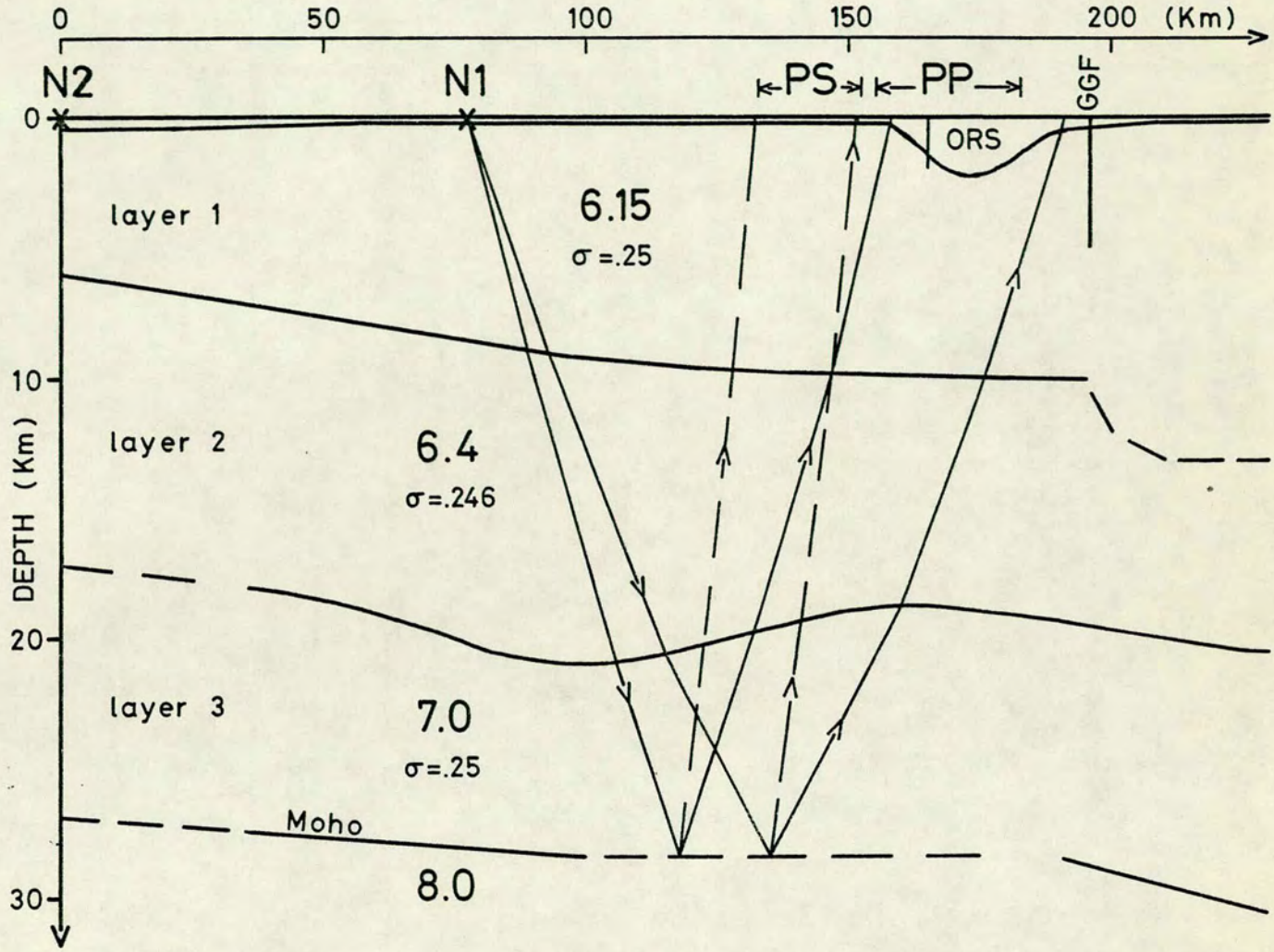

Fig. 5.5 Starting model of the crustal structure showing the ray paths of PP and PS reflections. ORS = Old Red Sandstone sedimentary basin, GGF = Great Glen Fault.

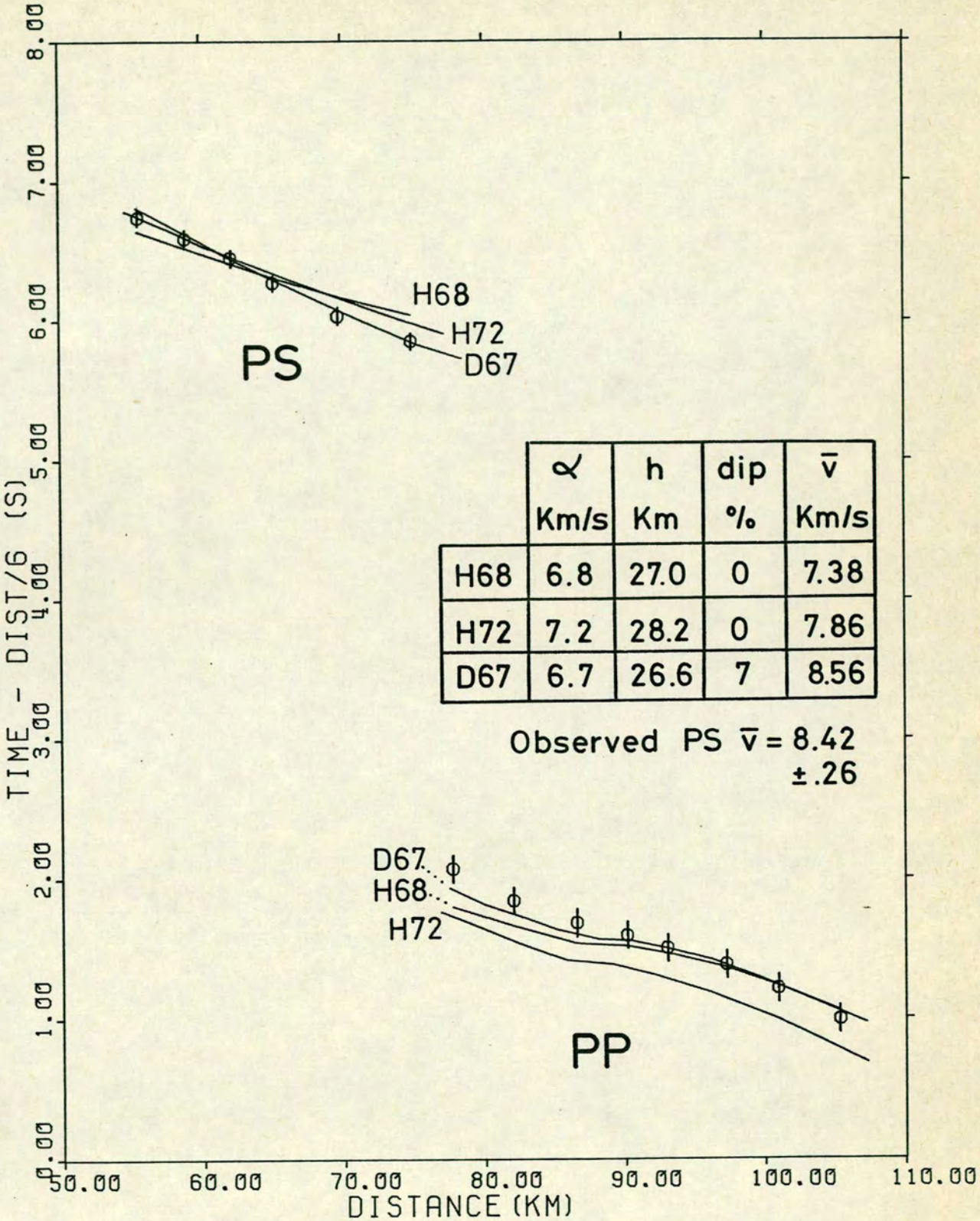

	α Km/s	h Km	dip %	$\bar{v}$ Km/s
H68	6.8	27.0	0	7.38
H72	7.2	28.2	0	7.86
D67	6.7	26.6	7	8.56

Fig. 5.6 PS and PP travel time data with results of various models of the lower crust. α = lower crust P velocity, h = Moho depth (at coord. 130 Km), $\bar{v}$ = PS apparent velocity. All models have Poisson's ratio 0.25 in the lower crust.

called H68 with α = 6.8Km/s and h = 27.0Km (Fig. 5.6) does not reproduce the correct PS apparent velocity. H68 has an apparent velocity of 7.38 Km/s much lower than the observed 8.42+/-0.26 Km/s. Because of the slight interdependence of velocity and depths in crustal models the velocity of the lower crust was arbitrarily fixed at 7.2 Km/s in an attempt to increase the apparent PS velocity. In this case the best fitting depth of h = 28.2 Km was found (model H72) but the apparent velocity was still only 7.86 and the fit was considerably worse as Fig 5.6 shows. Poisson's ratio in the lower crust does not affect the PS apparent velocity very much. For example if σ in the bottom layer was 0.23 (as low as the σ model of Fig. 4.15(b) allows) PS apparent velocities would not increase by more than 0.02 Km/s and the lower crust parameters would not change significantly. Poisson's ratio in the upper layers have equally small effects.

One parameter that could produce the observed PS apparent velocity is a dip in the Moho towards the shot. The best model with a dipping Moho was found to be α = 6.7 Km/s(+/-.1), h = 26.6 Km(+/-.3) and dip = 7%(+/-1.5) towards the north, model D67 Fig. 5.6 .

5.4 Pn DATA

The Moho discontinuity in northern Scotland as determined by the LISPB experiment generally dips southwards contrary to the dip of model D67 above. Nevertheless a discontinuity in the regional dip in that area had already been suspected by Bamford et al.(1978) on the basis of Pn time-terms. Fig. 5.7 shows Moho depths determined from time-terms of Pn waves from the LISPB shot-points N2, N1 and 1. The time-terms were recalculated with the following parameters taken from the model of Bamford et al. : Pn mantle velocity of 8.0 Km/s; Moho depth of 27.5 Km at shot-point N2 and 32.0 Km at shot-point 1 (offsets taken into consideration); lower crust P velocity of 7.0 Km/s except from horizontal coordi-

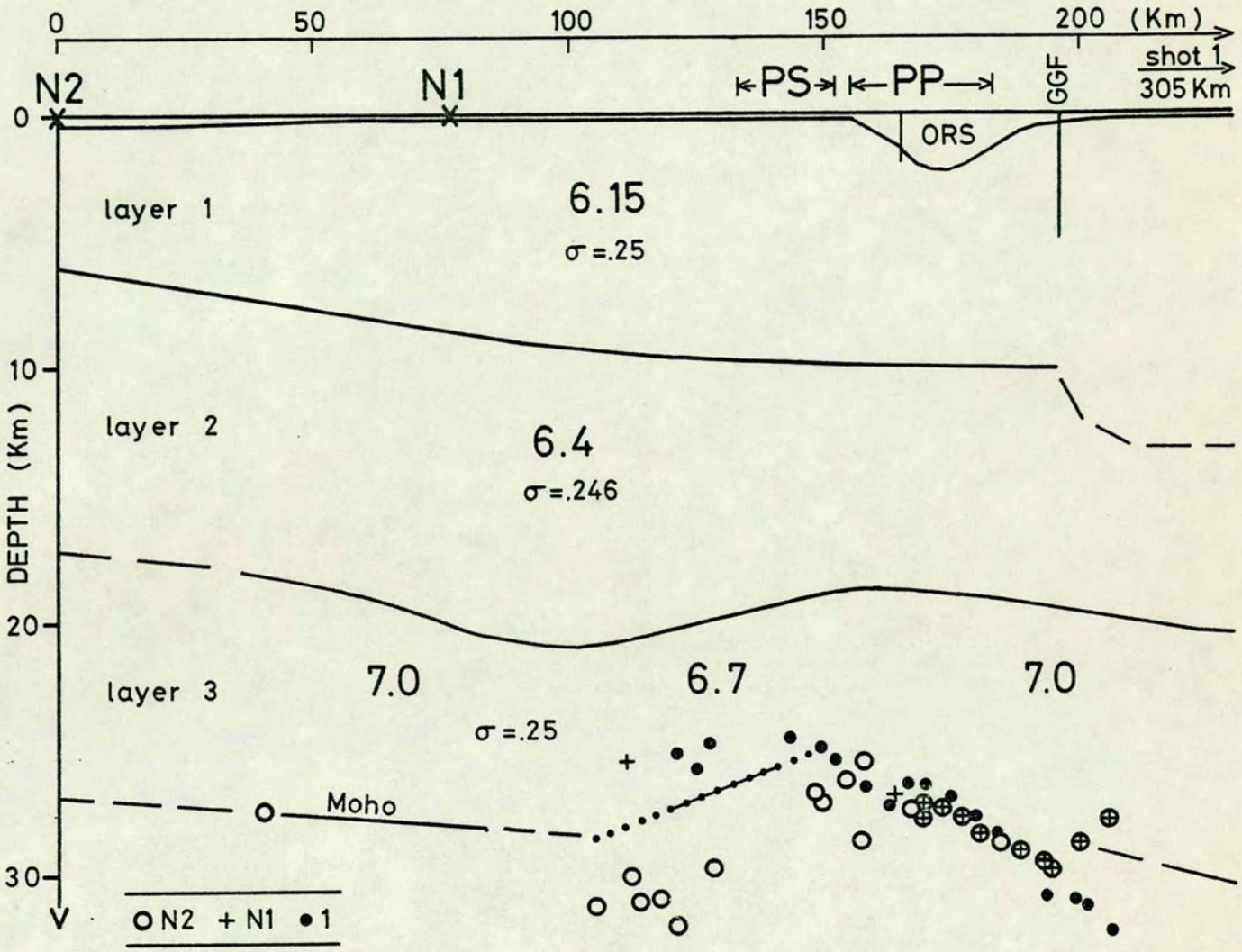

Fig. 5.7 Moho depths determined from Pn time-terms. Line with dots indicates common PP and PS reflection points from model D67.

nates 90 to 160 Km where a velocity of 6.7 from our model D67 was used. The time-term of shot-point N1 was found with the condition that stations recording Pn from both N2 and N1 should have equal time-terms. All points in Fig 6.7 were plotted with the appropriate offsets between station and Moho. It can be seen that the Pn time-term depths from N2 have a very clear step between horizontal distances 120 and 150 Km which agrees fairly well with the location of the dip determined from PS reflection. (It should be remarked that if the Pn time-term depths had been calculated with a constant velocity throughout the lower crust that step would be bigger by about 1 Km). Shots at N1 and 1 do not show any clear step but seem to show some kind of discontinuity in the slope around horizontal coordinate 150 Km. This last "discontinuity" can be seen more clearly in the seismic section 1-->ALPHA of Bamford et al.1978.

Time-term depths are usually very scattered partly because of crustal inhomogeneities and partly because of the non-uniqueness of velocity-depth determinations. This case is no exception with Moho depths having uncertainties of about +/- 1 to 2 Km. Nevertheless the localized dip of 7% was suggested by two independent sets of data, that is, PS and PP phases from shot-point N1 and Pn phase from N2 recorded at different stations (and to some degree by Pn from shot-point 1). So, in spite of the scatter in Fig 5.7 there is good evidence for the existence of a short localized dip in the Moho towards the north superimposed on a regional dip south.

5.5 LATERAL VARIATIONS

The evidence for the localized dip of 7% (= 4^{o}) is based mainly on the high apparent velocity of the PS phase assuming that the P (and S) velocities in all 3 layers of the crust did not vary laterally. This is not necessarily correct as refraction studies only give averages of velocities in each layer and local variations from the model of Fig. 5.5 cannot be

excluded. A few examples of strong lateral variation, with a horizontal Moho, were tried as alternative explanations for the high PS apparent velocity.

a) A horizontal velocity gradient was introduced in layer 1 under the stations recording the PS waves. The resulting model had an S velocity in layer 1 increasing from 3.4 to 3.8 Km/s over a horizontal distance of 20 Km (and lower crust α = 6.7, h = 26.6 Km). This corresponds to an increase in P velocity from 5.8 to 6.5 Km/s for a constant Poisson's ratio (or a decrease in Poisson's ratio from 0.29 to 0.20 for a constant P velocity) throughout the 10 Km thickness of layer 1. This is a rather big variation in velocity and there is no evidence of an anomalous upper crust either from surface geology or from the Pg phase of shot-point N1.

b) If a velocity gradient in layer 3 instead of the upper layer is considered the S velocity variation would have to be from 3.9 to 4.3 Km/s (h = 27.5 Km) corresponding to a P velocity from 6.7 to 7.5 Km/s spread over 30 Km. This velocity also seems rather high but would nevertheless reduce the step in the Pn time-term depths from shot-point N2 from 5 to 1.5 Km.

c) Another possibility in terms of lateral variation is to place the dip not in the Moho but in some other discontinuity in the crust (in a way this is equivalent to horizontal gradient). For example if the Moho is taken to be horizontal and a dip in the interface between layers 2 and 3 is introduced, this dip would have to be around 17^{o} (30%) over 20 Km horizontal distance to produce the high PS apparent velocity. Such a high slope does not seem to be allowed by the data of Bamford et al.(1978).

The examples above indicate that the localized dip of model D67 is likely to be real although one cannnot at this stage exclude other forms of lateral variation as alternative explanations.

5.6 CONCLUSION

It is difficult to determine Moho topography because of the usual non-uniqueness of velocity depth determination. Absolute Moho depths determined from Pn (and PP) data have usually an uncertainty of at least +/- 1 to 2 Km. Analysis of PS waves seems to provide good control on Moho dips mainly because its apparent velocity is rather insensitive to Poisson's ratio and also to slight lateral variations in velocity. For example a PS wave from shots in the North Minch Basin recorded by a station at Cape Wrath (NW Scotland, Jacob & Booth 1977) has an apparent velocity lower than the fitted horizontal plane-layer model (Booth, private communication) which seems to indicate that the Moho in that area is dipping south in general agreement with the regional time-term map of Bamford et al.(1978).

PS waves offer very little control on determination of Poisson's ratio and unfortunately could not be used to check the Poisson's ratio model of Fig. 4.15(b). On the other hand this means that only an approximate knowledge of S velocities is sufficient for PS waves to be used in determining lower crustal structure and especially Moho topography. Unfortunately PS waves are extremely rare in refraction work and if they are to be searched for, not only horizontal components and large density of station/shots (spacing < 3 Km) should be used but also low frequency sources (~3 Hz) seem to be necessary to produce strong reflections from the Moho.

CHAPTER 6

KINTAIL EARTHQUAKE SERIES

6.1 INTRODUCTION

During August 1974 a swarm of about 20 earthquakes occurred in the Kintail area of NW Scotland, the biggest of them with magnitude ML = 4.4 . These earthquakes were all recorded by the permanent Lowlands Seismic Network (LOWNET) as well as by a temporary 4-station array in the Grampian Highlands (ATHOLL NET, Fig. 6.1). By a fortunate accident one earthquake of that series was also recorded by the 60 LISPB stations while positioned on profiles ALPHA and BETA at 6-7 Km interval forming an array about 400 Km long. Fig. 6.1 shows this earthquake (henceforth referred to as KEQ) and all the recording stations (only LISPB stations with clear first P arrivals are shown).

Kaminsky et al.(1976) determined the KEQ hypocentre as well as a plane-layered model fitting the P arrivals (first and secondary P arrivals were used). The purpose of this study was to relocate KEQ using P and S arrivals with the LISPB crustal model determined by Bamford et al.(1978) and the Poisson's ratio determined in chapter 4. Once the KEQ location was known it was used as a master event to locate other earthquakes of the Kintail series.

6.2 DETERMINATION OF KEQ EPICENTRE

6.2.1 The crustal model

The crustal structure along the LISPB profile is well determined, Fig. 4.15(a) and Bamford et al.1977, 78. For the LOWNET stations on the other hand a crustal model more in accordance with the LISPB results and allowing for lateral variation had to be calculated. This was done by using LISPB

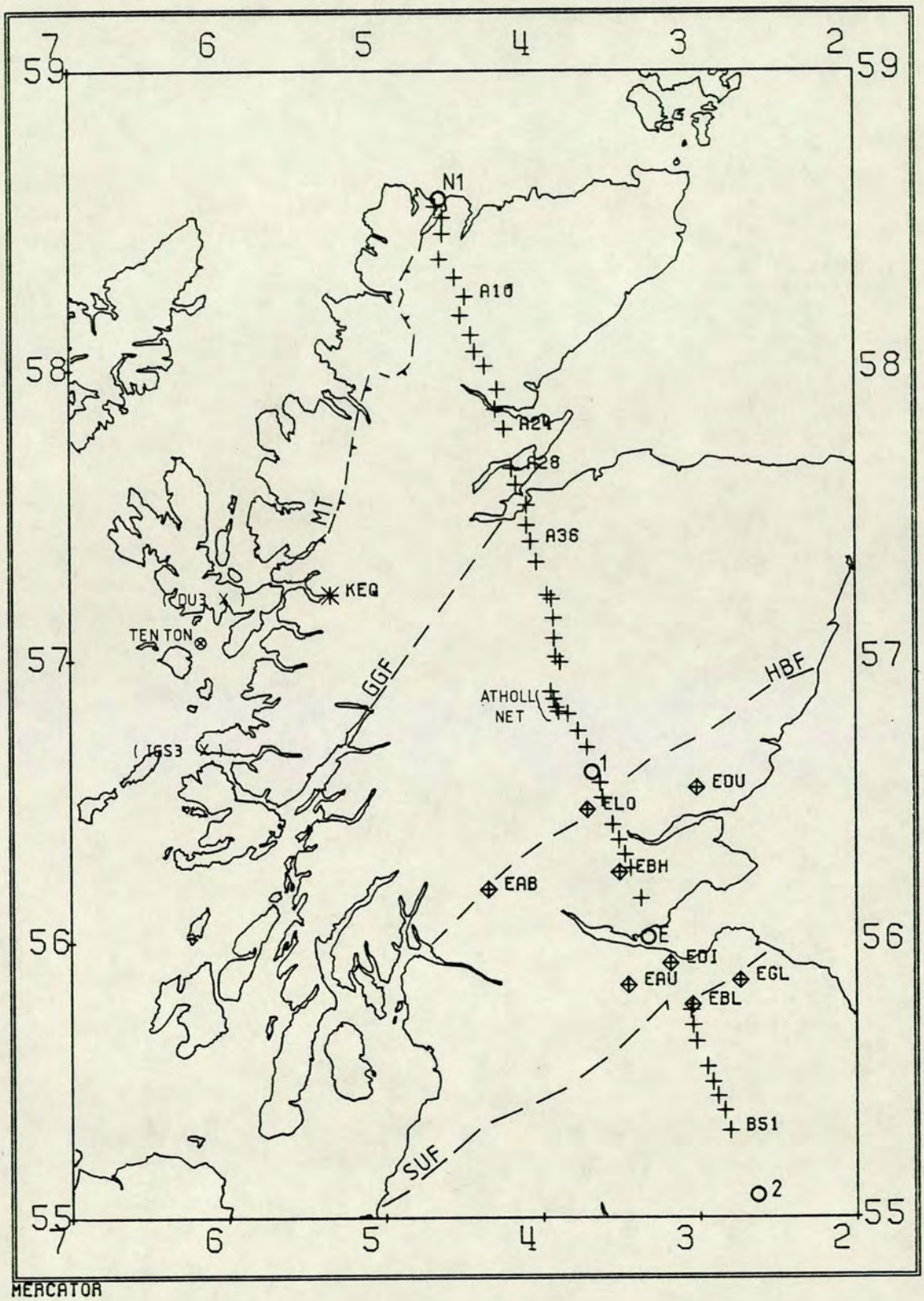

Fig. 6.1 Map of stations. MT = Moine Thrust, GGF = Great Glen Fault
HBF = Highland Boundary Fault, SUF = Southern Upland Fault.

\+ LISPB stations that recorded KEQ.
⊕ permanent LOWNET stations.
O LISPB shot-points N1, 1, E and 2.
(X temporary stations not operating in 1974)

shots E and 1 and a 10 ton explosion fired off the west coast of Scotland (part of the 10 ton series started by Jacob & Willmore 1972). The P velocities of the various layers were taken according to the LISPB results for the Midland Valley, that is : a low velocity superficial layer of about 4.6 Km/s, an upper crust of 5.8 Km/s, a mid crustal layer of 6.4 Km/s, a lower crust of 7.0 Km/s and Pn velocity of 8.0 Km/s. Travel times from shots 1 and E fix the thickness of the first two layers for every LOWNET station. The thickness of the 6.4 Km/s layer was taken equal to the LISPB profile. The thickness of the lower crustal layer (and Moho depth) was derived from the travel times of the 10 ton shot. The 10 ton shot was chosen because it is near the KEQ epicentre and has very clear Pn arrivals all over LOWNET. (The Pn time-term at the 10 ton shot-point was taken as 2.94 s from the time-terms of two nearby temporary stations (DU3 and IGS3, Fig 6.1) used in an earlier refraction work by Smith & Bott 1975). This LOWNET structural model with lateral variations was tested by locating explosions fired off the west coast of Scotland giving on average better locations than other homogeneous crustal models (the location errors were smaller by an average of 30%).

The computer program used to relocate the KEQ epicentre was FAMG written by Crampin 1970, 1973. The program accepts a maximum number of 3 layers over a halfspace with constant velocity within each layer and different layer thicknesses for each station. For this reason the first two layers of the structure described above (superficial and upper crustal layers) were substituted by an equivalent single layer with P velocity 6.0 Km/s having the same time-term for the 6.4 Km/s refractor. This alteration did not affect the epicentre determination as there were no upper crustal phases from KEQ (Kaminsky et al. 1976).

While the structure at the stations is well defined that of the epicentre is not so well Known. Nevertheless it can be reasonably assumed

on geological grounds that the crustal structure should be similar to that of the LISPB profile north of the Loch Tay Fault (all Moine metamorphic formation) and that a 3 layered crustal model with velocities 6.0, 6.4, and 7.0 Km/s is suitable for the epicentre. The 6.4 Km/s which has been interpreted as a continuation of the Lewisian Granulites (Smith & Bott 1975, Bamford et al. 1978) is assumed to get shallower towards the NW. For this reason its depth at the epicentre was taken as 7 Km equal to the stations around A10 (Fig.6.1). The other two layers (6.4 and 7.0 Km/s) were taken with thicknesses of 12.8 Km each so that the total crustal thickness (32.5Km) would give a Pn time-term of 2.85 s in agreement with the time-term of DU3, which also agrees with the time-term of the nearest LISPB station A36 (Fig 6.1).

The S velocities were taken by converting the P velocities with the Poisson's ratio determined in chapter 4 assuming that the Poisson's ratio along the LISPB segment ALPHA can be extrapolated for the rest of the Highlands. For the upper crust an average Poisson's ratio of 0.245 was taken. 0.246 was used for the second layer and 0.25 for the lower crust. For the upper mantle the nominal value of 0.25 was assumed. The lower values of Poisson's ratios in the Midland Valley (segment BETA, Fig. 4.15(b)) did not affect the results because no S arrivals from that part of the profile were used to locate KEQ.

6.2.2 The data

First arrivals only of P and S waves were used in the KEQ epicentre determination. First P arrivals were usually accurate to +/- 0.03s or better. S arrivals (SV and SH) were read with the help of particle-motion plots as described in chapter 3 (after rotating the horizontals to get true radial and transverse components) and only those with estimated accuracy of +/- .20 s or better were used. This limited the S arrivals to only 13

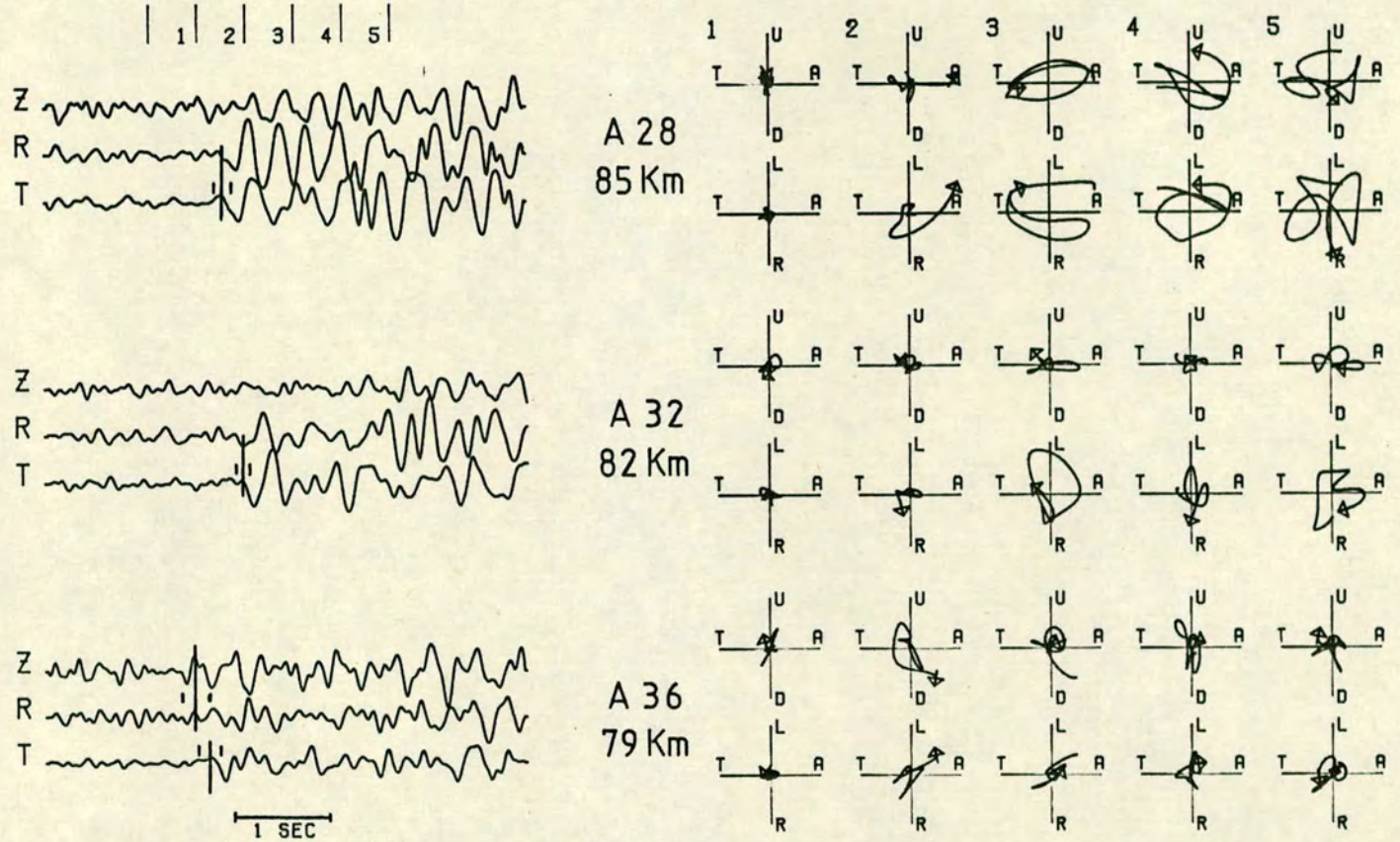

Fig. 6.2 Examples of S onsets from KEQ.

stations in segment ALPHA, mostly crustal refractions. Fig. 6.2 shows three examples of particle-motion plots used to pick S onsets. On the whole the quality of the S arrivals was comparable to those of the LISPB explosions.

Secondary P arrivals were not used because generally they are not refractions but wide-angle reflections and the FAMG program only works with refractions. Secondary P arrivals can be useful in controlling the focal depth of the event, provided the correct phases are identified. In this case the focal depth was controlled by the relative difference of arrival times between the crustal P phase and the upper mantle Pn phase. The use of S wave arrivals also helped control the focal depth by better restraining the origin time and so removing much of the trade-off between depth and origin time.

6.2.3 The KEQ solution

The FAMG program holds the focal depth fixed and solves for the epicentre latitude, longitude and origin time. The depth is then chosen as the one with the minimum arrival time residuals. Initially the program was run with only the P waves to determine the correct phases, that is, for every depth the program would identify the phases treating them as first P arrivals. Having identified the correct phase for each station (phase 'a_1' up to about 120 Km and Pn for distances greater than about 130 Km) these phases were fixed and S arrivals were included in the data. Fig. 6.3(a) shows the variations with depth of the epicentre parameters when only P waves were used. Fig. 6.3(b) shows the solution when P and S arrivals were used and it can be seen that the minimum in the arrival time residuals is much sharper than the previous case. The variations of the epicentre parameters with depth are also smaller when S waves are included. Table 6.1 shows the KEQ epicentre solution.

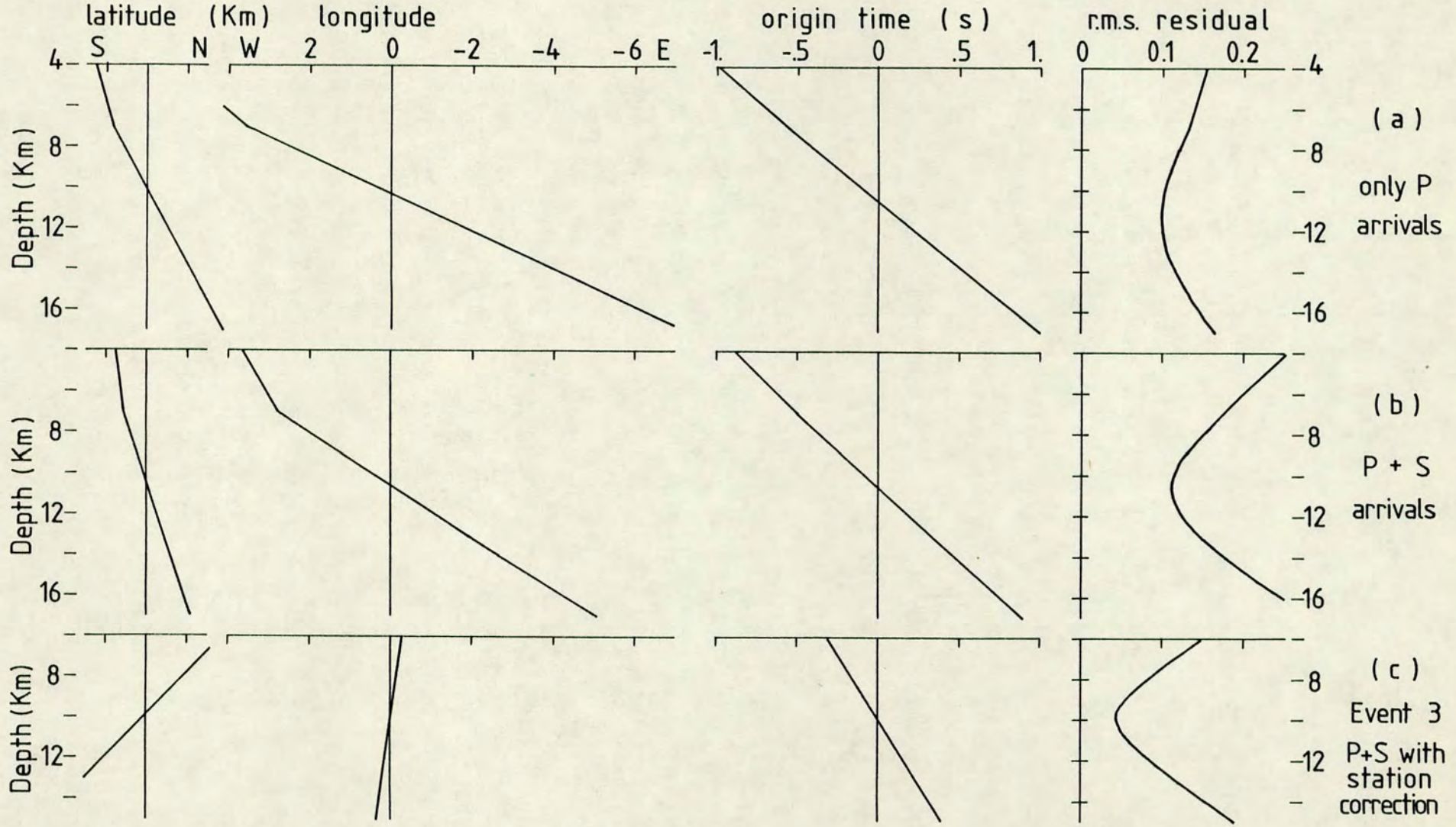

Fig. 6.3 (a),(b) Variation of KEQ epicentre solution with depth.
(c) Variation of epic. solution for event no. 3, with station corrections.

Table 6.1

Epicentre solution for KEQ (recorded by LISPB)

Date 6/8/74, Origin time: 18h 17min 36.93s +/- .04s
latitude : 57.2271° N +/- 0.16 Km
longitude: 5.3381° W +/- 0.40 Km
Depth : 10.6 Km
National Grid : 198.5 Km E, 820.1 Km N

FAMG program : 51 P and 17 S arrivals,
largest residual = 0.29 s,
r.m.s residual = 0.11 s .

Table 6.2

Effect of model variations on KEQ epicentre.

Model	Structure modification	Offset(Km) lat.	Offset(Km) long.	Depth (km)	Res. (s)
KEQ	- none -	0.00	0.00	10.6	0.11
A1	All Poisson's ratios = 0.25	0.21	-.94	11.2	0.11
A2	All Poisson's ratios = 0.24	-.49	1.74	9.1	0.14
A3	All Poisson's ratios = 0.26	0.92	-3.66	13.3	0.14
B1	Layer 2 P vel. = 6.5 Km/s instead of 6.4	-.22	0.62	11.0	0.14
B2	Layer 2 P vel. = 6.3 Km/s	0.20	-.42	10.1	0.11
C1	Pn vel. = 7.95 Km/s instead of 8.00	-.26	0.31	11.3	0.11
C2	Pn vel. = 8.05 Km/s	0.24	-.23	9.8	0.13
D1	Layer 1 1Km shallower north of and 1Km deeper south of GGF	-.95	0.16	10.5	0.11
D2	Layer 1 1Km deeper north of and 1Km shallower south of GGF.	0.94	-.10	10.8	0.12
E1	Moho depth increased by 2Km (Pn time-term changed by 0.14s)	0.08	-.15	12.5	0.12
E2	Moho depth decreased by 2Km	-.03	-.01	8.9	0.11

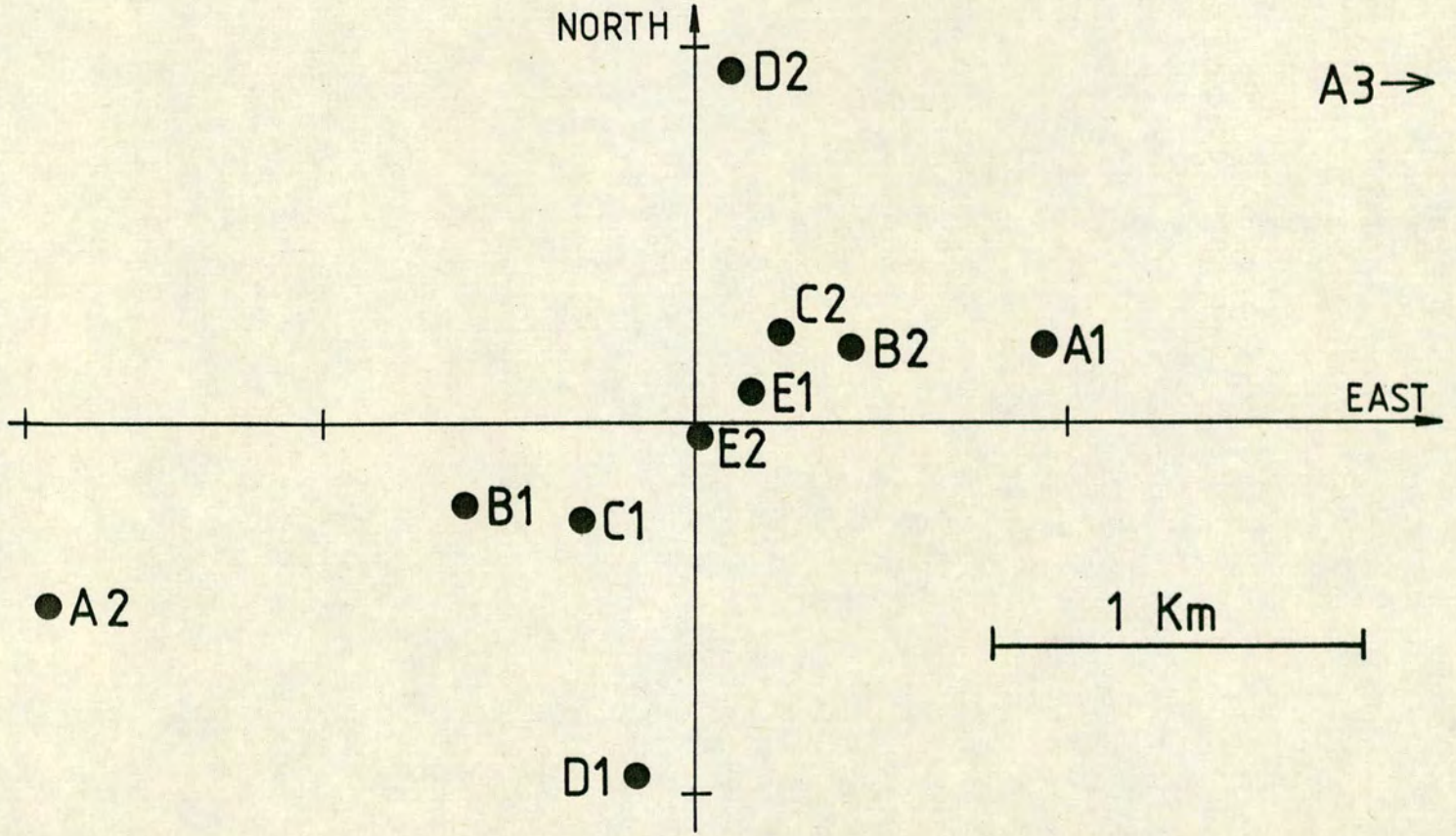

Fig. 6.4 KEQ epicentre solutions for the crustal models shown in Table 6.2 .

This epicentre is only about 0.7 Km east of the solution of Kaminsky et al. 1976, whereas the depth is over 3 Km shallower. As pointed out before the depth in these solutions is controlled by the relative time difference between the direct crustal phase and Pn, which means in effect that it is the distance between the hypocentre and the Moho that is being determined. This means that uncertainties in the Moho depth will directly affect the focal depth. Considering that no detailed structure at the epicentre is known such difference in the focal depth is not really significant. However the focal depth of 10.6 Km determined here is consistent to within 1 Km with the difference in arrival times between the direct P phase and the Moho reflection for the Atholl Net stations where the PmP phase is very clear. Nevertheless the uncertainty in the focal depth should still be at least +/- 2 Km this value being the uncertainty of Moho depths determined by LISPB.

6.2.4 Effect of uncertainties in the crustal model.

The uncertainties in the epicentre shown in Table 6.1 above only reflect the internal consistency of the arrival time data used in the program and do not take into account possible deviations of the crustal model used from the actual structure. The only way to see the effect on the epicentre of such structure variations is to relocate the epicentre for a few slightly different crustal models. Table 6.2 shows 11 variations in the crustal model together with the epicentre offset caused by such model modifications. Fig 6.4 is a plot of those offsets showing the relocated KEQ epicentres relative to the initial solution. Considering that the variations in the models of Table 6.2 are reasonably large and that the correct structure should not be very far from the range of models tested it seems plausible to conclude that the KEQ epicentre is accurate to about +/- 2 Km

in latitude and about +/- 3 Km in longitude. The origin time should be accurate to about +/- .2 s. It should be noted from Table 6.2 that models A2 and A3 (with constant σ = 0.24 and 0.26 respectively) give a higher travel time residual than the adopted model. This confirms the assumption made earlier that Poisson's ratio for the rest of the Highlands is very close to 0.25 as found along the LISPB segment ALPHA.

6.3 LOCATION OF THE KINTAIL SERIES EVENTS OF AUGUST 1974

All Kintail events recorded during August 1974 by LOWNET and Atholl Net had a very similar pattern of arrival times and also highly correlated signal waveforms, at each station, in spite of differences in magnitude. As an example Fig. 6.5 shows the S waves (vertical component) recorded by LOWNET station EAB for a few of the Kintail events. It could be concluded then that all events were concentrated in a small area. The aim of this section is to determine how small this area was by locating the other events (specially the big one of 10/8/74) using the KEQ solution of Table 6.1 as a reference event.

6.3.1 Arrival time data

In the KEQ epicentre determination described in section 6.2 Atholl Net and LOWNET contributed with first P arrivals only (in fact, only EAB, ELO and EDU from LOWNET had clear first arrivals to be used). For the relative epicentre determination of the other events of the series it was essential to use secondary P arrivals and S arrivals too. So, these were picked in the KEQ records (with uncertainties of at least +/- 0.1s) and station corrections were calculated for every phase using the KEQ solution of Table 6.1 above. These corrections were mostly about .2 or .3s with a maximum of 0.5s .

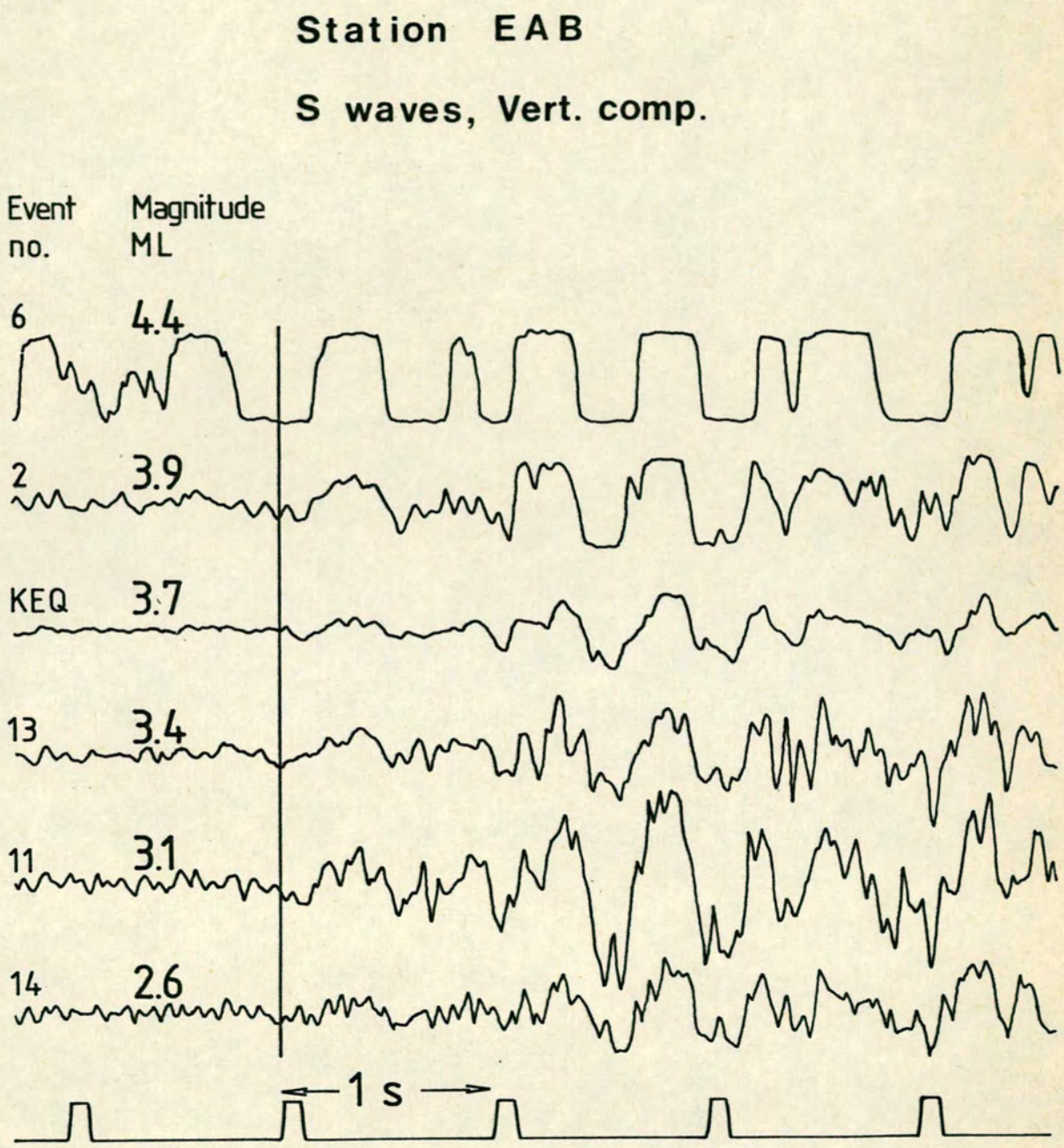

Fig. 6.5 Shear waves from various Kintail events of August 1974 recorded at LOWNET station EAB showing the same waveform. Amplitudes not to scale.

The 14 largest events were chosen for this study. Fast play-outs were obtained (with scale 1 s = 3 cm) and the signals of each event were correlated with the corresponding KEQ signal. It was found that no computer correlation was necessary and that simply visually correlating the records by overlaying one on top of the other gave results sufficiently accurate to about +/- 0.03s (equivalent to +/- 1mm in the seismogram). This means that although the absolute uncertainty of each secondary arrival is greater than +/- .1 or .2s, the arrival time for any event, relative to KEQ, after station correction, is accurate to about +/- 0.03 s . Although there was excellent correlation between signals from different events recorded at the same station, the correlation between stations for the same event was rather poor, specially for LOWNET. This is not surprising in view of the different paths and distances travelled by the waves to the LOWNET stations.

Up to two P arrivals and one S arrivals were picked for each station. First P arrivals were not picked by correlation with KEQ but the first break in the seismogram was picked instead.

The identification of the secondary phases presented a slight problem. On the whole they were not refractions but wide-angle reflections from the bottom of the 6.4 Km/s layer (LOWNET) or from the Moho (Atholl Net). As the FAMG program does not accept reflections these secondary phases were approximated by the refraction branch with the closest apparent velocity. Although the absolute error in this approximation can be as high as 0.5s the travel time error relative to KEQ after station corrections are applied are estimated to be about 0.01s only.

6.3.2 Relative Epicentre Determination

The FAMG program was modified to incorporate time corrections for up to 3 phases per station. No Joint Epicentre Determination was done with the

Kintail events and the epicentre parameters for each earthquake was determined separately. Nevertheless because of the applied station corrections and the accuracy of the relative arrival times the location of each event relative to KEQ is as accurate as can possibly be determined. The standard deviations of the epicentres thus determined (which is an indication of the accuracy of the location relative to KEQ) range from about 0.1 to 0.5 Km .

Table 6.3 shows the epicentre parameters for the 15 Kintail events studied. Fig. 6.3(c) shows the solution variations with depth for event number 3. Fig 6.6 is a plot of the location of all events relative to KEQ. Error bars are 1 st. deviations in latitude and longitude. It can be concluded from these results that all Kintail events of August 1974 are certainly contained in an area about 3 Km across or perhaps in an area as small as 1 Km across.

The apparent trend of the epicentres along the SW-NE direction is most likely due to network bias because all stations are situated SE of the events. To test this the KEQ event was relocated using its own station corrections, in a similar way to the other events, with random errors added to the arrival times. Random errors with normal distribution and st. deviation of 0.03s were used, comparable to the r.m.s residuals of Table 6.3 . The results are shown in Fig. 6.7 . It can be seen that there is a zone of uncertainty in the epicentre location along the SW-NE direction. If there is any NE trend in the epicentre locations it is probably masked by the epicentre uncertainties.

The depths of the relocated KEQ with random errors were fairly stable with a maximum deviation of 0.3 Km from the depth of 10.6 Km of Table 6.1. This together with the results shown in Table 6.3 seems to indicate that the depths of the Kintail events were confined to a limited range of about 2 or 3 Km only.

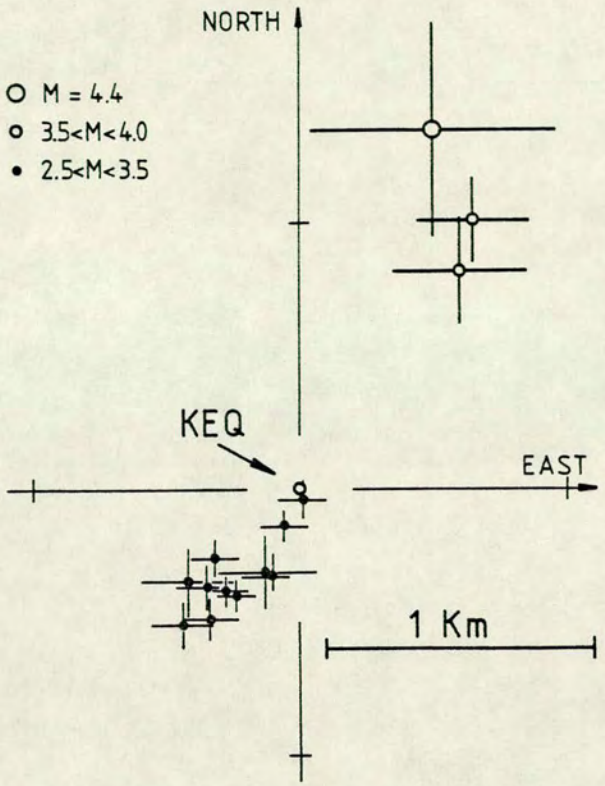

Fig. 6.6 Location of the Kintail events relative to KEQ. Error bars are 1 st.dev. .

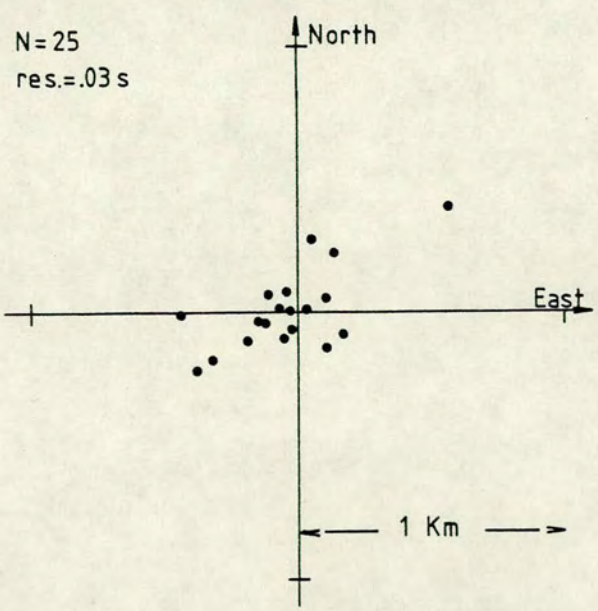

Fig. 6.7 Epicentre variations (LOWNET + Atholl Net with station corrections) with artificial reading errors having st. deviation of 0.03s .

6.4 FOCAL MECHANISM AND THE EVENT OF 10/8/74

The observation that all events of this Kintail series had exactly the same signal shape on all Lownet and Atholl Net stations is a good evidence that they all had the same focal mechanism. For this reason a composite focal plane solution was attempted for the Kintail events using polarities (compression or dilation) of first P arrivals. This amounts to using P polarity data of KEQ recorded by the LISPB stations and P polarities of the big event number 6 (10/8/74, ISC mb=4.3, IGS ML=4.4) as recorded by LOWNET and other British stations as well as a few European stations reported on ISC bulletins. S wave polarization angle could not be used because of the generally emergent character of the S arrivals.

The focal plane solution is shown in Fig 6.8, which is a stereographic projection of the lower focal hemisphere. It can be seen that in spite of the far from ideal distribution of stations it seems possible to say that the focal mechanism was predominantly strike-slip with possibly a small component of normal fault. The strike of the two focal planes are reasonably well defined by two clear changes of polarity : one along the LISPB line near stations A24-A28 (Fig. 6.1) and another one over LOWNET which shows clear compression for all stations except EAB showing clear dilation for events number 3, 6 and KEQ (other events had emergent P arrivals). The dip of the plane striking 52^{o} E of N is about 74^{o} South (measured from the horizontal) but is not very well constrained depending essentially on only one data point.

In the Kintail area there is a major fault system striking SW-NE, called Strathconon Fault which is known to have suffered left-lateral movements. The location of the earthquake swarm is very close to the fault as shown by Fig. 6.9 . In addition the strike of one of the focal planes (52^{o} E of N, Fig. 6.8) is very close to the SW-NE direction of the fault.

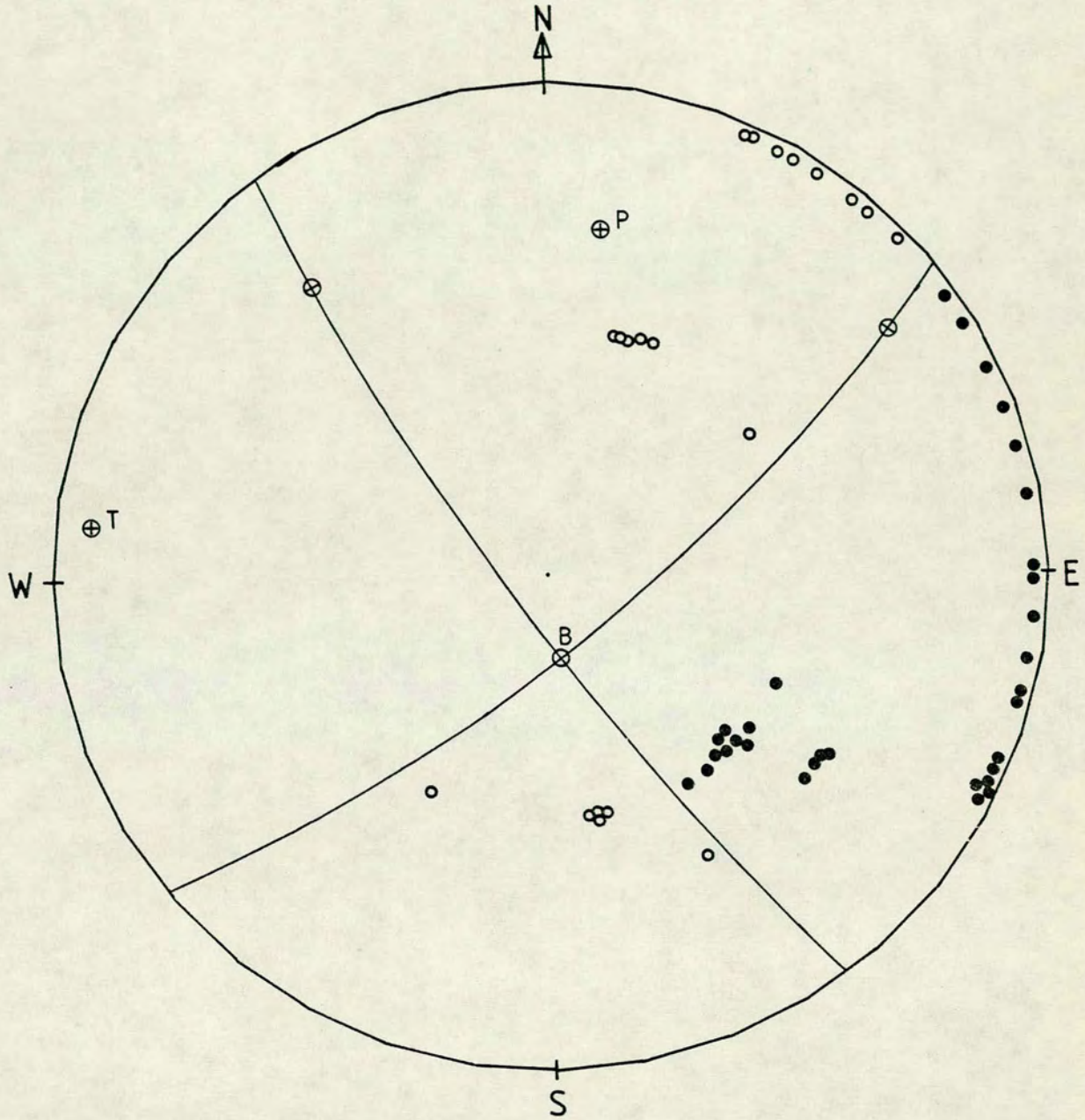

Fig. 6.8 Composite fault-plane solution for the Kintail events. Stereographic projection of the lower focal hemisphere. Open circles = dilation, dots = compression.

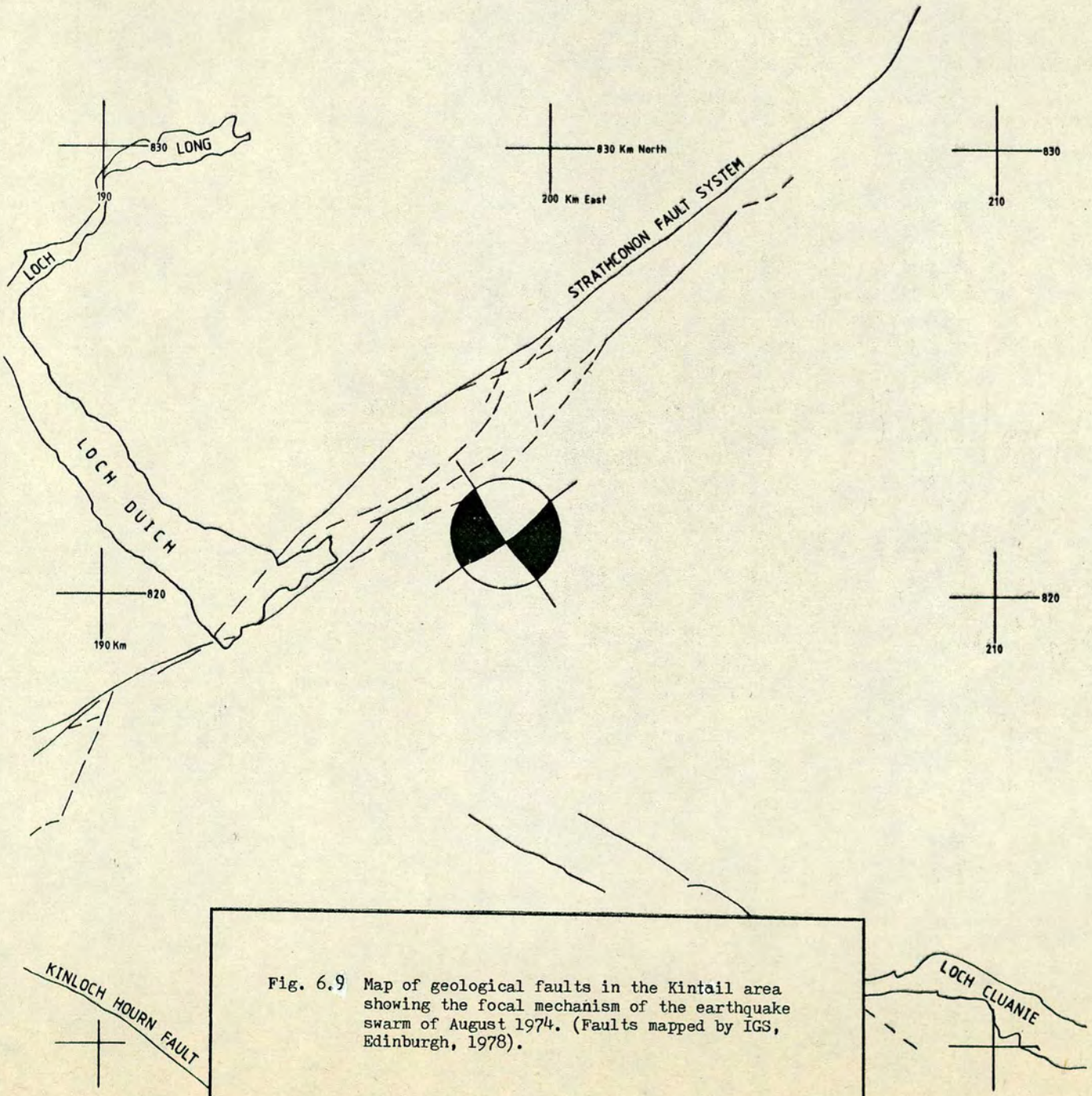

Fig. 6.9 Map of geological faults in the Kintail area showing the focal mechanism of the earthquake swarm of August 1974. (Faults mapped by IGS, Edinburgh, 1978).

It seems appropriate then to associate the earthquake swarm of August 1974 with the Strathconon Fault. If that focal plane is taken to be the rupture plane then the earthquake mechanism is a sinistral strike-slip in agreement with past movement of the Strathconon Fault.

The parameters of the earthquake of 10/8/74 are shown in Table 6.4 .

6.5 CONCLUSION

In spite of the absence of stations near the events accurate location for the Kintail swarm of earthquakes of August 1974 was possible because of two reasons:

1) a good epicentre determination for one event (KEQ) obtained by using P and S waves well recorded by the LISPB stations, and which was used as a reference for all other events of the series, and

2) correlation of the seismic signals from different events at the same station which allowed determination of epicentres relative to KEQ with an accuracy of about 1 Km.

Application of station correction on its own would not ensure good epicentre resolution. When signal correlation is not possible the usual uncertainties in the onsets (specially secondary arrivals) of the order of .2s produce an uncertainty in the epicentre of at least 5 to 10 Km.

The focal mechanism solution helped identify the earthquake swarm with the Strathconon fault system. The predominant rupture mechanism is left-lateral strike-slip with possibly a slight component of normal fault which would indicate tensional forces in the Kintail area roughly in the E-W direction.

A few other events of the Kintail region (March and June 1978) were very briefly examined showing poor signal correlation with the series of August 1974. This helps confirm the evidence from the IGS routine epicentre determination for LOWNET that the centre of seismic activity has changed

places in NW Scotland although part of it is still associated to other points of the Strathconon fault.

Table 6.3 - Kintail series of August 1974

No.	Day	Time h min sec	Latitude North	Longitude West	Depth (Km)	ML	N	RES (s)
1	4	09 45 49.9	57.227°	5.338°	10.8	3.0	27	0.01
2	4	09 48 16.2	57.236	5.328	9.9	3.9	29	0.04
3	6	08 07 32.2	57.234	5.328	9.9	3.8	27	0.04
4	6	08 14 20.0	57.226	5.339	10.8	3.0	19	0.01
KEQ	6	18 17 36.9	57.227	5.338	10.6	3.7		
5	6	19 47 54.7	57.224	5.340	10.8	2.9	17	0.02
6	10	12 49 42.1	57.239	5.330	9.5	4.4	31	0.08
7	10	17 27 05.1	57.224	5.345	10.8	3.1	19	0.02
8	11	23 38 35.7	57.224	5.340	10.7	3.0	18	0.01
9	13	19 27 10.8	57.224	5.343	10.5	3.3	20	0.01
10	14	11 53 46.6	57.224	5.342	10.4	3.0	19	0.01
11	16	08 52 47.4	57.225	5.344	10.4	3.1	26	0.02
12	18	05 31 44.3	57.223	5.344	10.4	2.8	23	0.02
13	27	23 32 20.7	57.224	5.344	10.6	3.4	19	0.02
14	29	15 20 56.3	57.222	5.346	10.4	2.6	18	0.02

Dates are August 1974
N = Number of arrivals
RES = r.m.s arrival time residual

Table 6.4

KINTAIL EVENT OF 10/8/74

Origin time : 12h 49min 42.1s
Epicentre : 57.24° N 5.33° W
(National Grid : 199Km E, 821 Km N)
Depth : 9.5 Km
Magnitude : mb=4.3(ISC), ML=4.4(IGS)
Strike-slip with fault plane striking 52 E of N
Dip of fault plane : 74 South (?)

CHAPTER 7

SUMMARY AND FINAL CONCLUSIONS

Shear waves are not used as often as P waves in crustal seismic refraction investigations because of difficulties in recording and picking their onsets accurately. Analysis of LISPB S data demonstrate that explosions can be used in the study of shear waves and determination of crustal Poisson's ratio when a large density of 3-component stations are employed. Difficulties in recording shear waves may not be due to lack of S energy generated by the explosions but rather to the fact that S waves are more easily destroyed (either by attenuation or by conversion) when they propagate through highly heterogeneous media with many velocity discontinuities as shown in chapter 2.

Difficulties in picking shear wave onsets are not only due to the fact that they are secondary arrivals (and so will always appear in a background of signal generated noise following the P waves), but also seem to be related to a more complex type of ground motion (as compared to the P waves) for shallow angle arrivals, depending strongly on the station site. Shear wave onsets should then be determined after careful examination of 3-component records and an uncertainty should be assigned to every pick and taken into account when determining S velocity structure. Large station density as in LISPB is necessary to compensate for the occasional large uncertainty in the S arrivals. Transverse components are also very important - quite often the amplitude in the transverse component is bigger than either vertical or radial.

A method was developed (chapter 4) to determine Poisson's ratio distribution in the crust using the travel time ratio ts/tp and taking into account the uncertainties of P and S onsets. The method involves linearization of the ts/tp value at each station as a function of the Poisson's

ratios of various crustal blocks. It is of course necessary to have a crustal model already determined from the P waves. The advantage of the method is that uncertainties in the P velocity model hardly affect the resulting Poisson's ratio. In this way reflections and refractions can be successfully used to determine Poisson's ratio with resulting uncertainties down to 0.01 or less.

LISPB Poisson's ratio were generally close to 0.25 except for layer 2 under the Midland Valley ($\sigma < 0.23$). No difference in Poisson's ratio was found in layer 1 (lower palaeozoic basement) between the Midland Valley and Southern Uplands so that the similarity between those two regions (in terms of seismic velocity) as found with the P waves (Vp = 5.8 Km/s) is essentially confirmed. The pre-Caledonian basement on the other hand (Vp = 6.4 Km/s) does show a difference in Poisson's ratio betwen the Highlands and its possible continuation beneath the Midland Valley. An interpretation in terms of compositional differences is suggested (higher content of quartz beneath the Midland Valley), although other explanations might be possible such as anisotropy or crack density differences (e.g. a higher density of dry cracks beneath the Midland Valley).

The lower crust in segment ALPHA has a P velocity in the range 6.7 to 7.0 Km/s and Poisson's ratio in the range 0.23 to 0.26 which is consistent with recent interpretation of lower crustal composition in terms of intermediate granulite-facies rocks. Unfortunately it was not possible to determine Poisson's ratio for the lower crust in segment BETA (Midland Valley and Southern Uplands) as the seismic return from the Moho was very poor for both P and S waves.

The Poisson's ratio structure of segment ALPHA found in chapter 4 was used to help analyse a PS reflection from the Moho recorded from shot-point N1. Good evidence for the existence of a localized topography in the Moho was found as well as some evidence that the P velocity in that part of the

lower crust could be 6.7 Km/s instead of the average 7.0 Km/s of Bamford et al. These results point to the accumulating evidence of recent years that the continental lower crust has a fine structure and heterogeneities not previously suspected. As seismic experiments become more sophisticated and interpretation techniques more developed it might turn out that the lower crustal structure is as complex as surface geology. It is suggested that Moho topography as found in chapter 5 might be a common feature not easily detected by the usual refraction methods, in which case PS reflections might offer new prospects for Moho investigations.

Finally as an important application of the Poisson's ratio structure an earthquake swarm in the Kintail area of NW Scotland was accurately located using P and S arrivals. The S wave arrivals are consistent with an average value of Poisson's ratio very close to 0.25 for the whole of the Highlands and so generally support the results found along the LISPB line.

REFERENCES

Aggarwal Y.P., Sykes L.R., Simpson D.W. & Richards P.G., 1975. Spatial and temporal variations in ts/tp and in the P wave residuals at the Blue Mountain Lake, N.Y.: application to earthquake prediction. J.Geophys.Res., 80, 718-732.

Bamford D., Faber S., Jacob B., Kaminsky W., Nunn K., Prodehl C., Fuchs K., King R. & Willmore P., 1976. A lithospheric seismic profile in Britain I. Preliminary results, Geophys.J.R.astr.Soc., 44, 145-160.

Bamford D., Nunn K., Prodehl C. & Jacob B., 1977. LISPB-III. Upper crustal structure of northern Britain. J.geol.Soc.London, 133, 481-488.

Bamford D., Kominskaya I., Mueller S. & Prodehl C., 1977. The results of the CCSS-workshop at Karlsruhe. Presented at the IASPEI meeting, Durham, 1977.

Bamford D., Nunn K., Prodehl C. & Jacob B., 1978. LISPB-IV. Crustal structure of northern Britain. Geophys.J.R.astr.Soc., 54, 43-60.

Berckhemer H., 1969. Direct evidence of the composition of the lower crust and Moho. Tectonophysics, 8, 97-105.

Berry M.J. & Fuchs K., 1973. Crustal studies of the Superior and Grenville provinces of the NE Canadian shield. Bull.seism.Soc.Am., 63, 1393-1432

Birch F., 1960. The velocity of compressional waves in rocks to 10Kb, part 1. J.geophys.Res., 65, 1083-1102.

" 1961. The velocity of compressional waves in rocks to 10Kb, part 2. J.geophys.Res., 66, 2199-2224.

" 1969. Density and composition of the Upper Mantle: first approximation as an Olivine layer. THE EARTH'S CRUST AND UPPER MANTLE, Am.Geophys. Union Monograph, 13, 18-36.

Braile L.W. & Smith R.B., 1975. Guide to the interpretation of crustal refraction profiles. Geophys.J.R.astr.Soc., 40, 145-176.

Cerveny V., 1961. The amplitude curves of reflected harmonic waves around the critical point. Studia geoph. et geod., 5, 319-351.

" 1965. On dynamic properties of reflected and head waves in the n-layered Earth's crust. Geophys.J.R.astr.Soc., 11, 139-147.

Cerveny V. & Hron F., 1961. Reflection coefficients for spherical waves. Studia geoph. et geod., 5, 122-132.

Cerveny V., Langer J. & Psencik I., 1974. Computation of geometrical spreading of seismic body waves in laterally inhomogeneous media with curved interfaces. Geophys.J.R.astr.Soc., 38, 9-19.

Chesher J.A. & Bacon M., 1975. A deep seismic survey in the Moray Firth. Rep. Inst. Geol. Sci., No. 75/11, 13pp.

Christensen N.I., 1965. Compressional wave velocities in metamorphic rocks at pressures to 10Kb. J.Geophys.Res., 70, 6147-6164.

" 1966a. Shear wave velocities in metamorphic rocks at pressures to 10Kb. J.geophys.Res., 71, 3549-3556.

" 1966b. Elasticity of ultrabasic rocks. J.geophys.Res., 71, 5921- .

" 1969. Granulite facies metamorphic of the lower continental crust. (Abstract). Trans.Am.Geophys.Union, 50, 673.

" 1971. Elastic moduli and anisotropy of dunite at 10Kb. J.gephys.Res., 76, 4003- .

" 1972. Compressional and shear wave velocities at pressures to 10Kb for basalts from the East Pacific Rise. Geophys.J.R.astr.Soc.,28,425-429.

" 1974. Compressional wave velocities in possible mantle rocks to pressures of 30Kb. J.geophys.Res., 79, 407-412.

Christensen N.I. & Fountain D.M., 1975. Constitution of the lower continental crust based on experimental studies of seismic velocities in granulite. Geol.Soc.Am.Bull., 86, 227-236.

Crampin S., 1970. A method for the location of near seismic events using travel times along ray paths. Geophys.J.R.astr.Soc., 21, 535-539.

Crampin S., 1973. A computer program for the location of local earthquakes recorded by large-aperture low-density seismic networks. Inst.Geol. Sci., Global Seismology Unit, Edinburgh. Internal Report No. 33 .

" 1978. Seismic wave propagation through a cracked solid: polarization as a possible dilatancy diagnostic. Geophys.J.R.astr.Soc., 53, 467-496

Crosson R.S. & Christensen N.I., 1967. Composition of the Earth's crust and upper mantle from Poisson's ratio. (Abstract). Trans.Am.Geophys.Union, 48, 200.

Dewey J.F., 1969. Evolution of the Appalachian/Caledonian orogen. Nature, 222, 124-129.

" 1976. Ancient plate margins : some observations. Tectonophysics, 33, 379-385.

Dunning F.W. & Stubblefield J., 1966. Tectonic map of Great Britain and Northern Ireland. Institute of Geological Sciences, London.

Edel J.B., Fuchs K., Gelbke C. & Prodehl C., 1975. Deep structure of the southern Rhinegraben area from seismic refraction investigations. J.Geophys., 41, 333-356.

Erickson E.L., Miller D.E. & Waters K.H., 1968. Shear wave recordings using continuos signal methods,II -later experiments. Geophysics,33, 240-254

Faber S.,1978. Refraktionsseismische untersuchung der Lithosphare unter der Britischen Inseln. Ph.D. thesis, University of Karlsruhe.

Fagernes V. & Kanestrom R., 1973. Variations in the upper mantle strucrure as derived from Pn and Sn waves. Pure & Appl.Geophys., 109, 1762-1772.

Fielitz K., 1976. Compressional and shear wave velocities as a function of temperature in rocks at high pressure. In EXPLOSION SEISMOLOGY IN CENTRAL EUROPE (ed. Giese, Prodehl & Stein). Springer-Verlag, p40-44.

Fuchs K., 1975. Synthetic seismograms of PS-reflections from transition zones computed with the reflectivity method. J.Geophys., 41, 445-462.

Fuchs K. & Müller G., 1971. Computation of synthetic seismograms with the reflectivity method and comparison with observations. Geophys.J.R.astr.Soc., 23, 417-433.

Garson M.S. & Plant J., 1972. Possible dextral movements on the Great Glen and Minch Faults in Scotland. Nature Phys. Sci., 240, 31-35.

Geyer R.L. & Martner S.T., 1969. SH waves from explosive sources. Geophysics, 34, 893-905.

Giese P., 1976. General remarks on travel time data and principles of correlation. In EXPLOSION SEISMOLOGY IN CENTRAL EUROPE (ed. Giese, Prodehl & Stein). Springer-Verlag, p130-136.

Gunn P.J. 1973. Location of the Proto-Atlantic suture in the British Isles. Nature, 242, 111-112.

Gregory A.R., 1976. Fluid saturation effects on dynamic elastic properties of sedimantary rocks. Geophysics, 41, 895-921.

Griffiths D., King R., Khan M. & Blundel D., 1971. Seismic refraction line in the Gregory Rift (Kenya). Nature Phys.Sci., 229, 69-71.

Hagedoorn J.G., 1959. The plus-minus method of interpretation of seismic refraction sections. Geophys.Prosp., 7(2), 158-182.

Hall D.H. & Hajnal Z., 1969. Refraction seismology in NW Ontario. Can.J.Earth Sci., 6, 83- .

" 1973. Deep seismic crustal studies in Manitoba. Bull.seism.Soc.Am., 63, 885-910.

Hall J. & Al-Haddad F.M., 1976. Seismic velocities in the Lewisian metamorphic complex, northwest Britain - 'in situ' measurements. Scott.J.Geol., 12, 305-314.

Haskell N.A., 1962. Crustal reflections of plane P and SV waves. J.geophys.Res., 67, 4751-4767.

Hirn A., Prodehl C. & Steinmetz L., 1975. An experimental test of models of the lower lithosphere in Bretagne (France). Ann.Geophys., 31, 517-530.

Holgate N., 1969. Palaeozoic and Tertiary transcurrent movement on the Great Glen Fault. Scott.J.Geol., 5, 97-139.

Jacob A.W.B., 1975. Dispersed shots at optimum depth - an efficient seismic source for lithospheric studies. J.Geophys., 41, 63-70.

Jacob A.W.B. & Booth D.C., 1977. Observation of PS reflections from the Moho. J.Geophys., 43, 687-692.

Jacob A.W.B. & Willmore P.L., 1972. Teleseismic P waves from a 10 ton explosion. Nature, 236, 305-306.

Jolly R.N., 1956. Investigation of shear waves. Geophysics, 21, 905-938.

Johnstone G.S., 1975. The Moine succession. In A CORRELATION OF PRECAMBRIAN ROCKS IN THE BRITISH ISLES. Geological Society of London, Special report no. 6 .

Kaminsky W., Bamford D., Faber S., Jacob B., Nunn K. & Prodehl C., 1976. A Lithospheric Profile in Britain, II : Preliminary report on the recording of a local earthquake. J.Geophys., 42, 103-110.

Kennedy W.Q., 1946. The Great Glen Fault. Q.J.Geol.Soc.Lond., 102, 41-72.

Kind R., 1974. Long range propagation of seismic energy in the lower lithosphere. J.Geophys., 40, 189-202.

King M.S., 1966. Wave velocity in rocks as a function of changes in overburden pressure and pore fluid saturatns. Geophysics, 31, 50-73.

Kisslinger C. & Engdahl E.R., 1973. The interpretation of the Wadati diagram with relaxed assumptions. Bull.seism.Soc.Am., 63, 1723-1736.

Lachenbruch A.H., 1970. Crustal temperature and heat production : implications of linear heat flow relations. J.Geophys.Res., 75, 3291-3300.

Landisman M. & Mueller S., 1966. Seismic studies of the Earth's crust in continents, II. Analysis of wave propagation in continents and adjacent areas. Geophy.J.R.astr.Soc., 10, 539-548.

Landisman M., Mueller S. & Fuchs K., 1967. Further evidence of the sialic low velocity zone in continental areas. Geophys.J.R.astr.Soc., 13, 367-368 .

MacKenzie D., 1969. The Mohorovicic Discontinuity. In : THE EARTH'S CRUST AND UPPER MANTLE. AGU monograph 13, 660-664.

Meissner R., 1965. P and SV-waves from uphole shooting. Geophys. Prosp., 13, 433-459.

Moseley F., 1977. Caledonian plate tectonics and the place of the English Lake District. Bull.Geol.Soc.Am., 88, 764-768.

Mueller S. & Landisman M., 1966. Seismic studies of the earth's crust in continents, I : Evidence for a low velocity zone in the upper part of the lithosphere. Geophys.J.R.astr.Soc., 10, 525-538.

Mueller S. & Landisman M., 1971. An example of the unified method of interpretation of crustal seismic data. Geophys.J.R.astr.Soc., 23, 365-371.

Montalbetti J.F. & Kanasewich E.R., 1970. Enhancement of teleseismic body phases with a polarization filter. Geophys.J.R.astr.Soc., 21, 119-129.

Nunn K.R. & LISPB working group, 1978. Crustal structure beneath Wales from the LISPB line DELTA. (Abstract). Geophys.J.R.astr.Soc., 53, 170.

Nur A., 1972. Dilatancy, pore fluids and premonitory variations of ts/tp travel times. Bull.seism.Soc.Am., 62, 1217-1222.

Nuttli O., 1961. The effect of the Earth's surface on the S wave particle motion. Bull.seism.Soc.Am., 51, 237-246.

O'Brien P.N.S., 1967a. The efficient use of large charges. In SEISMIC REFRACTION PROSPECTING, Soc. Explor. Geophys., p. 152-170.

" 1967b. Quantitative discussion on seismic amplitudes produced by explosions in Lake Superior. J.geophys.Res., 72, 2569-2575.

" 1967c. Analysis of a small number of seismic records in a E-W Alpine profile. Boll. Geof. Teor. Appl., 9, 22-65

O'Connell R.J. & Budiansky B., 1977. Viscoelastic properties of fluid saturated cracked solids. J.geophys.Res.,82(36),5719-5735.

Powell D.W., 1971. A model for the lower palaeozoic evolution of the southern margin of the early Caledonides of Scotland and Ireland. Scott.J.Geol., 7, 369-372.

Richards T.C., 1961. Motion of the ground on arrival of reflected longitudinal and transverse waves at wide-angle reflection distances. Geophysics, 26, 277-297.

Ringwood A.E. & Green D.H., 1966. Petrological nature of the stable continental crust. In THE EARTH BENEATH THE CONTINENTS, Am.Geophys. Union monograph, 10, 611-619.

Ronov A.B. & Yaroshevsky A.A., 1969. Chemical composition of the earth's crust. In THE EARTH'S CRUST AND UPPER MANTLE, Am.Geophys.Union monograph, 13, 37-57.

Ruegg J.C.,1975. Structure profonde de la croute et du manteau superieur du SE de l'Afar d'apres les donnes sismiques. Ann. de Geoph.,31, 329-360.

Scarascia S., Colombi B. & Cassinis R.,1976. Some experiments on transverse waves. Geophys.Prosp., 24, 549-568.

Scholtz C.H., Sykes L.R. & Aggarwal Y.P., 1973. Earthquake prediction: a physical basis. Science, 181, 803-810.

Simmons G., 1964. Velocity of shear waves in rocks to 10Kb, 1. J.geophys.Res., 69, 1123-1130.

Smith A.G., 1976. Plate tectonics and orogeny : a review. Tectonophysics, 33, 215-285.

Smith P.J. & Bott M.H.P., 1975. Structure of the crust beneath the Caledonian Foreland and Caledonian Belt of the North Scottish shelf region. Geophys.J.R.astr.Soc., 40, 187-205.

Sutton G.H. & Pomeroy P.W., 1963. Analog analyses of seismograms recorded on magnetic tape. J.geophys.Res., 68, 2791-2815.

Suzuki Z., 1965. Maine seismic experiment : a study of shear waves. Bull.seism.Soc.Am., 55, 425-439.

Tatham R.H. & Stoffa P.L., 1976. Vp/Vs - a potencial hydrocarbon indicator. Geophysics, 41, 837-849.

Todd T. & Simmons G., 1972. Effect of pore pressure on the velocity of compressional waves in low porosity rocks. J.Geophys.Res., 77, 3731-3743.

Whitcomb J.H., Garmany J.D. & Anderson D.L., 1973. Earthquake prediction: variation of seismic velocities before the San Fernando earthquake. Science, 180, 632-635.

Wielandt E., 1975. Generation of seismic waves by underwater explosions. Geophys.J.R.astr.Soc., 40, 421-439.

Wilson J.T., 1966. Did the Atlantic close and then re-open ? Nature, 211, 676-681.

Wittlinger G. & Haessler H., 1976. Etude du rapport des vitesses sismiques avant et apres la mise en eau d'un lac-barrage. C.R.Acad.Sc.Paris, 282, 137-140.

Wright A.E., 1976. Alternating subduction direction and the evolution of the Atlantic Caledonides. Nature, 264, 156-160.

APPENDIX A

Seismic sections of S waves

Seismic sections of P waves can be found in Bamford et al. 1978.

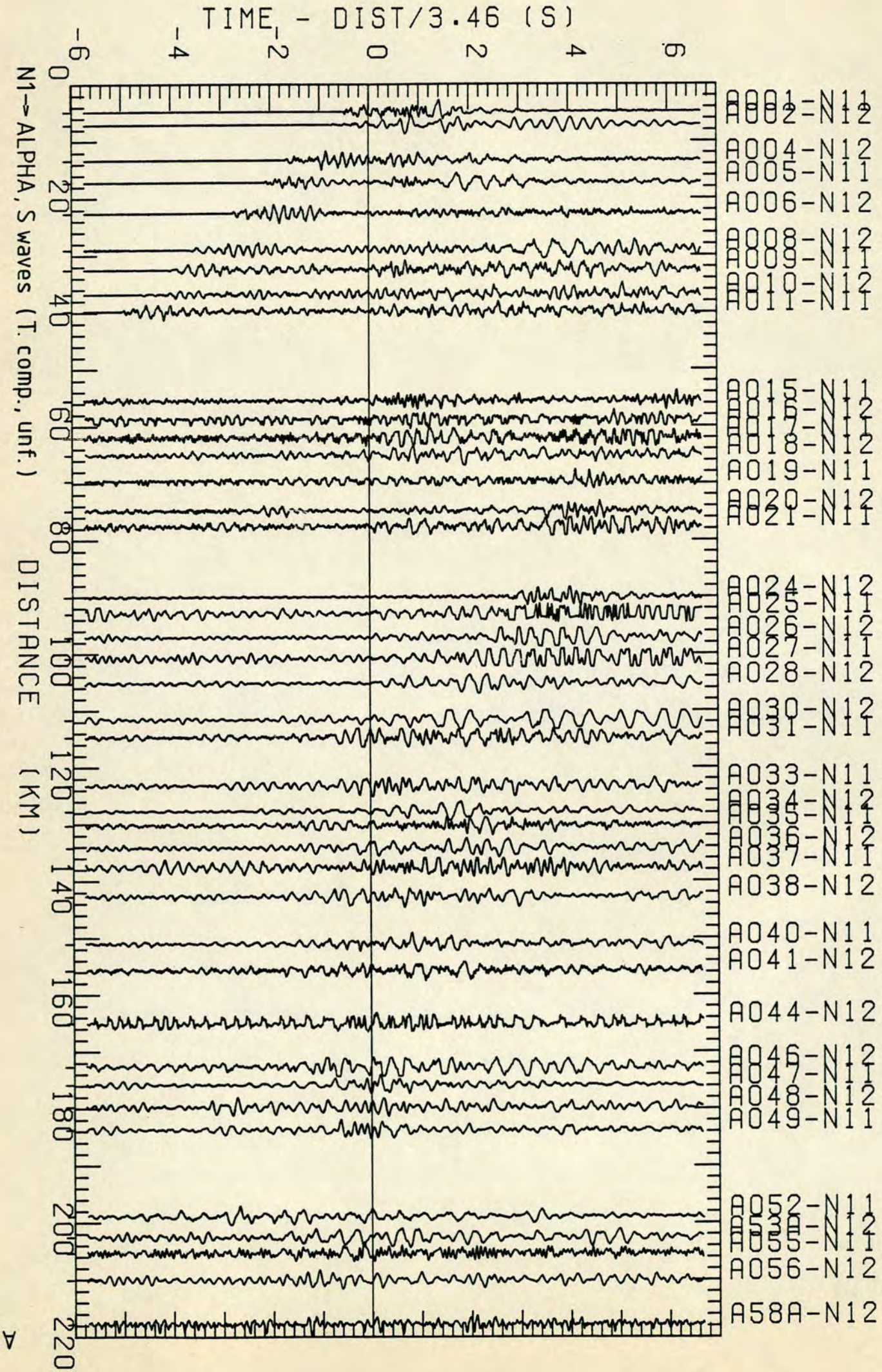
TIME - DIST/3.46 (S)
-6
-4
-2
0
2
4
6
N1-> ALPHA, S waves (T. comp., unf.)
DISTANCE (KM)
0
20
40
60
80
100
120
140
160
180
200
220
A001-N11
A002-N12
A004-N12
A005-N11
A006-N12
A008-N12
A009-N11
A010-N12
A011-N11
A015-N11
A017-N12
A018-N12
A019-N11
A020-N12
A021-N11
A024-N12
A025-N11
A026-N12
A027-N11
A028-N12
A030-N12
A031-N11
A033-N11
A034-N12
A035-N11
A036-N12
A037-N11
A038-N12
A040-N11
A041-N12
A044-N12
A046-N12
A047-N11
A048-N12
A049-N11
A052-N11
A053-N12
A055-N11
A056-N12
A58A-N12

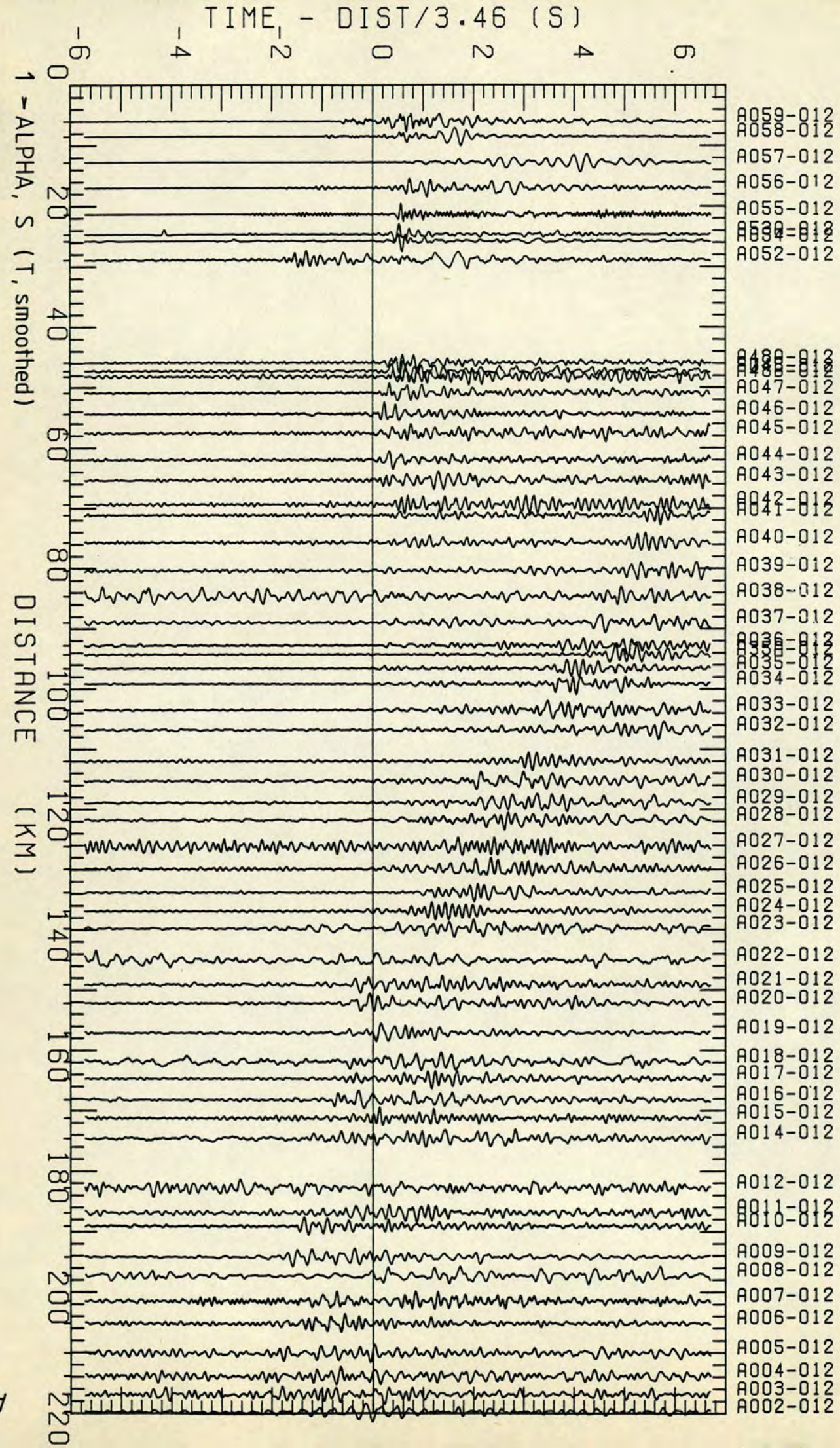
TIME - DIST/3.46 (S)
-6
-4
-2
0
2
4
6
0
20
40
60
80
100
120
140
160
180
200
220
1 - ALPHA, S (T, smoothed)
DISTANCE (KM)
A059-012
A058-012
A057-012
A056-012
A055-012
A052-012
A047-012
A046-012
A045-012
A044-012
A043-012
A041-012
A040-012
A039-012
A038-012
A037-012
A034-012
A033-012
A032-012
A031-012
A030-012
A029-012
A028-012
A027-012
A026-012
A025-012
A024-012
A023-012
A022-012
A021-012
A020-012
A019-012
A018-012
A017-012
A016-012
A015-012
A014-012
A012-012
A009-012
A008-012
A007-012
A006-012
A005-012
A004-012
A003-012
A002-012

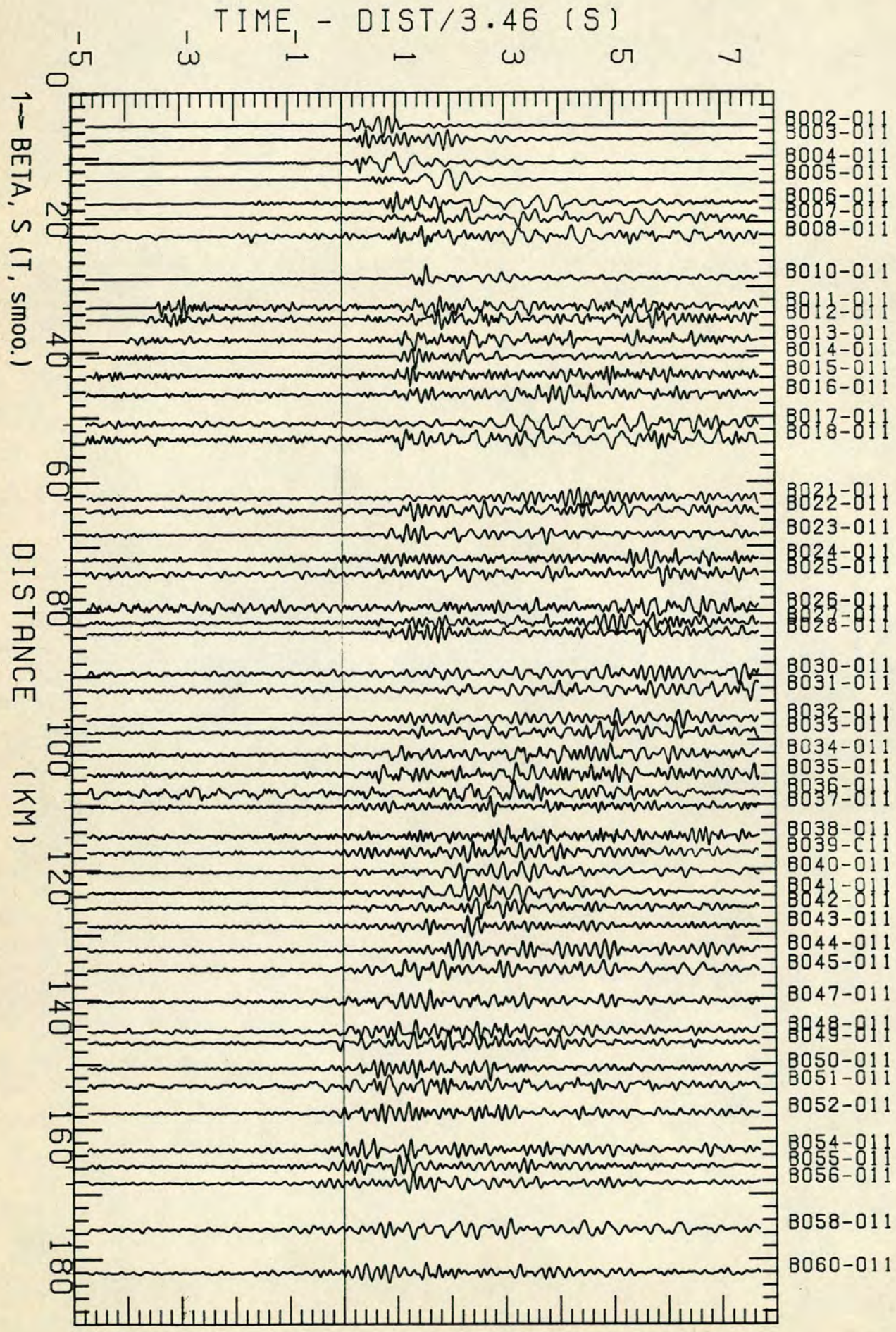
TIME - DIST/3.46 (S)
-5
-3
-1
1
3
5
7
0
20
40
60
80
100
120
140
160
180
DISTANCE (KM)
1--- BETA, S (T, smoo.)
B002-011
B003-011
B004-011
B005-011
B006-011
B007-011
B008-011
B010-011
B011-011
B012-011
B013-011
B014-011
B015-011
B016-011
B017-011
B018-011
B021-011
B022-011
B023-011
B024-011
B025-011
B026-011
B027-011
B028-011
B030-011
B031-011
B032-011
B033-011
B034-011
B035-011
B036-011
B037-011
B038-011
B039-011
B040-011
B041-011
B042-011
B043-011
B044-011
B045-011
B047-011
B048-011
B049-011
B050-011
B051-011
B052-011
B054-011
B055-011
B056-011
B058-011
B060-011

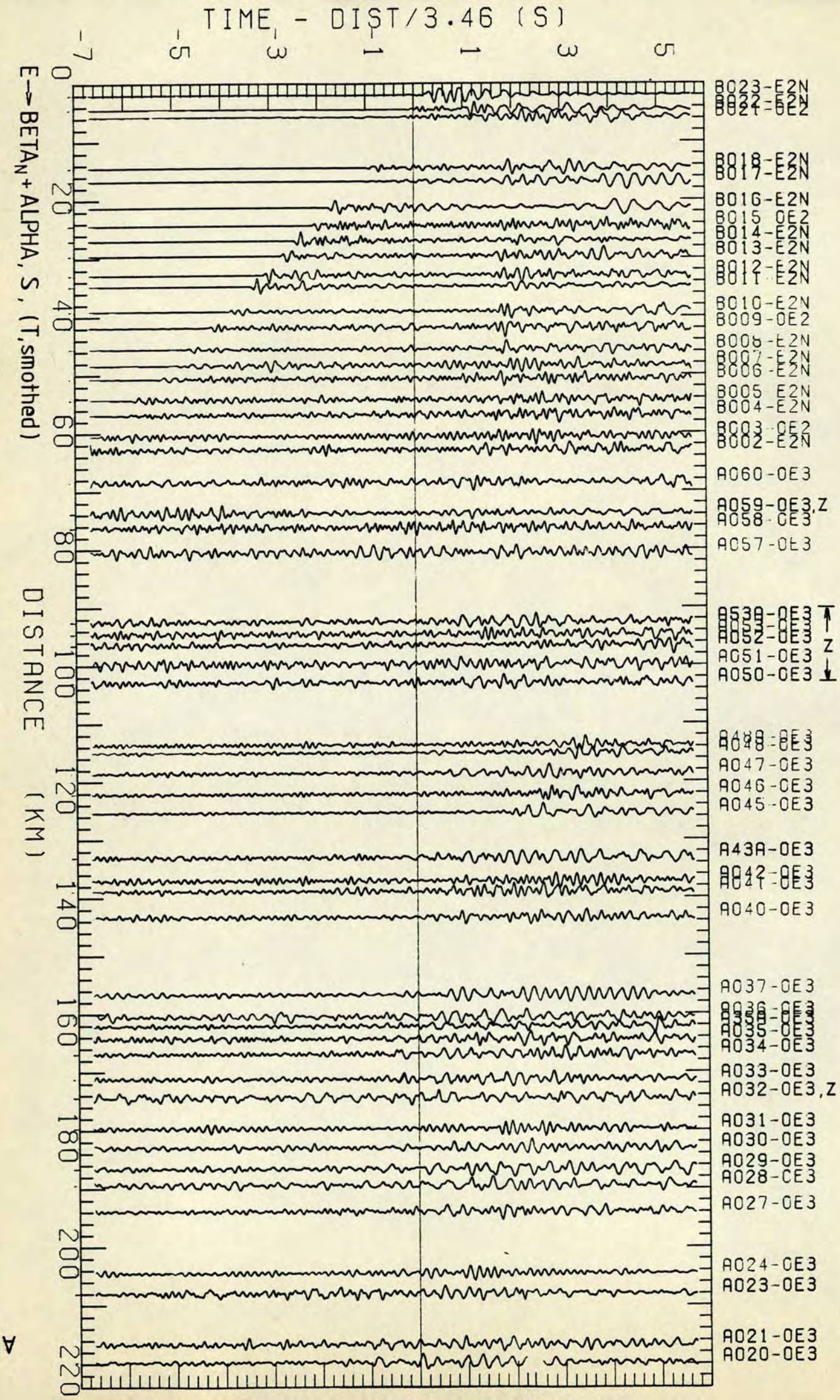
TIME - DIST/3.46 (S)
-7
-5
-3
-1
1
3
5
0
20
40
60
80
100
120
140
160
180
200
220
E→ BETA$_N$ + ALPHA, S, (T,smothed)
DISTANCE (KM)
B023-E2N
B022-E2N
B021-0E2
B018-E2N
B017-E2N
B016-E2N
B015 0E2
B014-E2N
B013-E2N
B012-E2N
B011 E2N
B010-E2N
B009-0E2
B008-E2N
B007-E2N
B006-E2N
B005 E2N
B004-E2N
B003 0E2
B002-E2N
A060-0E3
A059-0E3,Z
A058-0E3
A057-0E3
A53A-0E3
A053-0E3
A052-0E3
A051-0E3
A050-0E3
Z
A048-0E3
A047-0E3
A046-0E3
A045-0E3
A43A-0E3
A042-0E3
A041-0E3
A040-0E3
A037-0E3
A036-0E3
A035-0E3
A034-0E3
A033-0E3
A032-0E3,Z
A031-0E3
A030-0E3
A029-0E3
A028-0E3
A027-0E3
A024-0E3
A023-0E3
A021-0E3
A020-0E3

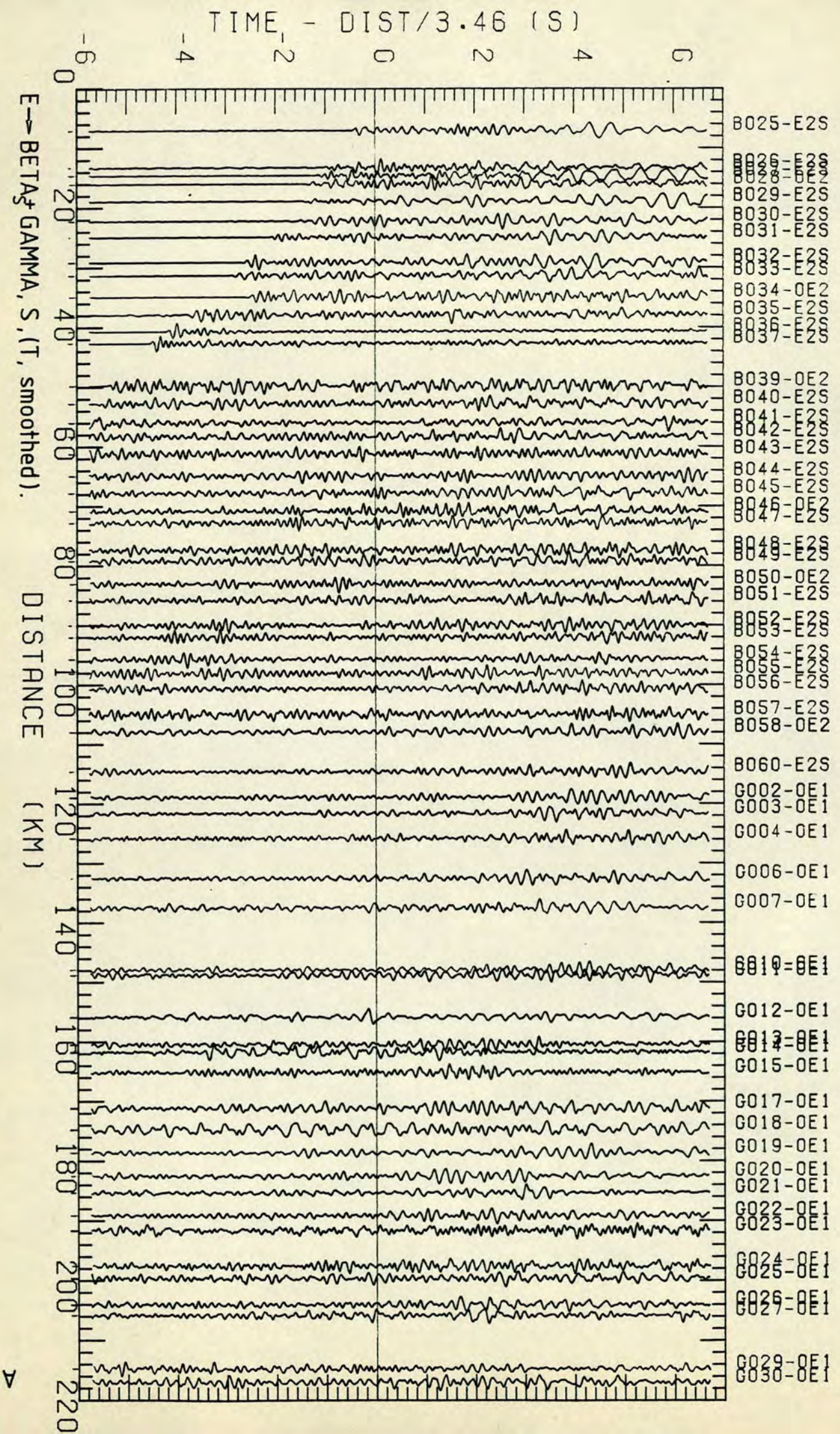
TIME - DIST/3.46 (S)
-6
-4
-2
0
2
4
6
0
20
40
60
80
100
120
140
160
180
200
220
DISTANCE (KM)
E→ BETA, GAMMA, S, (T, smoothed).
B025-E2S
B026-E2S
B028-E2S
B029-E2S
B030-E2S
B031-E2S
B032-E2S
B033-E2S
B034-0E2
B035-E2S
B036-E2S
B037-E2S
B039-0E2
B040-E2S
B041-E2S
B042-E2S
B043-E2S
B044-E2S
B045-E2S
B046-0E2
B047-E2S
B048-E2S
B049-E2S
B050-0E2
B051-E2S
B052-E2S
B053-E2S
B054-E2S
B055-E2S
B056-E2S
B057-E2S
B058-0E2
B060-E2S
G002-0E1
G003-0E1
G004-0E1
G006-0E1
G007-0E1
G012-0E1
G015-0E1
G017-0E1
G018-0E1
G019-0E1
G020-0E1
G021-0E1
G022-0E1
G023-0E1
G024-0E1
G025-0E1
G029-0E1
G030-0E1

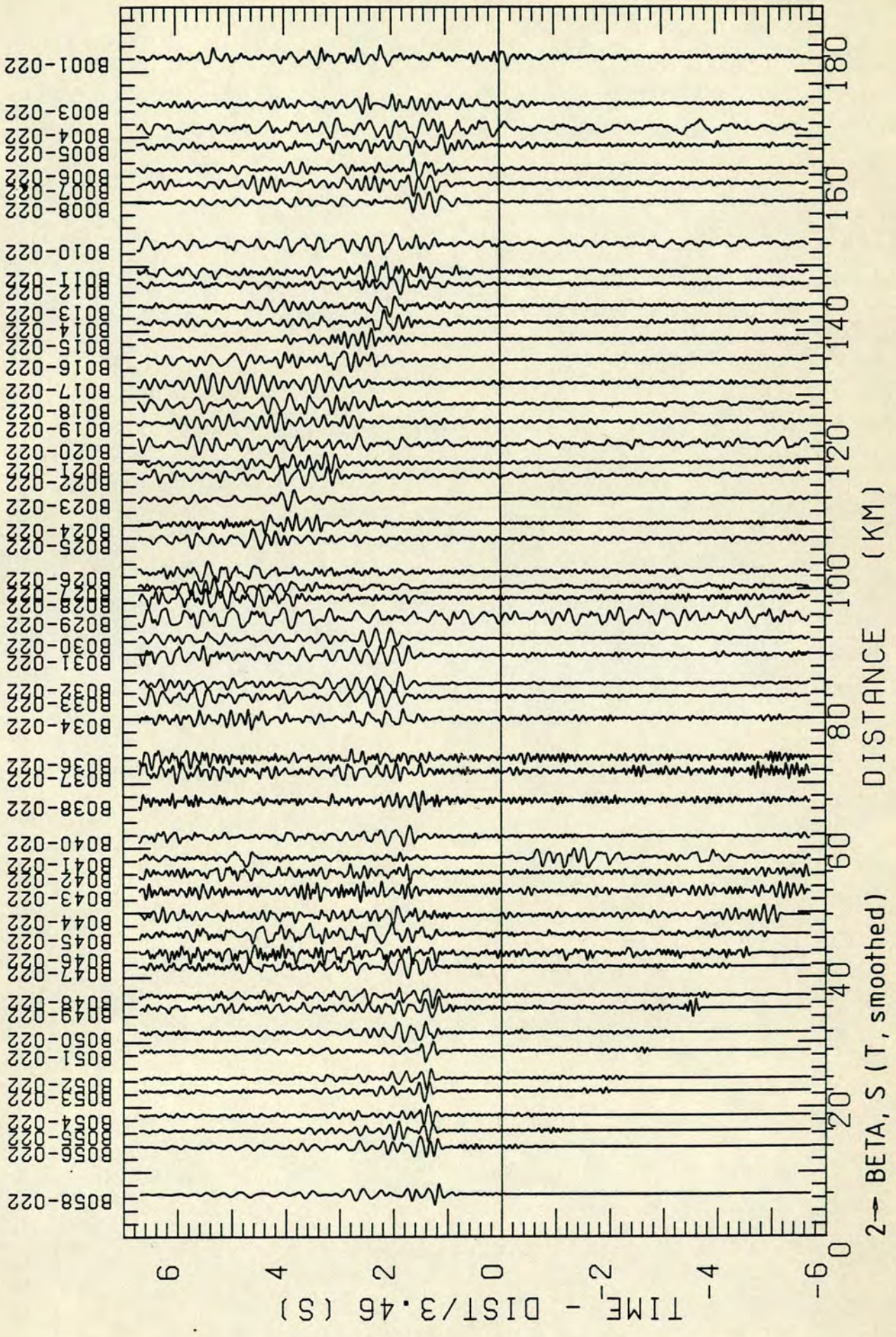
B001-022
B003-022
B004-022
B005-022
B006-022
B007-022
B008-022
B010-022
B011-022
B012-022
B013-022
B014-022
B015-022
B016-022
B017-022
B018-022
B019-022
B020-022
B021-022
B022-022
B023-022
B024-022
B025-022
B026-022
B027-022
B028-022
B029-022
B030-022
B031-022
B032-022
B033-022
B034-022
B036-022
B037-022
B038-022
B040-022
B041-022
B042-022
B043-022
B044-022
B045-022
B046-022
B047-022
B048-022
B049-022
B050-022
B051-022
B052-022
B053-022
B054-022
B055-022
B056-022
B058-022
0
20
40
60
80
100
120
140
160
180
DISTANCE (KM)
2→ BETA, S (T, smoothed)
TIME - DIST/3.46 (S)
6
4
2
0
-2
-4
-6

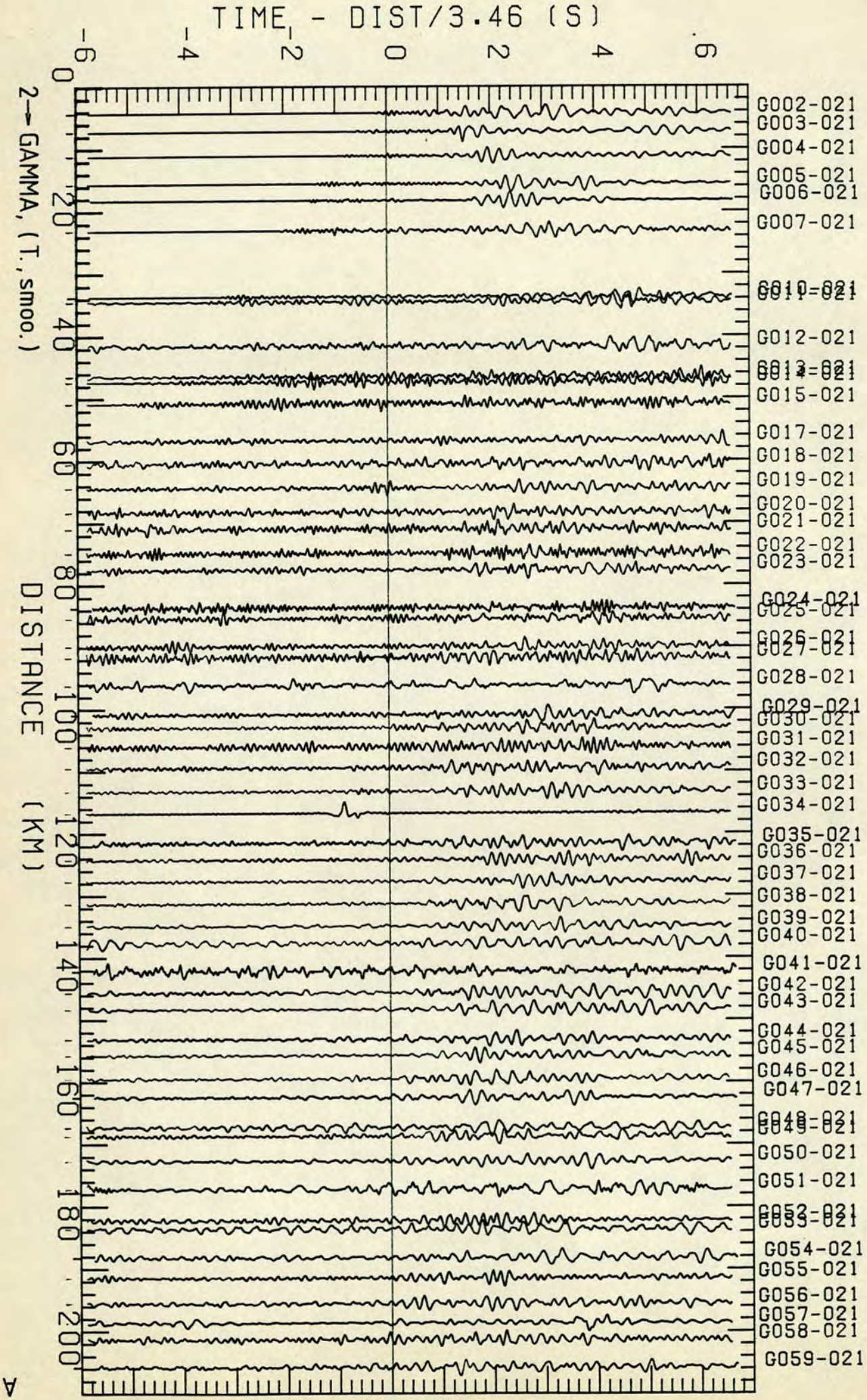
TIME - DIST/3.46 (S)
-6
-4
-2
0
2
4
6
2→ GAMMA, (T., smoo.)
DISTANCE (KM)
0
20
40
60
80
100
120
140
160
180
200
G002-021
G003-021
G004-021
G005-021
G006-021
G007-021
G010-021
G011-021
G012-021
G013-021
G014-021
G015-021
G017-021
G018-021
G019-021
G020-021
G021-021
G022-021
G023-021
G024-021
G025-021
G026-021
G027-021
G028-021
G029-021
G030-021
G031-021
G032-021
G033-021
G034-021
G035-021
G036-021
G037-021
G038-021
G039-021
G040-021
G041-021
G042-021
G043-021
G044-021
G045-021
G046-021
G047-021
G048-021
G049-021
G050-021
G051-021
G052-021
G053-021
G054-021
G055-021
G056-021
G057-021
G058-021
G059-021

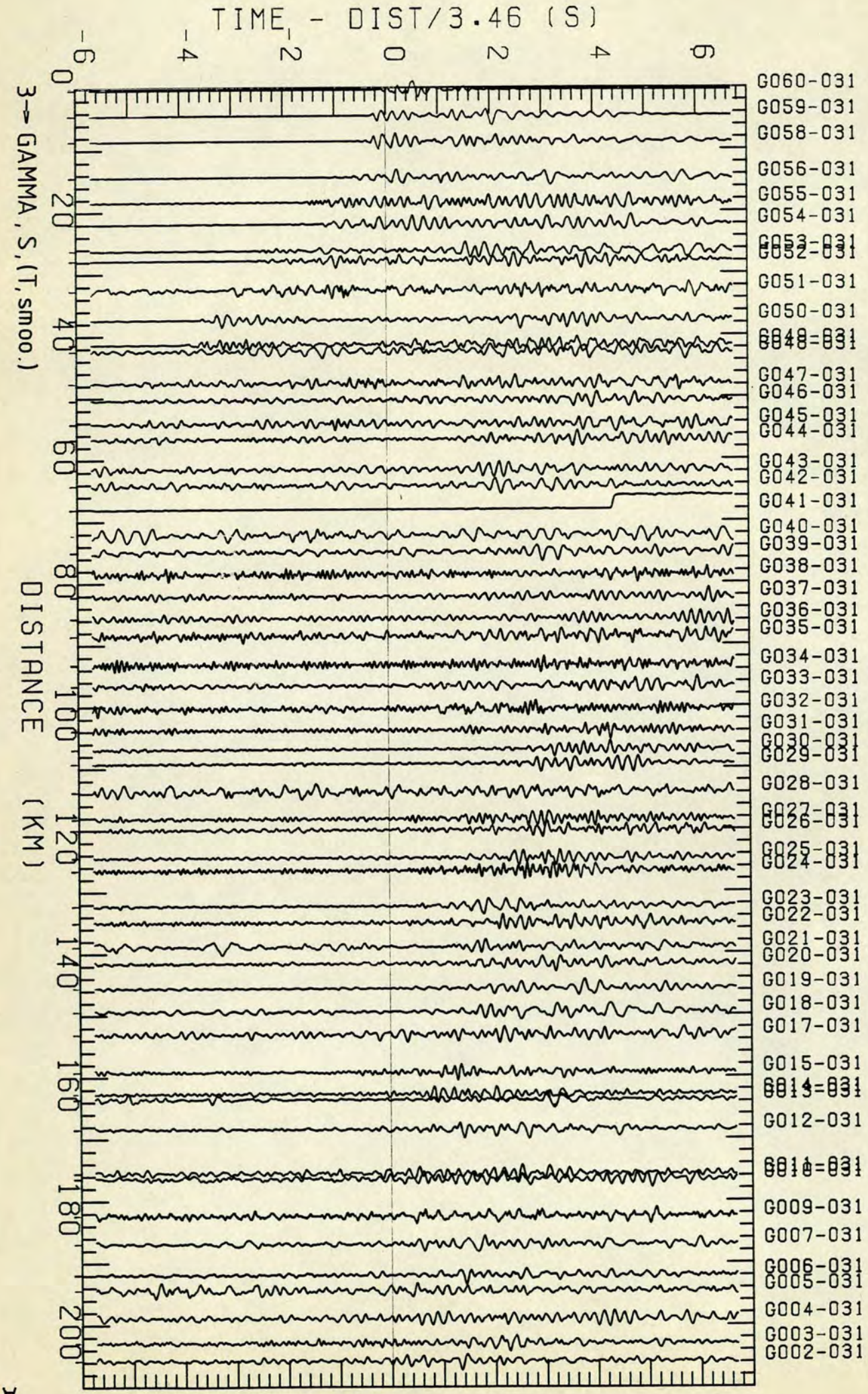
TIME - DIST/3.46 (S)
-6
-4
-2
0
2
4
6
0
20
40
60
80
100
120
140
160
180
200
DISTANCE (KM)
3→ GAMMA, S, (T, smoo.)
G060-031
G059-031
G058-031
G056-031
G055-031
G054-031
G053-031
G052-031
G051-031
G050-031
G049-031
G048-031
G047-031
G046-031
G045-031
G044-031
G043-031
G042-031
G041-031
G040-031
G039-031
G038-031
G037-031
G036-031
G035-031
G034-031
G033-031
G032-031
G031-031
G030-031
G029-031
G028-031
G027-031
G026-031
G025-031
G024-031
G023-031
G022-031
G021-031
G020-031
G019-031
G018-031
G017-031
G015-031
G014-031
G013-031
G012-031
G011-031
G010-031
G009-031
G007-031
G006-031
G005-031
G004-031
G003-031
G002-031

APPENDIX B

S wave particle-motion plots

In the diagrams of particle-motion the following abbreviations are used:

sagittal plane : U=Up, D=Down, T=Towards, A=Away

horizontal plane : L=Left, R=Right

The numbers following the station codes are the station distances in Km. ST is the start time of the seismograms, i.e, the time of the first sample on the 3-component set (in reduced time with reduction velocity of 3.464 Km/s).

The lines crossing the seismograms are the picked onsets (SV crossing the vertical(Z) and SH crossing the transverse (T) components). The two small lines on each side of the pick indicate its estimated uncertainty.

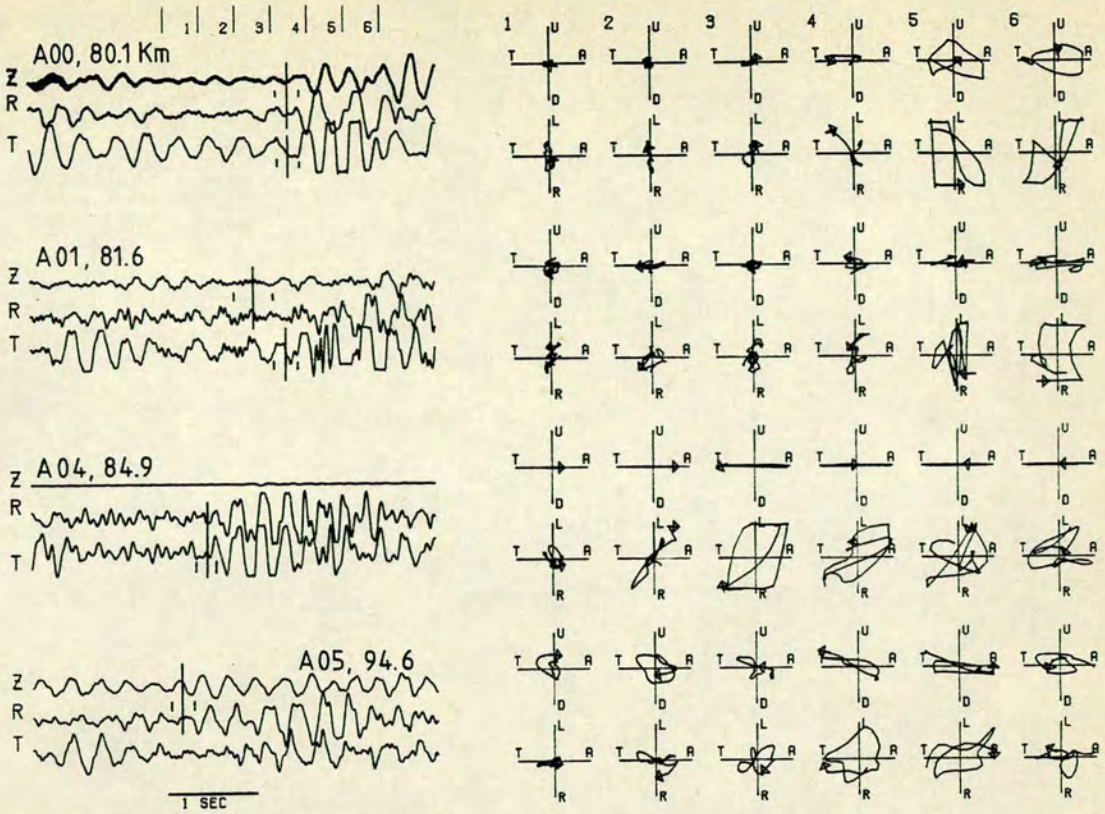

N2-ALPHA S 'C' UNF.
ST=0.0 A00 TO A05

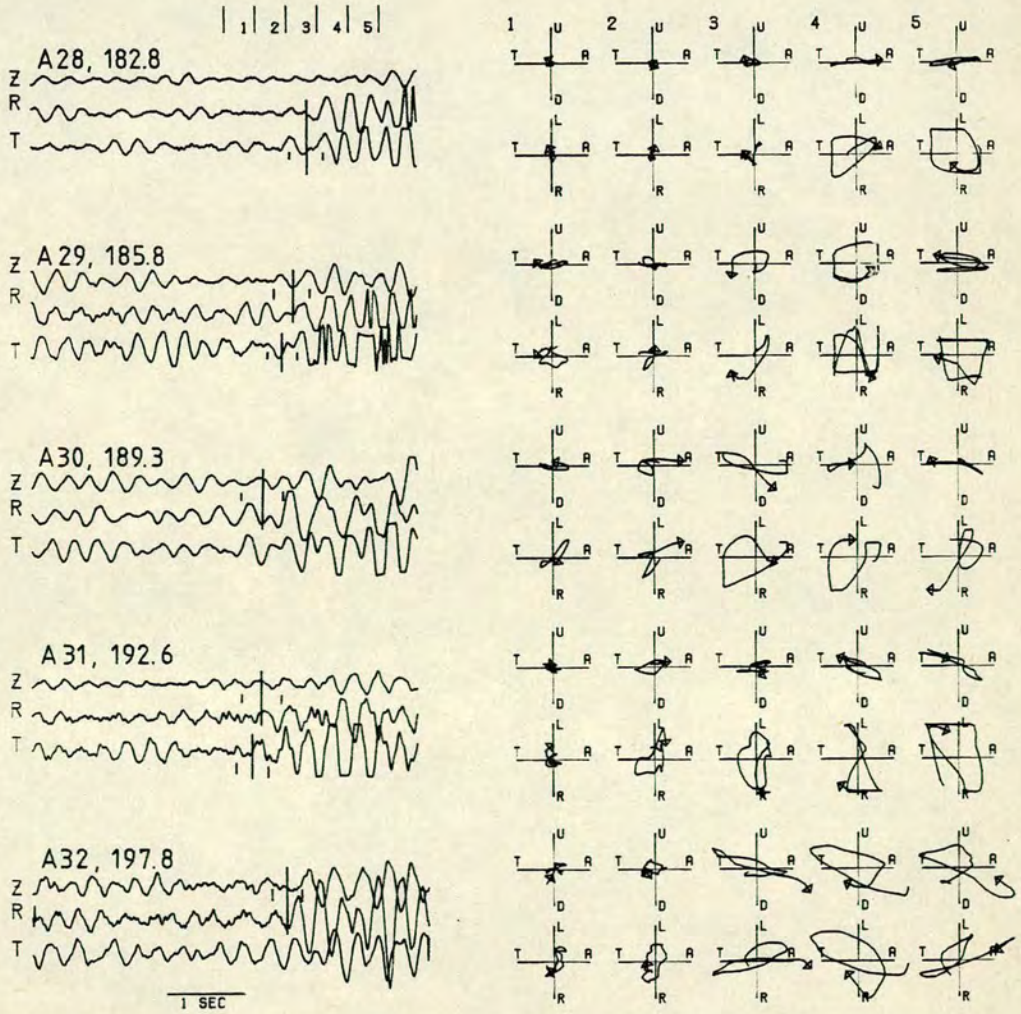

N2-ALPHA. S 'E' A-28 TO A-32
ST=-5.00 WINDOW=0.40 S.

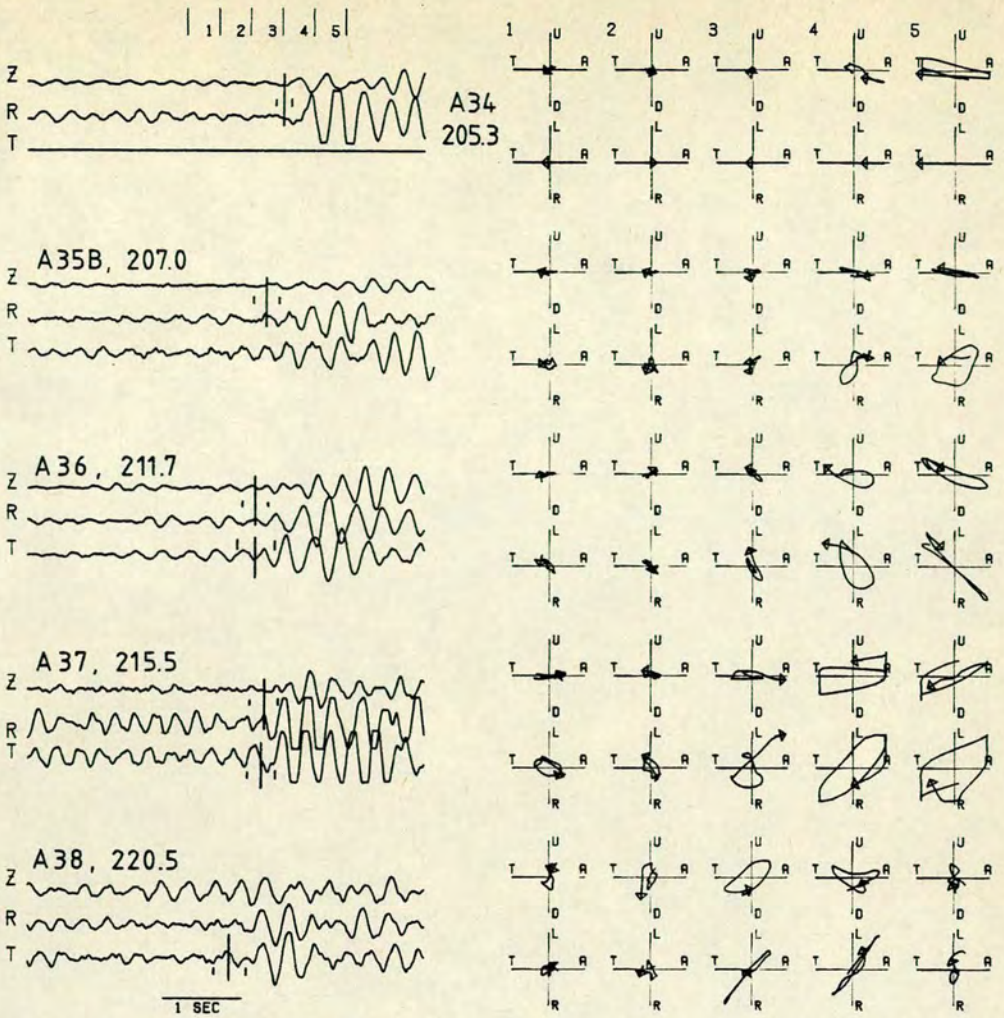

N2-ALPHA. S 'E' A34 TO A38
ST=-5.0 WINDOW=0.40 S.

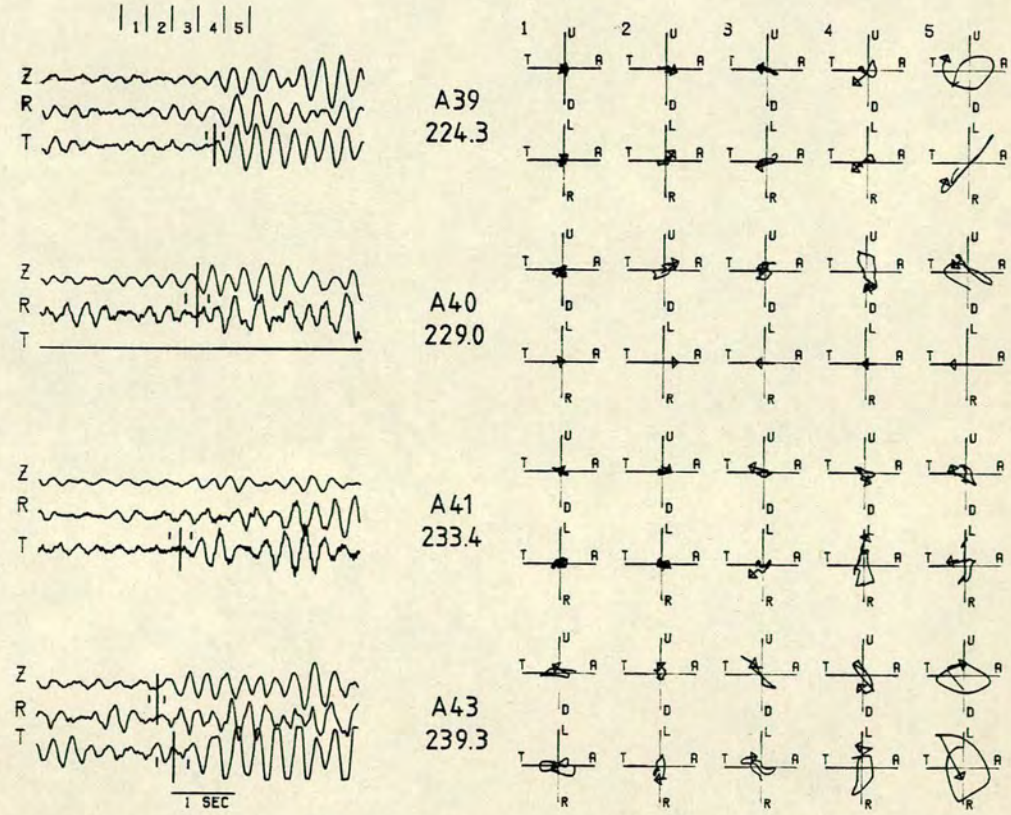

N2-ALPHA. S 'E' A39 TO A43
ST=-5.0 WINDOW=0.40 S.

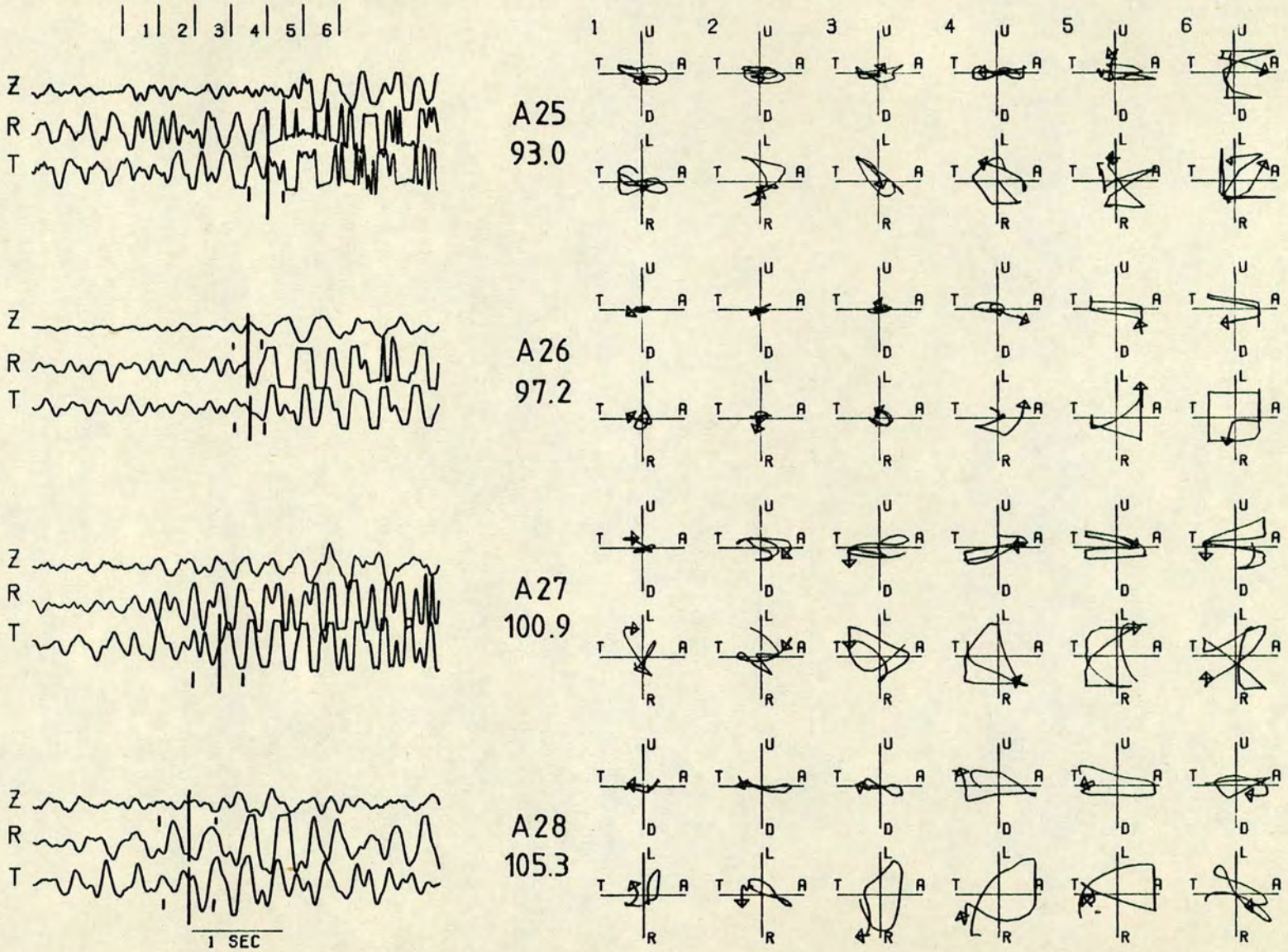

N1-ALPHA S , 'C' , A25 TO A28

ST=0.0 , UNF. , WINDOW=0.40 S.

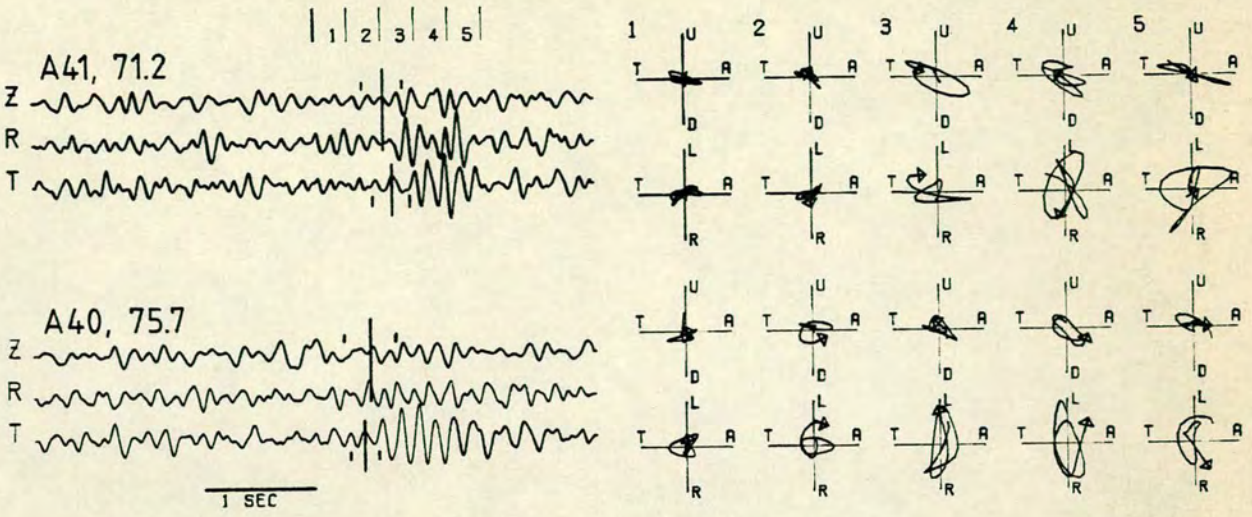

1-ALPHA S. 'C'. A41. A40
ST=2.0 . SMOO.. WINDOW=0.30 S.

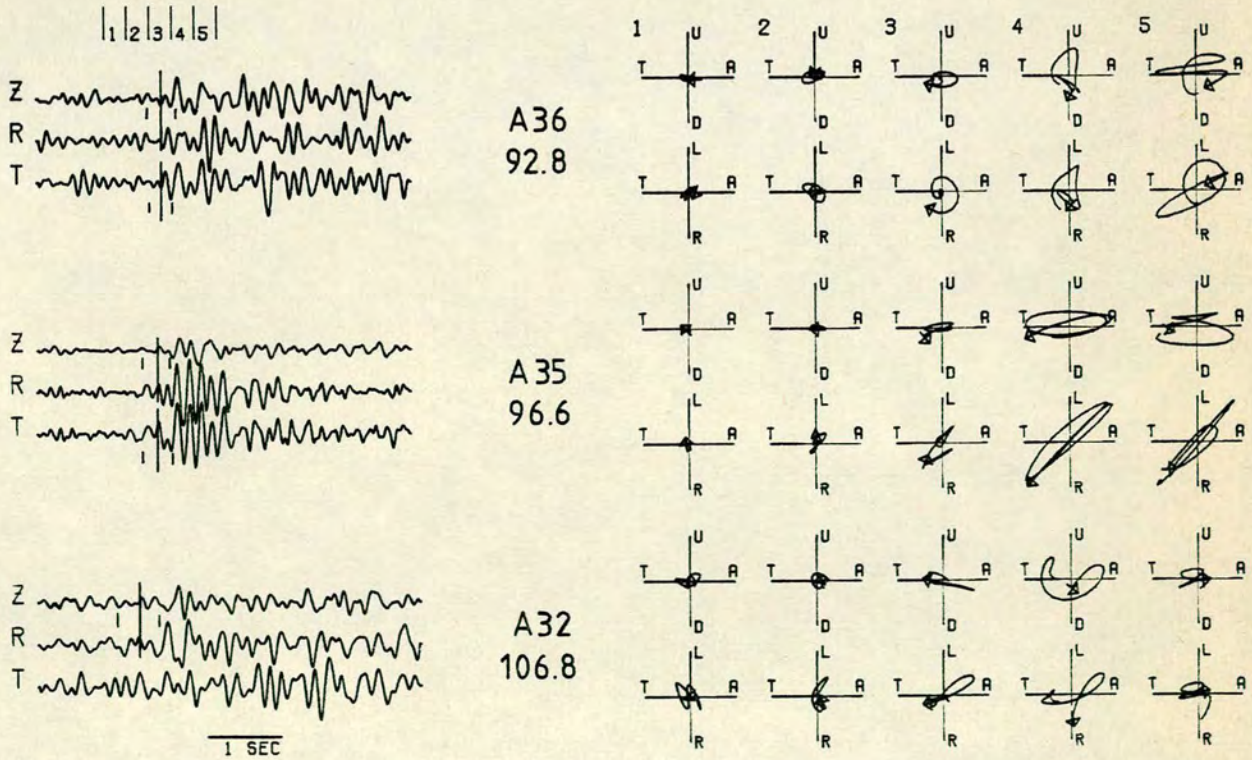

1-ALPHA . S . 'C'. A36 TO A32
ST=2.0 . SMOO. . WINDOW=0.30 S.

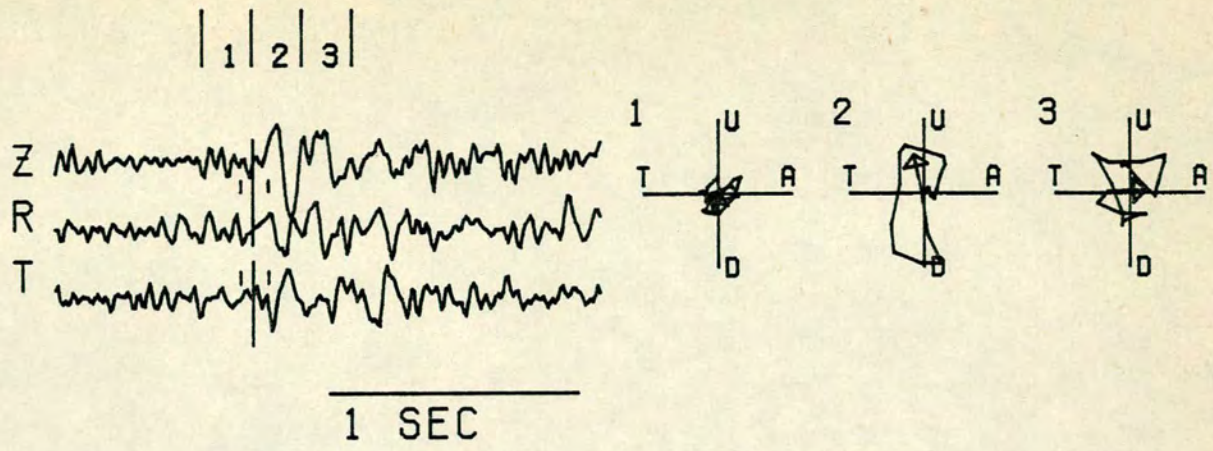

1-ALPHA SG A-56 17.0KM, 'a_o', ST=-.20
(UNFILT.)

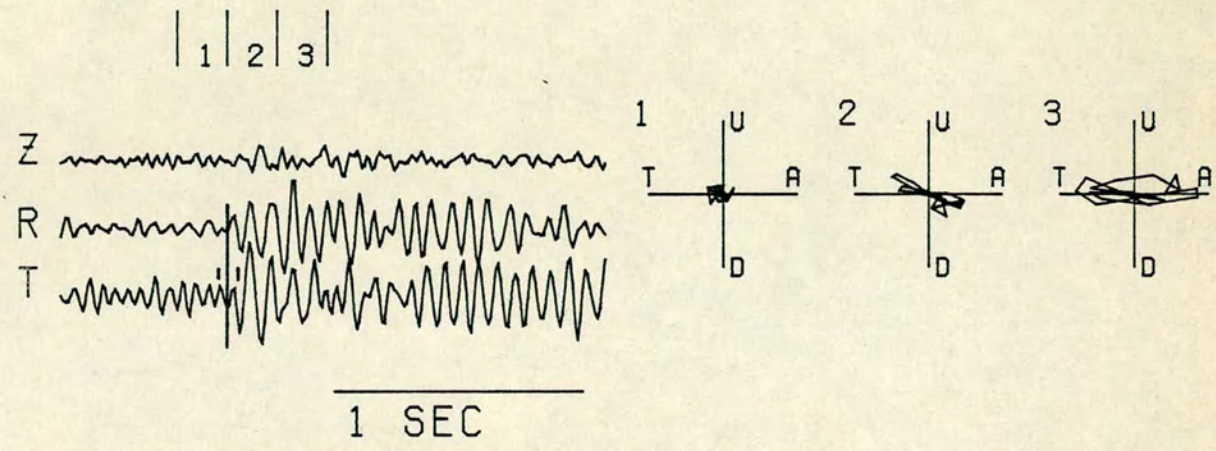

1-ALPHA SG A-55 21.4KM, 'a_o' ST=-.20
(UNFILT.)

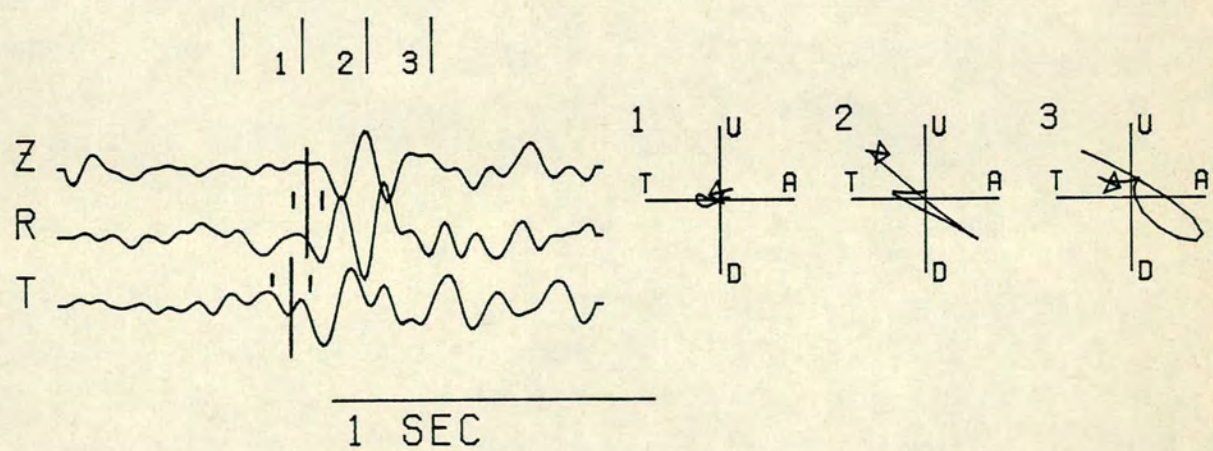

1-BETA S* B-18 53.6KM, 'a_1', ST=0.30
(SMOOTHED)

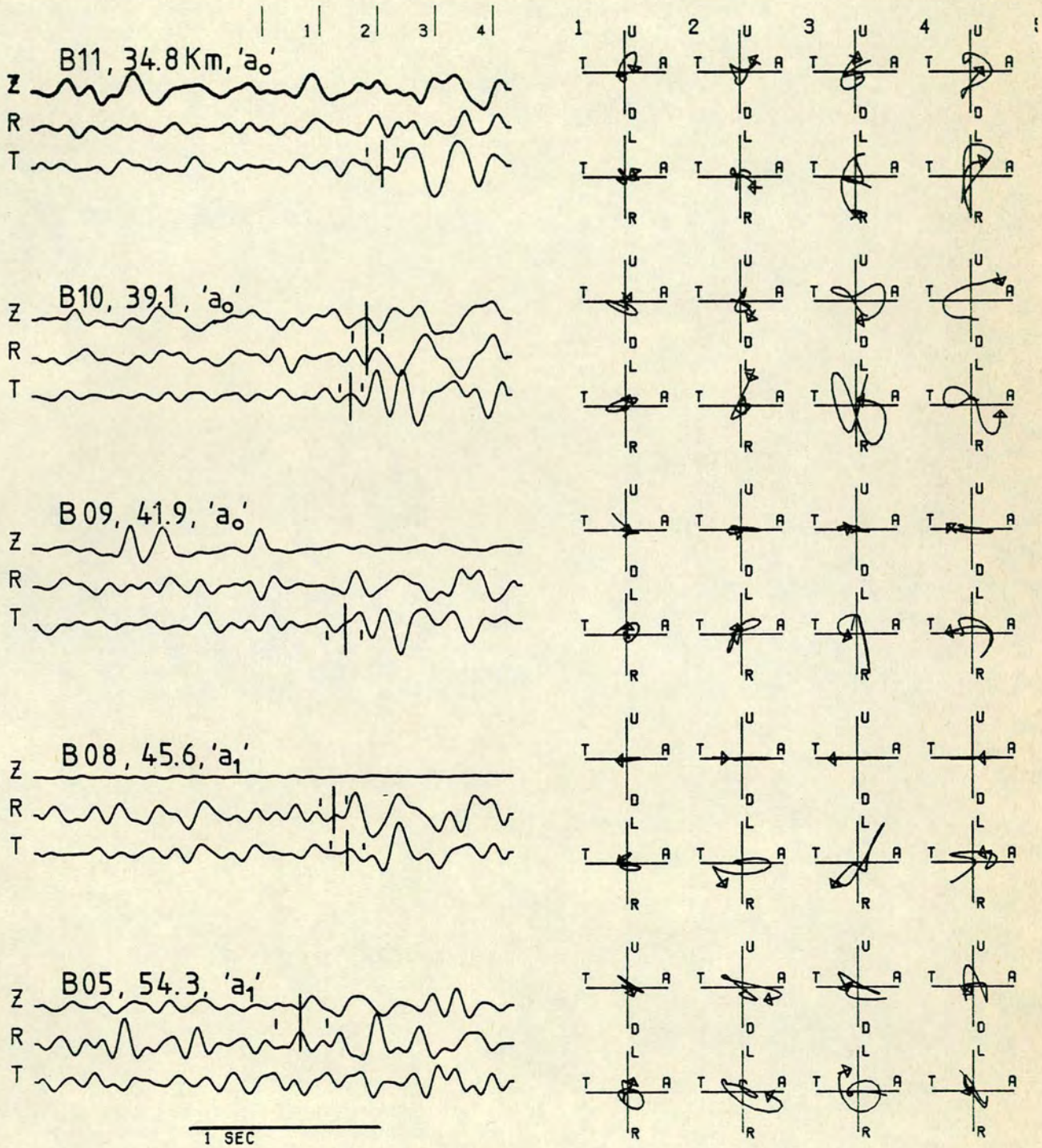

S WAVES E-BETA-N B11 TO B05

ST=0.00 WINDOW=0.30

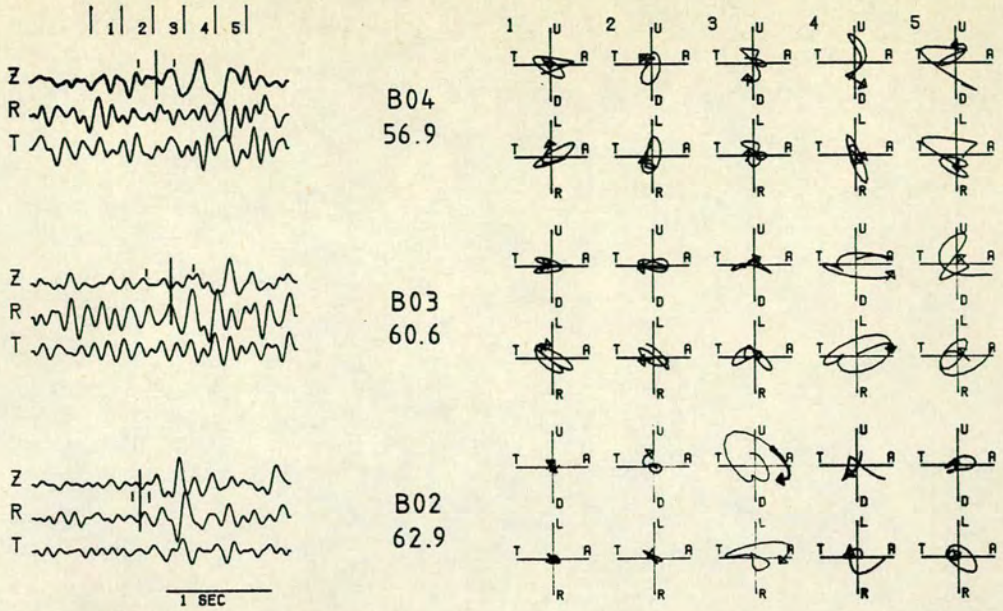

S WAVES E-NORTH B04 TO B02
ST=0.0 WINDOW=0.30 phase 'a_1'

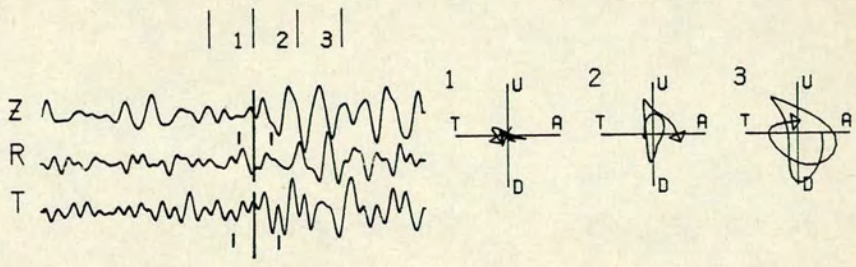

E-ALPHA SMS A-46 122.2KM, 'c', ST=0.50
(SMOOTHED)

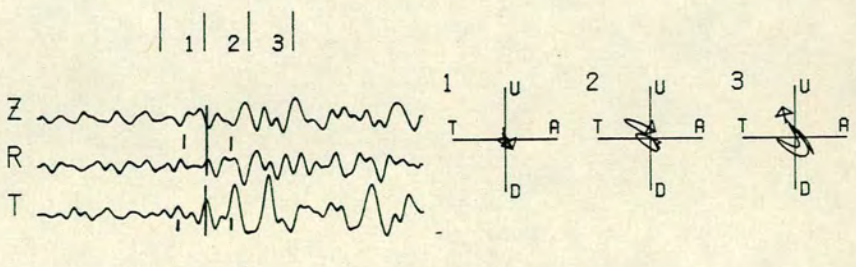

E-ALPHA SMS A-45 125.4KM, 'c', ST=0.50
(SMOOTHED)

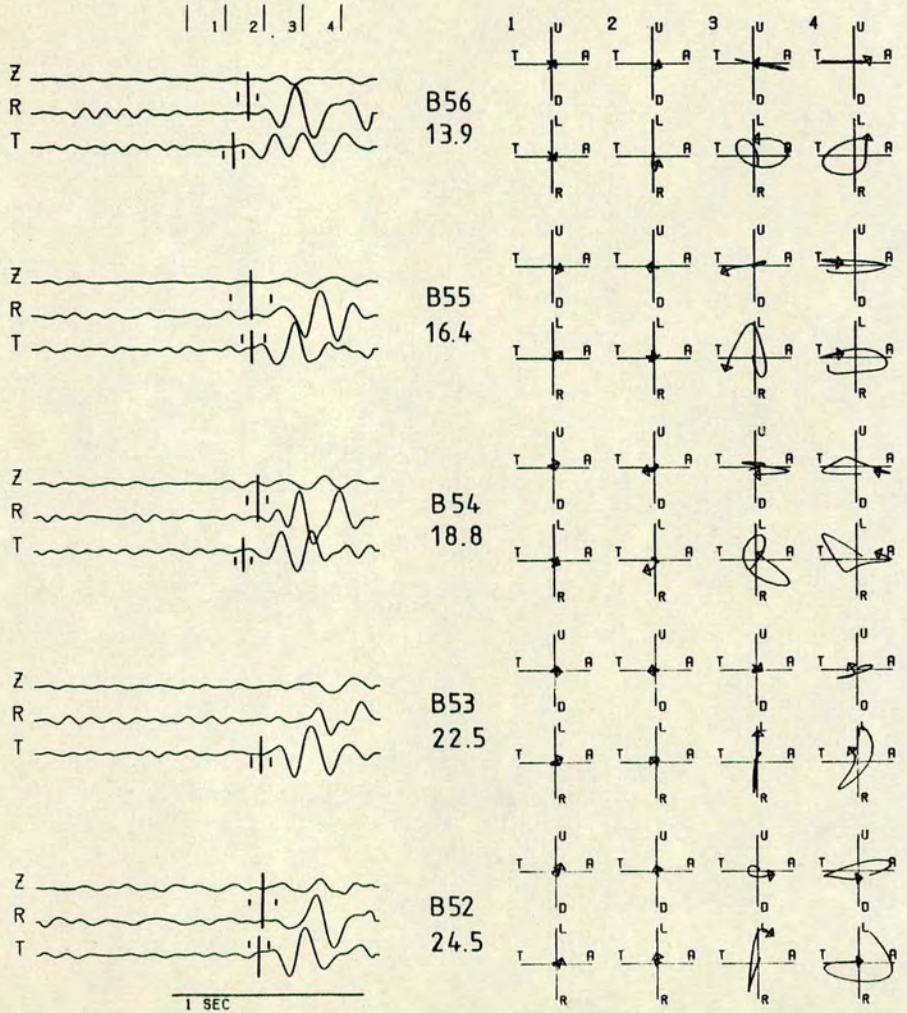

S WAVES 2-BETA
ST=0.0 WIN=0.20 phase 'a_o'

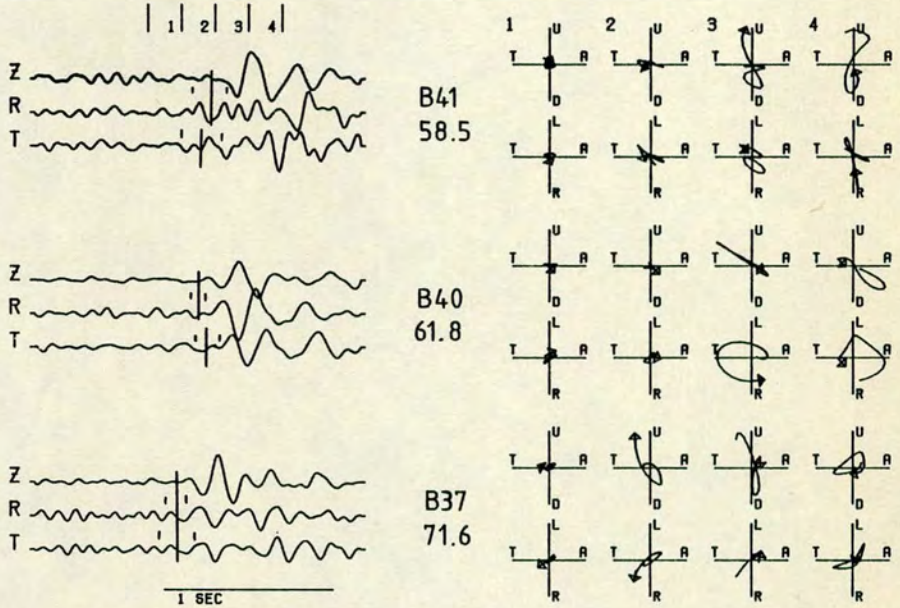

S WAVES, 2-BETA B-41 TO B-37
ST=0.40 WINDOW=0.20 phase 'a_o'

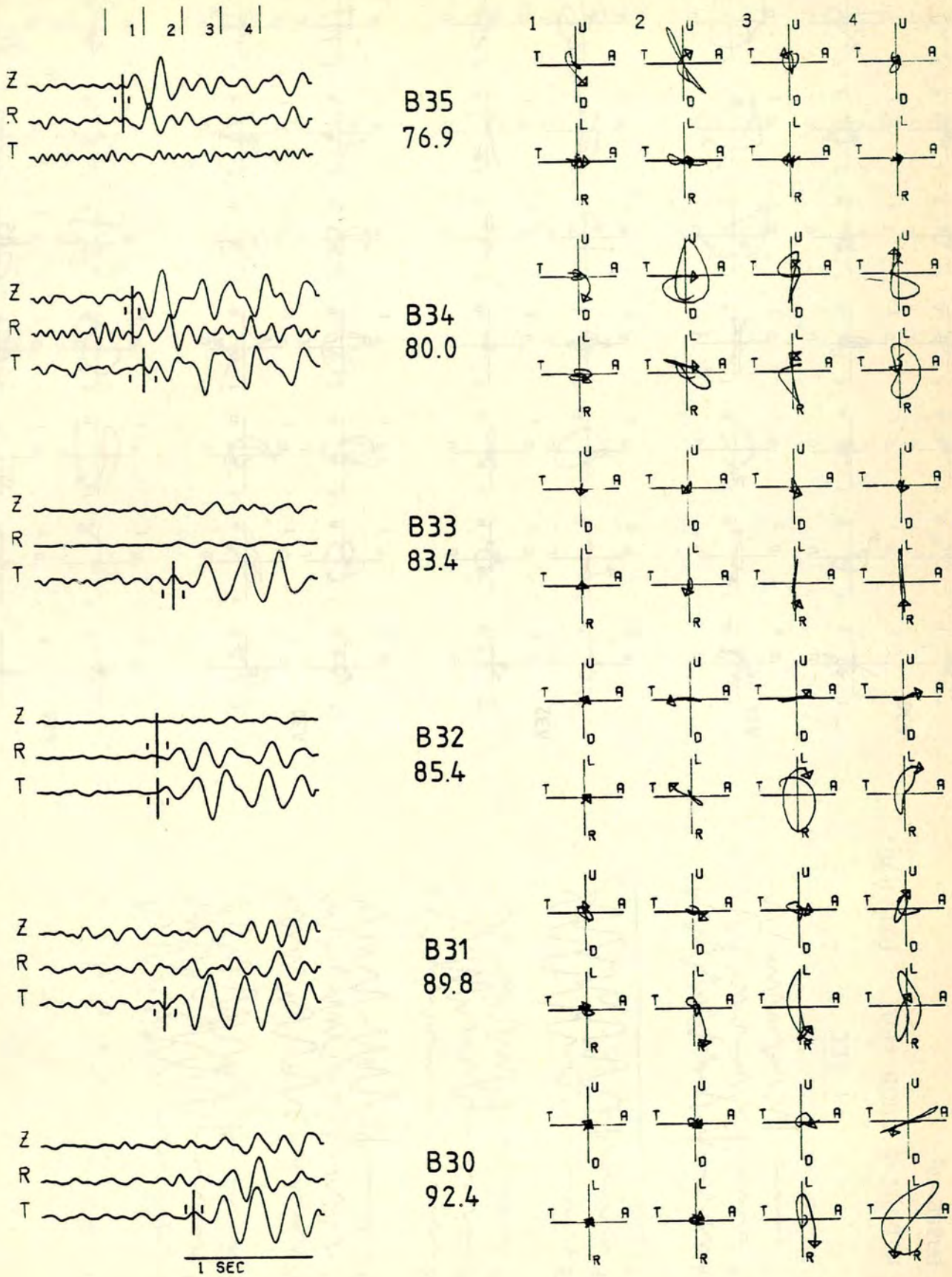

S WAVES 2-B35 TO B30

ST=0.50 WINDOW=.30

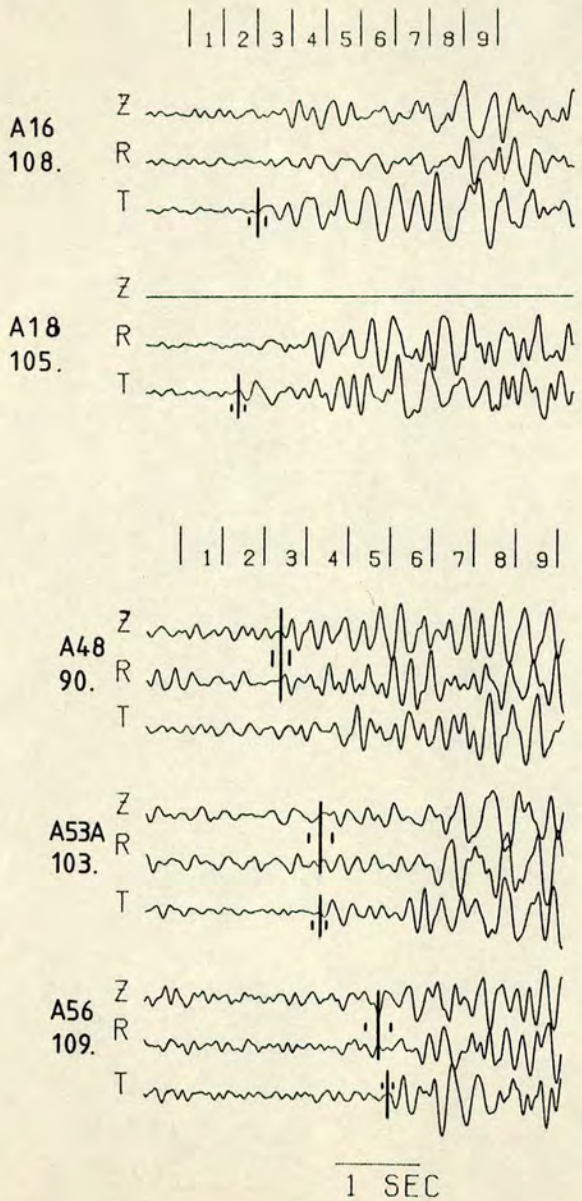
1 2 3 4 5 6 7 8 9
A16
108.
Z
R
T
A18
105.
A48
90.
A53A
103.
A56
109.
1 SEC

phase 'a_1'

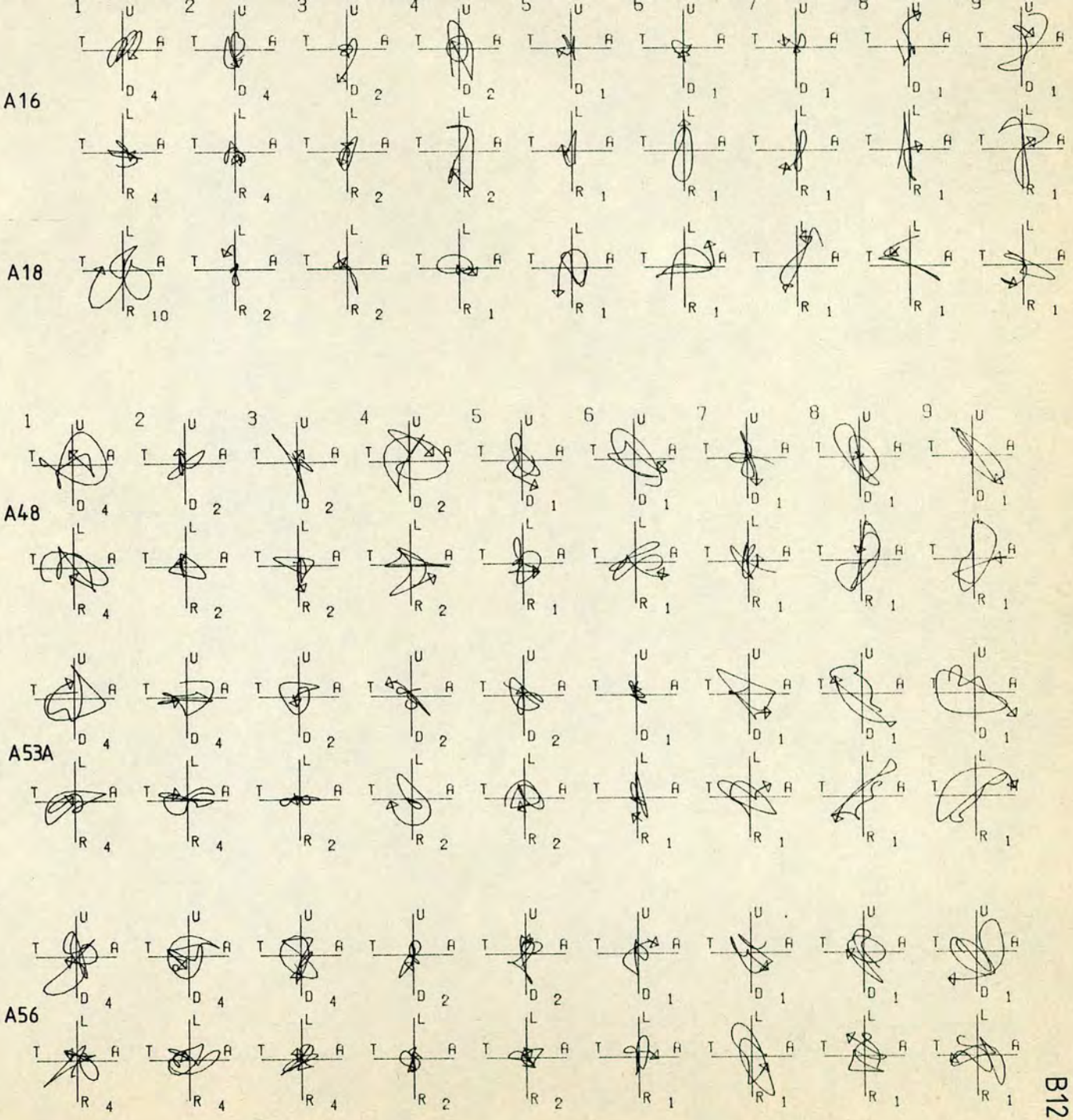
A16
A18
A48
A53A
A56
U
D
L
R
T
A

APPENDIX C

List of P and S travel times

The travel times are given in reduced time (in sec.) with reduction velocity of 6.0 Km/s for P and 3.464 Km/s for S. Distances are in Km. Only the travel times used in the ts/tp inversion are listed.

N2-->ALPHA 'c'

Station	Dist.	P	SV	SH
A00	80.1	1.35 ± .07	2.71 ± .11	2.71 ± .11
A01	81.6	1.43 "	2.46 .20	2.84 .13
A04	90.7	1.19 .10	---	1.95 .09
A05	94.6	1.01 .07	1.66 .11	---
A06	99.5	0.84 "	---	---
A07	103.3	0.73 "	---	1.49 .10
A08	106.3	0.66 "	0.88 .10	1.09 "
A09	100.5	0.23 "	0.22 "	---
A10	114.5	0.39 "	0.11 "	0.39 "

N2-->ALPHA 'e'

Station	Dist.	P	SV	SH
A27	178.8	-0.57 ± .05	-1.12 ± .37	---
A28	182.8	-0.70 "	-1.44 .23	---
A29	185.8	-0.85 "	-1.62 .25	-1.76 ± .18
A30	189.3	-0.94 "	-2.02 .28	---
A31	192.6	-0.98 "	-2.06 .28	-2.15 .21
A32	197.8	-1.00 .09	-1.80 .19	---
A34	205.3	-1.00 .05	-1.80 .10	---
A35B	207.0	-0.98 "	-2.11 .16	---
A35	208.1	-0.87 "	---	---
A36	211.7	-1.04 "	-2.14 .15	-2.15 .24
A37	215.5	-1.05 "	-2.05 .20	---
A38	220.3	-1.12 "	---	-2.46 .22
A39	224.3	-1.25 "	---	-2.35 .12
A40	229.0	-1.30 "	-2.60 .20	---
A41	233.4	-1.41 "	---	-2.80 .18
A42	235.2	-1.45 "	---	---
A43	239.3	-1.34 "	-3.16 .14	-2.87 .27
A44	242.5	-1.37 "	---	-2.79 .24

N1-->ALPHA 'c'

Station	Dist.	P	SV	SH
A21	77.7	2.06 ± .05	---	3.45 ± .23
A22	82.0	1.84 .15	3.18 ± .37	---
A23	86.5	1.70 .05	3.16 .22	---
A24	90.1	1.61 .10	3.03 .15	2.80 .17
A25	93.0	1.51 "	---	2.68 .30
A26	97.2	1.38 "	2.37 .15	2.40 .16
A27	100.9	1.20 "	---	2.08 .25
A28	105.3	0.98 "	1.70 .30	1.70 .30

N1-->ALPHA , phase PmS

Station	Dist. (Km)	PmS(*) (s)	E.C.(**) (s)
A15	55.6	6.78 ± .06	-.04
A16	58.9	6.61 "	-.02
A17	62.1	6.48 "	-.03
A18	65.1	6.31 "	-.04
A19	69.7	6.08 "	-.05
A20	74.9	5.86 "	-.03

(*) reduced time with red. vel. of 6.0 Km/s.
(**) station elevation correction.

1-->ALPHA 'a'

Station	Dist.	P	SV	SH
Phase 'a_s'				
A59	6.0	0.09 ± .03	---	0.22 ± .06
A58	8.5	0.11 .01	0.49 ± .04	0.49 .04
Phase 'a_o'				
A57	12.8	0.16 ± "	0.51 ± .05	0.55 ± .09
A56	17.0	0.23 "	0.59 .05	0.59 .05
A55	21.4	0.17 "	---	0.47 .03
A53A	24.7	0.22 "	0.55 .13	0.39 .05
A54	25.8	0.20 "	---	0.37 .09
A48	47.3	0.20 "	0.23 .11	0.29 .07
A48B	48.2	0.17 .02	0.25 .06	0.27 .08
A47	50.9	0.16 .01	0.10 .14	0.17 .08
A46	54.4	0.18 "	---	0.11 .05
A45	57.6	0.15 "	0.24 .13	0.16 .12
A44	62.0	0.18 .02	0.15 .09	0.14 .11
A43	65.4	0.19 .01	0.16 .08	0.13 .10
A42	69.4	0.22 "	0.32 .12	0.36 .11
A41	71.2	0.18 "	0.17 .07	---
A40	75.7	0.20 "	---	---
A36	92.8	0.18 .03	0.15 .06	0.14 .08
A35	96.6	0.12 .03	0.10 .08	-.02 .09
A34	99.2	0.18 .01	0.04 .09	0.08 .08

1-->ALPHA 'c'

Station	Dist.	P	SV	SH
A41	71.2	---	5.10 ± .17	5.18 ± .17
A40	75.7	---	4.99 .21	4.93 .13
A39	80.4	2.86 ± .15	---	4.79 .18
A37	89.0	2.40 .10	---	4.22 .14
A36	92.8	2.29 .08	3.63 .16	3.64 .15
A35	96.6	2.16 .06	3.58 .20	3.58 .20
A34	99.2	1.99 .11	3.52 .25	3.47 .17
A33	103.5	1.85 .11	3.42 .20	3.22 .20
A32	106.8	1.74 .10	3.32 .28	---

1-->BETA 'a'

Station	Dist.	P	SV	SH
Phase 'a_s'				
B02	5.3	0.00 ± .01	0.12 ± .03	---
B03	7.3	0.09 "	0.26 .04	0.26 ± .04
Phase 'a_o'				
B04	11.0	0.11 "	0.22 .03	0.22 .03
B05	13.6	0.25 "	---	0.50 .03
B06	17.2	0.42 "	---	0.79 .04
B07	19.5	0.45 "	---	---
B08	22.3	0.48 "	0.97 .05	0.96 .05
B09	26.0	0.59 "	1.29 .04	---
B10	28.8	0.65 "	1.30 .12	1.25 .06
B11	33.2	0.65 "	1.07 .05	1.09 .05
B12	35.1	0.66 "	1.23 .12	1.22 .09
B13	38.3	0.70 "	1.13 .06	1.06 .04
B14	40.9	0.69 "	0.98 .05	1.02 .04
B15	43.6	0.71 "	---	---
B16	46.7	0.70 "	1.07 .09	---
Phase 'a_1'				
B18	53.6	0.73 "	1.06 .04	1.00 .06
B22	64.6	0.64 .01	0.94 .06	0.94 .06
B23	68.3	0.59 "	---	0.75 .08
B24	72.1	0.54 "	---	0.63 .07
B26	79.6	0.48 "	---	---
B27	81.9	0.44 .02	0.34 .10	---

E-->ALPHA+BETA(North) 'a'

Station	Dist.	P	SV	SH
Phase 'a_s'				
B20	8.4	0.63 ± .01	1.31 ± .17	---
Phase 'a_o'				
B16	21.3	0.85 ± "	1.70 ± .18	---
B14	27.0	0.83 "	1.54 .07	---
B13	29.6	0.87 "	1.72 .05	1.56 ± .08
B12	32.9	0.90 "	1.75 .04	1.65 .11
B11	34.8	0.89 "	---	1.80 .06
B10	39.1	0.87 "	1.72 .07	1.64 .06
B09	41.9	0.87 "	---	1.58 .09
Phase 'a_1'				
B08	45.6	0.85 "	1.53 .07	1.62 .09
B05	54.3	0.80 "	1.38 .13	---
B04	56.9	0.76 "	1.21 .16	---
B03	60.6	0.82 "	1.31 .24	---
B02	62.9	0.70 "	1.03 .09	1.03 .09
A59	73.8	0.55 "	0.69 .25	0.69 .20
A55	89.1	0.39 "	0.29 .15	0.29 .15
A53A	92.5	0.40 "	---	0.06 .15
A54	93.5	0.38 "	---	0.16 .11
A52	96.5	0.42 "	---	---

E-->ALPHA 'c'

Station	Dist.	P	SV	SH
A48A	113.7	1.89 ± .07	---	3.11 ± .25
A48	115.1	1.84 "	---	3.06 .20
A48B	116.0	1.76 "	---	---
A47	118.6	1.69 "	2.81 ± .15	---
A46	122.2	1.55 "	2.43 .16	---
A45	125.4	1.46 "	2.02 .25	2.01 .25
A43A	133.1	1.20 .15	---	1.78 .20

2-->BETA 'a'

Station	Dist.	P	SV	SH	
Phase 'a_s'					
B58	6.6	0.28 ± .01	1.06? ± .02	1.06? ± .02	
B56	13.9	0.43 "	1.10 .05	1.04 .04	P: 'a_s'
B55	16.4	0.48 "	1.12 .10	1.14 .05	S: 'a_o'
B54	18.8	0.52 "	1.14 .05	1.07 .04	
Phase 'a_o'					
B53	22.5	0.63 ± .01	---	1.16 ± .04	
B52	24.5	0.63 "	1.16 .07	1.14 .05	
B51	28.7	0.64 "	1.25 .06	1.13 .02	
B50	31.5	0.69 "	1.25 .06	1.12 .04	
B49	35.3	0.63 "	1.14 .05	1.04 .05	
B48	37.2	0.64 "	1.11 .05	1.03 .04	
B47	41.7	0.75 "	1.30 .04	1.17 .07	
B46	43.7	0.73 "	1.20 .06	1.10 .05	
B45	46.7	0.73 "	1.16 .07	1.11 .12	
B44	49.6	0.82 "	1.35 .08	1.30 .12	
B43	53.3	0.82 "	1.28 .13	1.36 .10	
B42	56.2	0.90 "	1.45 .09	1.49 .11	
B41	58.5	0.95 "	1.46 .09	1.40 .12	
B40	61.8	0.92 "	1.40 .04	1.43 .08	
B38	67.3	0.90 "	1.32 .08	1.31 .10	
B37	71.8	0.96 "	1.26 .06	1.26 .11	
B36	73.9	0.92 "	1.21 .06	1.20 .08	
B35	76.9	0.93 "	1.22 .05	---	
B34	80.0	0.97 "	1.25 .05	1.35 .09	
B33	83.4	1.02 "	1.41 .12	1.57 .08	
B32	85.4	1.05 "	1.43 .06	1.43 .06	
B31	89.8	1.10 "	---	1.47 .08	
B30	92.4	1.22 "	---	1.67 .06	
B28	98.7	1.10 "	---	1.48 .17	
B27	100.4	1.11 "	---	1.29 .18	
B26	102.7	1.14 "	---	1.50 .30	

APPENDIX D

Linearization and least-squares - CURFIT program.

Suppose Y is a function of x with parameters K_1, K_2, etc.

$$Y = Y(x_n;\ K_1,\ K_2,\ \ldots) \qquad (I)$$

For example Y can be the ts/tp ratio of a particular station at distance x_n depending on the velocity ratios K_1, K_2, etc., in the various blocks of the crustal structure. Equation (I) can be approximated by a Taylor series expansion with respect to those parameters (linearization) :

$$Y(x_n) = Y_o(x_n) + \Delta K_1 \frac{\partial Y_o(x_n)}{\partial K_1} + \Delta K_2 \frac{\partial Y_o(x_n)}{\partial K_2} + \ldots \qquad (II)$$

where Y_o is the initial value of the function for a particular initial set of parameters, and ΔK_i are corrections to the initial set of parameters.

If a set of observational data $D(x_n)$ with associated uncertainties σ_n is to be fitted by least-squares, i.e., the sum of weighted squared residuals

$$\chi^2 = \sum_n \frac{1}{\sigma_n}[D(x_n) - Y(x_n)]^2$$

is to be minimized, then we get the normal equation :

$$\begin{bmatrix} a_{11} & a_{12} & \cdots & a_{1N} \\ a_{21} & & \cdots & a_{2N} \\ \cdot & & & \\ \cdot & & & \\ a_{N1} & & & a_{NN} \end{bmatrix} \cdot \begin{bmatrix} \Delta K_1 \\ \Delta K_2 \\ \cdot \\ \cdot \\ \Delta K_N \end{bmatrix} = \begin{bmatrix} d_1 \\ d_2 \\ \cdot \\ \cdot \\ d_N \end{bmatrix} \qquad (III)$$

where :

$$a_{ij} = \sum_n \frac{1}{\sigma_n^2} \frac{\partial Y_o(x_n)}{\partial K_i} \cdot \frac{\partial Y_o(x_n)}{\partial K_j} \qquad (a_{ij} = a_{ji})$$

$$d_i = \sum_n \frac{1}{\sigma_n^2}[D(x_n) - Y_o(x_n)] \cdot \frac{\partial Y_o(x_n)}{\partial K_i}$$

ΔK_i = increment in parameter K_i that minimizes χ^2.

This is an iterative process in which the first solution for the parameters K_i will constitute the initial model for the second iteration, and so on.

A program was written (called CURFIT) to solve equation (III) for the case when the partial derivatives $\frac{\partial Y_o(x_n)}{\partial K_i}$ could not be given by a simple formula but had to be calculated numerically by the difference between two values of Y_o calculated at K_i and $K_i + \Delta K_i'$. The program will use as input :

a) the initial values of the parameters and the parameter increments to be used to calculate the partial derivatives.

b) the observations x_n, $D(x_n)$ and uncertainties σ_n.

c) Initial values and perturbed values of Y_o calculated at a few key points x_n'. The derivatives will be calculated at these key points and values will be interpolated for all the observed data points.

The program allows any number of parameters to be fixed at specified values (and the theoretical initial value of Y_o will be corrected according to the calculated partial derivatives).

Fig. D.1(a) shows ts/tp data for phase 'a_o' (2—>BETA) where the vertical arrows indicate the key points (x_n') used in the CURFIT program. Contrary to chapter 4 we used here the P to S velocity ratio K = Vp/Vs as parameters instead of the Poisson's ratio. Three parameters as shown in Fig. D.1(b) were used. Their initial values were $K_1 = K_2 = K_3 = 1.732$ ($=\sqrt{3}$) and so all initial values $Y_o(x)$ were also 1.732 (as shown by the dashed line in Fig. D.1). Table D.1 is the input list for the program with added comments and explanations. The values under the columns Y1, Y2 and Y3 are the theoretical values of ts/tp at the key points calculated for the initial model with the parameters $K_1 + \Delta K_1'$, $K_2 + \Delta K_2'$ and $K_3 + \Delta K_3'$ respectively.

The list in Table D.1 is for the first iteration in the least-squares

process. The results of this first iteration are (with errors at 2 s.d.) :

K_1 = 1.872 +/- .033 (σ_1 = 0.300 +/- .010)

K_2 = 1.690 +/- .005 (σ_2 = 0.231 +/- .003)

K_3 fixed at 1.782 (σ_3 fixed at 0.27)

These results are almost identical to the final results shown in Table 4.2 (chapter 4), showing that two iterations only would be enough for inverting all ts/tp data for the segments ALPHA and BETA without any special initial model.

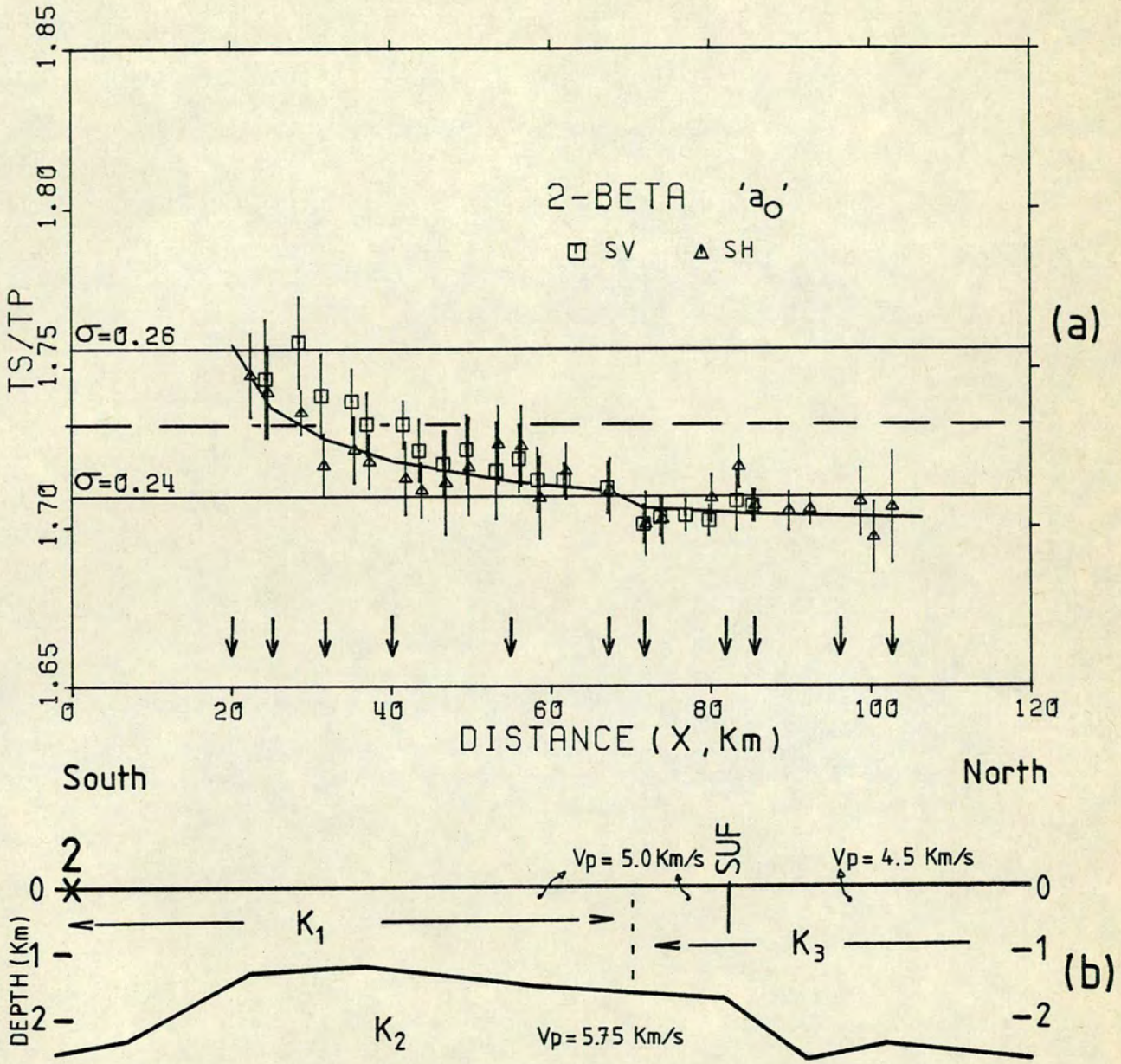

Fig. D.1 (a) t_s/t_p data of phase 'a_o' fitted with CURFIT program. Arrows indicate key points (x'_n). Horizontal dashed line is initial theoretical curve with all parameters $K = V_p/V_s = \sqrt{3}$ ($\sigma = 0.25$). Continuous line is the result of the first iteration (calculated with program SIGREFRA using the K solutions of CURFIT). (b) Structural model of superficial layer with parameters K_i in the three blocks.

Card no.	INPUT DATA	COMMENTS
1)	2-BETA 'A'	* Title
2)	03	No. of parameters
3)	(1F7.3,F7.3,001F7.3)	FMT format for cards 5, 6 and 10.
4)	(3F7.3,F7.3,001F7.3)	FMT " for cards 12 (Key points).
5)	1.732 1.732 1.732	Initial values of K_1, K_2, K_3 .
6)	0.050 0.050 0.050	K_i incr. used for Y1,Y2,Y3.
7)	01 FIXED PARAM.	No. of parameters to be fixed
8)	03 0.05	K_3 fixed at 1.732 + 0.05 .
9)	45	No. of data points.
10)	24.5 1.747 0.019	Data:
	28.7 1.758 0.014	
	31.5 1.741 0.013	Values of distance (Km), t_s/t_p,
	35.3 1.740 0.010	
	37.2 1.732 0.010	and uncertainties in t_s/t_p .
	41.7 1.732 0.007	
	43.7 1.724 0.010	
	46.7 1.720 0.010	
	. . .	
	. . .	
	. . .	
	53.3 1.726 0.012	
	56.2 1.725 0.012	
	58.5 1.709 0.013	
	61.8 1.718 0.009	
	67.3 1.712 0.010	
	71.8 1.701 0.010	
	73.9 1.702 0.007	
	80.0 1.709 0.007	
	83.4 1.719 0.007	
	85.4 1.707 0.005	
	89.8 1.705 0.006	
	92.4 1.705 0.005	
	98.7 1.708 0.011	
	100.4 1.697 0.011	
	102.7 1.706 0.017	
11)	11 X Y0 Y1 Y2 Y3	11 Key points.
12)	20.0 1.732 1.7521 1.7601	
	25.0 1.732 1.7461 1.7666	X = distance of key point.
	32.0 1.732 1.7432 1.7698	Y0 = initial value of t_s/t_p at X.
	40.0 1.732 1.7411 1.7721	Y1 = value of t_s/t_p when parameter 1 ($^pK1$) is increased by 0.05 (to calculate partial deriv.)
	55.0 1.732 1.7391 1.7743	
	67.3 1.732 1.7381 1.7753	
	71.8 1.732 1.7353 1.7756 1.7346	
	81.9 1.732 1.7349 1.7762 1.7344	
	85.4 1.732 1.7348 1.7768 1.7341	Y2 = same for K2
	96.5 1.732 1.7345 1.7766 1.7346	Y3 = same for K3 (blank = Y0).
	102.7 1.732 1.7343 1.7770 1.7344	
	0000000000000000000000000000000000000000	

Table D.1 Example of input data for program CURFIT.